CNIC-01718
CNDC-0035
INDC(CPR)-059/L

# COMMUNICATION OF NUCLEAR DATA PROGRESS

No.28(2002.12)

China Nuclear Data Center
China Nuclear Information Centre
China Nuclear Industry Audio & Visual Publishing House

# COMMUNICATION OF NUCLEAR DATA PROGRESS



## EDITORIAL NOTE

The editors hope that our readers and colleagues will not spare their comments in order to improve this publication. If you have any, please contact us by following address:


Mailing Address: Profs. LIU Tingjin and ZHUANG Youxiang
China Nuclear Data Center
China Institute of Atomic Energy
P.O. Box 275 (41), Beijing 102413
People's Republic of China
Telephone: 86-10-69357729 or 69357830
Facsimile: 86-10-6935 7008
E-mail: tjliu @ iris.ciae.ac.cn or yxzhuang @ iris.ciae.ac.cn

Abstract: This is the 28th issue of *Communication of Nuclear Data Progress* (CNDP), in which the progress and achievements in nuclear data field since 2001 in China are carried. It includes the measurement of neutron capture cross section of $^{50}$Cr in the energy range from 50 to 1052 keV; importance of $^{5}$He emission in neutron induced reactions, calculations of cross sections and energy spectra for neutron induced gamma-ray of $^{181}$Ta, $^{197}$Au and natural Ag, progress in making program MEND; evaluations of complete neutron data for n+$^{28,29,30,Nat}$Si, $^{85,87,Nat}$Rb, $^{89}$Y, $^{169}$Tm and $^{197}$Au, the mass distribution data for $^{238}$U and $^{239,242}$Pu fission, and n+$^{6}$Li reaction cross sections; data correction for mass resolution; implementation of the resonance analysis code SAMMY; the benchmark testing of $^{9}$Be data of CENDL-3.

# Communication of Nuclear Data Progress

**No.28 (2002) Beijing**

## CONTENTS

# Measurement of Neutron Capture Cross Section of $^{50}$Cr in the Energy Range from 50 to 1052 keV

XIA Yijun YANG Zhihua
*Institute of Nuclear Science and Technology, Sichuan University*

ZHENG Yiyun
*Department of Physics, Sichuan University*

**【abstract】** *The cross section for the $^{50}$Cr(n,γ)$^{51}$Cr reaction was measured relatively to that of $^{197}$Au for neutron energy from 50 to 1052 keV, using the activation technique. Neutrons were generated via the $^{7}$Li(p, n) $^{7}$Be and T(p,n) $^{3}$He reactions with a 2.5MV Van de Graaff accelerator at Sichuan University. The activities after irradiation were measured with a calibrated high resolution HPGe detector. The experiment results were compared with existing data.*

## Introduction

Capture cross section of chromium, as an important structural material of reactor, is required in reactor development. Natural Cr consists of four isotopes, i.e. $^{50}$Cr(4.35%), $^{52}$Cr(83.79%), $^{53}$Cr(9.5%), and $^{54}$Cr(2.36%). The abundance of $^{50}$Cr is fairly low. There are some data for the cross section of the $^{50}$Cr(n,γ)$^{51}$Cr reaction but they are quite discrepant. Because of the discrepancies, this cross section is not adequately known for fusion reactor applications. In this work we measured the cross sections in the energy range from 50 to 1052 keV by the activation method.

## 1 Measurement

The samples were made of naturally metallic chromium powder, which were pressed into a disk with 20mm in diameter and 1.5mm in thickness and packed in Al film. The gold disks each of 20mm in diameter and 0.1mm in thickness were used as the neutron flux monitors. Each sample was sandwiched between two gold disks. The sample groups were wrapped in cadmium foils of 0.5mm in thickness. The purity of Au and Cr samples is 99.99% and 99.9%, respectively.

The irradiations were performed at 0 degree with relation to the incident proton beam. The neutrons of 50 to 270 keV were produced by $^{7}$Li(p,n)$^{7}$Be reaction, and 437 to 1052 keV by T(p,n)$^{3}$He reaction. The distance between the samples and the target were 14~20mm. The proton beam currents were generally 8 to 12 μA and the duration of irradiation was about 30 to 40 hours for each energy. The neutron flux was monitored with a long counter at 0 degree and a distance of 1.8m from the target. In order to record the neutron flux as a function of time during the irradiation, the integral count rate of the long counter per 2 minutes was recorded continuously by microcomputer multiscaler and stored on magnetic disk for calculating the correction of nonuniform irradiation history.

The activities of the samples and the gold disks were measured with a calibrated high resolution HPGe detector. Because the activities of the samples were rather weak, they were placed on the surface of the detector for measurement. The relevant decay data of $^{51}$Cr and $^{198}$Au are listed in Table 1.

**Table 1 Decay data of products**

| Product nucleus | $T_{1/2}$ / day | $E_\gamma$ / keV | $I_\gamma$ / % |
|---|---|---|---|
| $^{51}$Cr | 27.704 | 302.08 | 9.92 |
| $^{198}$Au | 2.6935 | 411.8 | 95.5 |

## 2 Results

The cross section for the $^{50}$Cr(n,γ) $^{51}$Cr reaction measured relative to the standard cross section of $^{197}$Au(n,γ)$^{198}$Au reaction recommended by ENDF/B-6 are listed in Table 2 and plotted in Fig.1 together with experiment errors. For comparisons, the results given by Kenny [1], Beer [2] and Stieglitz [3] are also plotted in Fig.1.

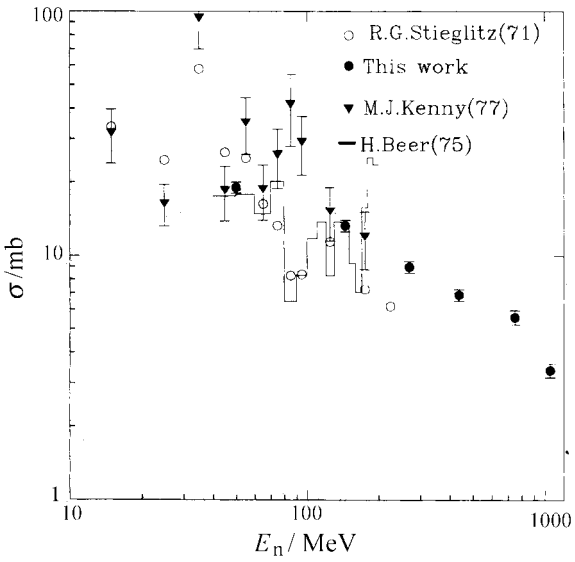


Fig. 1 The neutron capture cross section of $^{50}$Cr

The main uncertainties of the cross sections include the error of efficiency of γ-ray full energy peak (2.5%), the counting statistics of the γ-activities (1.2%~2.2%), the decay schemes (1.5%), the correction of γ-ray self absorption (1%), the neutron scattering back-ground (0.5%), the weight of samples (0.5%) and the standard cross section of gold (3%~4.5%).

**Table 2 Measured cross sections**

| $E_n$ / keV | $\sigma$ / mb |
|---|---|
| 50±13 | 19.1±1.0 |
| 145±23 | 13.3±0.7 |
| 270±24 | 9.0±0.5 |
| 437±89 | 6.9±0.4 |
| 750±89 | 5.6±0.4 |
| 1052±93 | 3.4±0.2 |

These are some resonance structure for the $^{50}$Cr(n,γ)$^{51}$Cr reaction cross section below 200 keV neutron energy. The data of Kenny, Beer and Stieglitz are average capture cross sections over wide energy intervals. It can be seen from Fig.1 that our results of 50 and 145 keV are in good agreement with the data of Kenny and Beer. Our result of 50 keV is lower than the data of Stieglitz, but is higher than the data of Stieglitz at 145 keV.

## Acknowledgment

The authors are indebted to China Nuclear Data Center for financial support. We would like to thank the crew of 2.5 MV Van de Graaff of Sichuan University too.

### References

[1] M.J.Kenny, B.J.Allen, R.AAEC/E-400, 7701
[2] H.Beer, R.R.Spencer, Nucl. Phys. A 240,29(1975)
[3] R.G.Stieglitz, et al., Nucl. Phys. A 163, 592(1971)

# Importance of $^5$He Emission in Neutron Induced Reactions

ZHANG Jingshang
*China Nuclear Data Center, CIAE, P.O.Box 271(41) Beijing 102413*

**【abstract】** *An important particle emission of $^5$He has never been included in the widely used statistical model codes as the evaluation tool. The threshold energies from light nuclei to heavy nuclei are given, which indicate that in general the compound nucleus induced by incident neutron would emit $^5$He rather than $^3$He. Being $^5$He unstable and separated into n+$\alpha$ spontaneously, the formulation of the double-differential cross section of the neutron from the $^5$He two-body breakup process is given. Because of stronger recoil effect than the other outgoing particles, the energy balance is strictly taken into account. The further improvement for the model calculation on this respect is proposed.*

## Introduction

The statistical model codes as the evaluation tool widely used in the world have long been performed to set up neutron data library below 20 MeV. However, an important emission channel has been ignored in all the way. Based on the calculated threshold energies of $^3$He and $^5$He emissions for various nuclei, one can find that the compound nucleus for neutron-induced reactions prefer emit $^5$He rather than $^3$He. Being $^5$He unstable and separated into n+$\alpha$ spontaneously with Q-value of 0.894 MeV, finally, the $^5$He emission belong to the (n,n$\alpha$) reaction channel. Unfortunately, this emission channel has never been considered in all the present codes for the model calculations. The calculated threshold energies from light nuclei to heavy nuclei are given for some important stable elements in Section 1. The reaction situation is also discussed. In general, $^3$He emissions have small reaction cross-sections, of which the measurements could rarely be found, while $^5$He has relative low threshold energies. The formula of the outgoing neutron from $^5$He separation is obtained and given in Section 2. The widths of the outgoing neutron spectra, as the example, have been calculated, which are all in the order of magnitude of MeV. Thus, the outgoing neutron spectrum should be treated as a continuum spectrum. The remarks are given in the last section.

## 1 Threshold Energies of $^3$He and $^5$He Emissions

The threshold energies of $^3$He and $^5$He emissions from neutron-induced reactions for the stable elements with the largest abundance from light nuclei to heavy nuclei are given in Table 1. From this Table one can find that the threshold energies of $^3$He emissions are larger than that of $^5$He emissions obviously, except $^{40}$Ca and $^{58}$Ni.

It should stress that the threshold energies of the alpha particle emissions become zero above $^{139}$La, which are very similar to that of $^5$He emissions. However, for these heavy nuclei, the reaction cross sections of the outgoing charged particles, like $^3$He, $^5$He, as well as alpha particle, become very small even without threshold due to the large Coulomb barrier. All of the He gas production cross sections could be neglected for these heavy nuclei.

For the medium nuclei, (see above $^{24}$Mg), both of the $^3$He emission and $^5$He emission become obvious. However, the $^5$He emissions have small values of the threshold energies compared with that of the $^3$He emissions. In this case the $^5$He emission and the $^3$He emission should be taken into account simultaneously in the model calculations.

In the case of light nuclei, from Table 1 one can see that the $^5$He emissions play an important role in the model calculations. The compound nuclei formed by incident neutron would emit $^5$He rather than $^3$He obviously. In general, the $^5$He emissions could be omitted, in particular, for the 1p shell nuclei as well as for $^{19}$F, $^{20}$Ne in 2s-1d shell.

## 2 The Double-differential Cross Section of the Neutron from $^5$He Separation

In pre-equilibrium emission processes, the emitted $^5$He has forward angular distribution, so the neutron from $^5$He two-body breakup process also has the same situation.

**Table 1 Threshold energies of $^3$He and $^5$He emissions for some elements in unit MeV**

| | $^3$He | $^5$He | | $^3$He | $^5$He |
|---|---|---|---|---|---|
| $^9$Be | 24.04 | 3.74 | $^{69}$Ga | 9.01 | 5.46 |
| $^{10}$B | 17.34 | 5.89 | $^{85}$Rb | 10.13 | 7.59 |
| $^{11}$B | 25.27 | 10.43 | $^{89}$Y | 10.08 | 8.96 |
| $^{12}$C | 21.10 | 8.95 | $^{90}$Zr | 7.80 | 7.66 |
| $^{14}$N | 18.62 | 13.41 | $^{93}$Nb | 7.80 | 2.86 |
| $^{16}$O | 15.64 | 8.56 | $^{98}$Mo | 9.63 | 4.21 |
| $^{19}$F | 17.08 | 5.17 | $^{106}$Pd | 8.76 | 4.17 |
| $^{20}$Ne | 13.79 | 5.91 | $^{107}$Ag | 8.39 | 4.95 |
| $^{23}$Na | 17.06 | 11.86 | $^{115}$In | 8.46 | 3.71 |
| $^{24}$Mg | 13.30 | 10.63 | $^{127}$I | 7.64 | 3.10 |
| $^{27}$Al | 15.25 | 11.39 | $^{133}$Cs | 5.37 | 0.75 |
| $^{28}$Si | 12.58 | 11.27 | $^{139}$La | 6.98 | 3.73 |
| $^{31}$P | 13.51 | 10.91 | $^{144}$Nd | 6.12 | 0 |
| $^{32}$S | 8.71 | 8.09 | $^{153}$Eu | 6.89 | 0.63 |
| $^{35}$Cl | 9.81 | 8.12 | $^{158}$Gd | 8.24 | 1.56 |
| $^{40}$Ar | 15.42 | 7.89 | $^{167}$Er | 6.58 | 0.23 |
| $^{39}$K | 9.14 | 8.32 | $^{175}$Lu | 5.80 | 0 |
| $^{40}$Ca | 7.17 | 8.14 | $^{180}$Hf | 6.98 | 0 |
| $^{45}$Se | 11.59 | 9.03 | $^{184}$W | 6.54 | 0 |
| $^{48}$Ti | 12.46 | 10.55 | $^{197}$Au | 6.53 | 0 |
| $^{51}$V | 12.75 | 11.41 | $^{208}$Pb | 7.70 | 0 |
| $^{52}$Cr | 11.06 | 11.41 | $^{209}$Bi | 3.49 | 0 |
| $^{55}$Mn | 12.96 | 8.99 | $^{226}$Ra | 6.22 | 0 |
| $^{56}$Fe | 10.72 | 8.66 | $^{232}$Th | 6.10 | 0 |
| $^{58}$Ni | 6.59 | 7.42 | $^{225}$U | 4.69 | 0 |
| $^{63}$Cu | 9.69 | 6.78 | $^{238}$U | 5.55 | 0 |
| $^{64}$Zn | 6.21 | 4.93 | $^{239}$Pu | 3.68 | 0 |

In this section the representation of the double-differential cross section of the neutron from $^5$He→n+α two-body breakup process is given. The derivation procedure can be found in Ref.[1] in detail. However, the formula in Ref.[1] is for the two-body breakup process of the residual nucleus, while in this paper the formula is for the two-body breakup process of emitted particle $^5$He. The emitted $^5$He in its ground state is assumed in this study, although $^5$He has its excited states.

Two motion systems are used in the formulation, the physical quantities are indicated by the superscript c, and r for center of mass system (CMS), and recoil residual nucleus system (RNS), respectively. The double-differential cross section of the neutron with the mass $m_n$ in CMS is represented by

$$\frac{d^2\sigma}{d\varepsilon_n^c d\Omega_n^c} = \sum_l \frac{2l+1}{4\pi} f_l^c(\varepsilon_n^c) P_l(\cos\theta_n^c) \tag{1}$$

the Legendre expansion coefficient of the emitted neutron in Eq. (1) is obtained by

$$f_l^c(\varepsilon_n^c) = \frac{1}{4\gamma\varepsilon_n^r} f_l^c(^5\mathrm{He}) P_l(\eta) \tag{2}$$

where $\eta$ is defined by

$$\eta \equiv \sqrt{\frac{\varepsilon_n^r}{\varepsilon_n^c}} \cdot \frac{\frac{\varepsilon_n^c}{\varepsilon_n^r} - 1 + \gamma^2}{2\gamma} \tag{3}$$

In Eq. (3) $\gamma$ is defined by

$$\gamma = \sqrt{\frac{E^c(^5\mathrm{He}) m_n}{\varepsilon_n^r m_{^5\mathrm{He}}}} \tag{4}$$

$E^c(^5\mathrm{He})$ = energy carried by $^5$He, which reads

$$E^c(^5\mathrm{He}) = \frac{M_1}{M_C}(E^* - B_{^5\mathrm{He}} - E_{k_1}) \tag{5}$$

where

$E_n$, $E^*$ are the incident neutron energy and excitation energy, respectively;

$B_{^5\mathrm{He}}$ is the binding energy of the emitted $^5$He in its compound nucleus;

$E_{k_1}$ is level energy of the residual nucleus after $^5$He emission;

$M_C$, $M_1$ are the masses of compound nucleus and the residual nucleus after $^5$He emission;

$m_{^5\mathrm{He}}$, $m_\alpha$ are the masses of $^5$He and alpha particle;

$f_l^c(^5\mathrm{He})$ is the Legendre expansion coefficients of the emitted $^5$He in CMS, calculated by the composite particle emission model[2,3].

$\varepsilon_n^r$ in Eq. (4) stands for the energy carried by the outgoing neutron in RNS , which is given by

$$\varepsilon_n^r = \frac{m_\alpha}{m_{^5\mathrm{He}}} Q \tag{6}$$

where $Q$=0.894 MeV is the reaction $Q$-value of $^5$He→n+α for two-body breakup process.

The maximum and the minimum energies of the neutron in CMS can be obtained by

$$\varepsilon_{n,\max}^c = \varepsilon_n^r (1+\gamma)^2 \tag{7}$$

$$\varepsilon_{n,\min}^c = \varepsilon_n^r (1-\gamma)^2 \tag{8}$$

Thus, the spectra of the emitted neutron are in ring type form. The width of the spectrum can be obtained by

$$\Delta\varepsilon \equiv \varepsilon^{\mathrm{c}}_{\mathrm{n,max}} - \varepsilon^{\mathrm{c}}_{\mathrm{n,min}} = 4\gamma\varepsilon^{\mathrm{r}}_{\mathrm{n}}$$

$$= 4\sqrt{\frac{m_{\mathrm{n}} m_{\alpha}}{m_{^5\mathrm{He}} M_{\mathrm{C}}}(E_{k_1} + Q)(E^* - B_{^5\mathrm{He}} - E_{k_1})} \qquad (9)$$

In general speaking, the larger the target mass is, the smaller the spectrum width is. Meanwhile, the spectrum width increases as $E^*$ increasing.

Because of relative heavy mass, the recoil effect must be taken into account in a strict way. The energy carried by the residual nucleus in CMS is given by [1]

$$E^{\mathrm{c}}(M_1) = \frac{m_{^5\mathrm{He}}}{M_{\mathrm{C}}}(E^* - B_{^5\mathrm{He}} - E_{k_1}) \qquad (10)$$

The energies carried by the neutron and alpha particle in CMS from $^5$He two-body breakup process are given, respectively, by

$$E^{\mathrm{c}}(m_{\mathrm{n}}) = \int_{\varepsilon^{\mathrm{c}}_{\mathrm{n,min}}}^{\varepsilon^{\mathrm{c}}_{\mathrm{n,max}}} \varepsilon^{\mathrm{c}}_{\mathrm{n}} f^{\mathrm{c}}_0(\varepsilon^{\mathrm{c}}_{\mathrm{n}}) \mathrm{d}\varepsilon^{\mathrm{c}}_{\mathrm{n}}$$

$$= \frac{m_{\alpha}}{m_{^5\mathrm{He}}} Q + \frac{m_{\mathrm{n}}}{m_{^5\mathrm{He}}} E^{\mathrm{c}}(^5\mathrm{He}) \qquad (11)$$

By using the same procedure for the outgoing alpha particle we have

$$E^{\mathrm{c}}(m_{\alpha}) = \frac{m_{\mathrm{n}}}{m_{^5\mathrm{He}}} Q + \frac{m_{\alpha}}{m_{^5\mathrm{He}}} E^{\mathrm{c}}(^5\mathrm{He}) \qquad (12)$$

In laboratory system, the energy carried by the residual nucleus $M_1$ is obtained by [1]

$$E^{\mathrm{l}}(M_1) = \frac{m_{\mathrm{n}} M_1}{M_{\mathrm{C}}^2} E_{\mathrm{n}} + \frac{m_{^5\mathrm{He}}}{M_1} E^{\mathrm{c}}(^5\mathrm{He})$$

$$- \frac{2}{M_{\mathrm{C}}} \sqrt{m_{\mathrm{n}} m_{^5\mathrm{He}} E_{\mathrm{n}} E^{\mathrm{c}}(^5\mathrm{He})} f^{\mathrm{c}}_1(^5\mathrm{He}) \qquad (13)$$

By means of the composition of velocities

$\vec{v}^{\mathrm{l}} = \vec{v}^{\mathrm{c}} + \vec{V}_{\mathrm{C}}$, where $\vec{V}_{\mathrm{C}}$ is the velocity of the center of mass, $V_{\mathrm{C}} = \frac{\sqrt{2m_{\mathrm{n}} E_{\mathrm{n}}}}{M_{\mathrm{C}}}$. So the energy of a particle with mass $m$ in LS can be obtained by

$$E^{\mathrm{l}}(m) = \frac{m}{2} \int (v^{\mathrm{l}})^2 \frac{\mathrm{d}^2\sigma}{\mathrm{d}\varepsilon^{\mathrm{c}} \mathrm{d}\Omega^{\mathrm{c}}} \mathrm{d}\varepsilon^{\mathrm{c}} \mathrm{d}\Omega^{\mathrm{c}}$$

To do so in this way the energies carried by the outgoing neutron and the outgoing alpha particle in LS are obtained

$$E^{\mathrm{l}}(m_{\mathrm{n}}) = \frac{m_{\mathrm{n}}^2}{M_{\mathrm{C}}^2} E_{\mathrm{n}} + E^{\mathrm{c}}(m_{\mathrm{n}}) + \frac{2m_{\mathrm{n}}}{M_{\mathrm{C}} m_{^5\mathrm{He}}}$$

$$\times \sqrt{m_{\mathrm{n}} m_{^5\mathrm{He}} E_{\mathrm{n}} E^{\mathrm{c}}(^5\mathrm{He})} f^{\mathrm{c}}_1(^5\mathrm{He}) \qquad (14)$$

$$E^{\mathrm{l}}(m_{\alpha}) = \frac{m_{\mathrm{n}} m_{\alpha}}{M_{\mathrm{C}}^2} E_{\mathrm{n}} + E^{\mathrm{c}}(m_{\alpha}) + \frac{2m_{\alpha}}{M_{\mathrm{C}} m_{^5\mathrm{He}}}$$

$$\times \sqrt{m_{\mathrm{n}} m_{^5\mathrm{He}} E_{\mathrm{n}} E^{\mathrm{c}}(^5\mathrm{He})} f^{\mathrm{c}}_1(^5\mathrm{He}) \qquad (15)$$

$E_{k_1}$ is the γ decay energy of the residual nucleus .

Thus, the total released energy reads

$$E^{\mathrm{l}}_{\mathrm{T}} = E^{\mathrm{l}}(m_{\mathrm{n}}) + E^{\mathrm{l}}(m_{\alpha}) + E^{\mathrm{l}}(M_1) + E_{k_1}$$

$$= \frac{m_{\mathrm{n}}}{M_{\mathrm{C}}} E_{\mathrm{n}} + E^{\mathrm{c}}(m_{\mathrm{n}}) + E^{\mathrm{c}}(m_{\alpha}) + E^{\mathrm{c}}(M_1) + E_{k_1}$$

$$= \frac{m_{\mathrm{n}}}{M_{\mathrm{C}}} E_{\mathrm{n}} + (1 + \frac{m_{^5\mathrm{He}}}{M_1}) E^{\mathrm{c}}(^5\mathrm{He}) + E_{k_1}$$

$$= \frac{m_{\mathrm{n}}}{M_{\mathrm{C}}} E_{\mathrm{n}} + Q + E^* - B_{^5\mathrm{He}}$$

$$= E_{\mathrm{n}} + B_{\mathrm{n}} - B_{^5\mathrm{He}} + Q \qquad (16)$$

where $B_{\mathrm{n}}$ is the neutron binding energy.

Obviously, the energy balance is held analytically.

The energy ranges of the outgoing neutron for some nuclei have been calculated at incident neutron energy of 14 MeV, and the results are given in Table 2. The residual nuclei are at their ground state in the calculations. From Table 2 one can find that the neutron energy regions are all in the order of magnitude of MeV. In general, the spectrum width decreases as target mass increasing. Meanwhile, the spectrum width increases as incident neutron energy increasing.

The discrete level energies of the residual nucleus affect the value of spectrum width. From Eq. (9), the maximum spectrum width is given at the residual excitation energy as below

$$E_{k_1} = \frac{1}{2}(E^* - B_{^5\mathrm{He}} - Q) \qquad (17)$$

For a given excitation energy, when the excited level energy of the residual nucleus after $^5$He emission is near the value determined by Eq. (17), then the largest value of the spectrum width could be occurred.

This kind of outgoing neutron spectrum should be treated as the continuum spectrum, which contributes to the low energy region of the total outgoing neutron spectra and belongs to the (n, nα) reaction channel.

## Remarks

Based on the aforementioned analysis numerically, the importance of $^5$He emissions in neutron induced reactions could be revealed for various elements. On the other hand, this reaction channel can have the important contribution to the outgoing neutron, especially, for light nuclei. Of course, the main reaction channel of He gas production is (n,α), while $^3$He and $^5$He productions are small quantities compared with $^4$He production. However, in general $^5$He production is greater than that of $^3$He productions.

**Table 2 The energy range of neutron from $^5$He breakup process for some elements in unit MeV**

| | $\varepsilon^{c}_{n,min} - \varepsilon^{c}_{n,max}$ | $\Delta\varepsilon$ |
|---|---|---|
| $^9$Be | 0.013-3.265 | 3.25 |
| $^{10}$B | 0.016-2.785 | 2.77 |
| $^{11}$B | 0.009-1.777 | 1.77 |
| $^{12}$C | 0.008-2.034 | 2.03 |
| $^{14}$N | 0.105-0.759 | 0.65 |
| $^{16}$O | 0.092-1.949 | 1.86 |
| $^{19}$F | 0.402-2.593 | 2.19 |
| $^{20}$Ne | 0.373-2.422 | 2.05 |
| $^{23}$Na | 0.019-1.008 | 0.99 |
| $^{24}$Mg | 0.088-1.305 | 1.22 |
| $^{27}$Al | 0.062-1.076 | 1.01 |
| $^{28}$Si | 0.076-1.096 | 1.02 |
| $^{31}$P | 0.121-1.157 | 1.04 |
| $^{32}$S | 0.396-1.806 | 1.41 |
| $^{35}$Cl | 0.426-1.775 | 1.35 |
| $^{40}$Ar | 0.502-1.792 | 1.29 |
| $^{39}$K | 0.442-1.701 | 1.26 |
| $^{40}$Ca | 0.473-1.736 | 1.26 |
| $^{45}$Se | 0.405-1.505 | 1.10 |
| $^{48}$Ti | 0.244-1.132 | 0.89 |
| $^{51}$V | 0.162-0.910 | 0.75 |
| $^{52}$Cr | 0.273-1.141 | 0.87 |
| $^{55}$Mn | 0.465-1.468 | 1.00 |
| $^{56}$Fe | 0.513-1.539 | 1.03 |
| $^{58}$Ni | 0.690-1.810 | 1.12 |
| $^{63}$Cu | 0.808-1.935 | 1.13 |
| $^{64}$Zn | 1.082-2.336 | 1.25 |
| $^{69}$Ga | 1.032-2.206 | 1.17 |
| $^{85}$Rb | 0.778-1.696 | 0.92 |
| $^{89}$Y | 0.586-1.382 | 0.80 |
| $^{90}$Zr | 0.784-1.672 | 0.89 |
| $^{93}$Nb | 1.549-2.707 | 1.16 |
| $^{98}$Mo | 1.350-2.408 | 1.06 |
| $^{106}$Pd | 1.382-2.403 | 1.02 |
| $^{107}$Ag | 1.258-2.232 | 0.97 |
| $^{115}$In | 1.484-2.487 | 1.00 |
| $^{127}$I | 1.616-2.599 | 0.98 |
| $^{133}$Cs | 2.031-3.091 | 1.06 |
| $^{139}$La | 1.536-2.449 | 0.91 |
| $^{144}$Nd | 2.363-3.448 | 1.08 |

The reaction mechanism included in the model calculation code, such as direct reaction, pre-equilibrium emission, and equilibrium emission, is an essential part. Meanwhile, the angular momentum conservation and the parity conservation for both continuum states and discrete states as well as the energy balance are also necessary. For composite particle emissions the pre-formation probability in the pickup mechanism is still important in the model calculation. On the other hand, the reaction channels designed in the code are also an important part. As the $^5$He emissions, if there is no this reaction channel included in the code, then in the fitting procedure to the measurement of (n,nα) cross sections, user has to increase the value of corresponding level density parameter of its residual nucleus. To do so in this way, the following reaction channels ($A$+1,$Z$)(n, nα) and ($A$,$Z$) (n, α), which have identical residual nucleus, could not use the same level density parameter, due to absent of $^5$He emission in the (n, nα) reaction channel.

The LUNF codes have been developed for neutron induced light nucleus reactions, in which the $^5$He emissions are already included in the model calculations. The calculated reaction cross sections of $^5$He-emission for neutron bombarding $^9$Be, $^{12}$C, $^{10}$B, $^{11}$B, as well as $^{16}$O are given in Table 3, which indicate that the $^5$He emissions play a very important role to reproduce the double-differential measurements fairly well.

Therefore, the $^5$He emissions process should be taken into account properly in the model calculations, in particular for the light nuclei in both equilibrium and pre-equilibrium mechanism.

Meanwhile, being $^5$He unstable, the optical model parameters of $^5$He need to be studied by means of the fitting to the double-differential measurements. The systematic representation of the parameters of optical potential ought to be studied.

**Table 3 Cross sections of $^5$He emission at 14 and 18 MeV for $^9$Be, $^{12}$C, $^{10}$B, $^{11}$B and $^{16}$O in unit mb**

| | 14 MeV | 18 MeV |
|---|---|---|
| $^9$Be | 33.51 | 13.36 |
| $^{10}$B | 24.26 | 39.46 |
| $^{11}$B | 86.41 | 110.88 |
| $^{12}$C | 73.95 | 118.31 |
| $^{16}$O | 26.28 | 36.92 |

The statistic model codes used for interpreting experimental data and for nuclear data evaluation should be improved further by adding the $^5$He emission channel properly. Especially, for the light mass nuclei, besides the 1p-shell elements, $^{19}$F as well as $^{20}$Ne, $^5$He emissions would play an important role.

On the other hand, the threshold energies of $^{6}$He emission from neutron induced reactions have been calculated, which are much higher than that of $^{3}$He, $^{4}$He and $^{5}$He emissions, so the $^{6}$He emission can be ignored at $E_n$ <20 MeV in model calculations.

## References

[1] ZHANG Jingshang, Y. L. Han. and L. G. Cao, Nucl. Sci. Eng. 133 (1999) 218

[2] ZHANG Jingshang, "Improvement of Computation on Nucleon-Induced Helium Gas Production," Proc. Int. Conf. on NuclearData for Science and Technology, Gatinburg, Tennessee, May 9-13 1994, Vol.2 p.932, American Nuclear Society (1994)

[3] ZHANG Jingshang et al., "Improvement of Pickup Mechanism for Composite Particle Emissions," Chin.J. Nucl. Phys., 18, 28 (1996)

# Calculations of Cross Sections and Energy Spectra for Neutron Induced γ-ray of $^{181}$Ta, $^{197}$Au and Natural Ag

LIU Jianfeng WANG Fengge JIA min
*Department of Physics, Zhengzhou University, Zhengzhou, 450052*

【**abstract**】*Using the hypothesis proposed before that in the primary and cascade γ de-excitation processes of the compound nucleus, in addition to the giant dipole resonance model, there exist the de-excitation processes of the excited states of $^{6}$He, $^{6}$Li, $^{6}$Be, $^{7}$Li and $^{7}$Be particle cliques, of which the γ-ray strength function was proposed. The cross sections of the (n,γ) reactions and the energy spectra both for (n,γ) and (n,n′γ) reactions were calculated in the neutron incident energy regions from 0.01 MeV to 5 MeV for natural Ag and $^{181}$Ta, from 0.01 MeV to 10 MeV for $^{197}$Au. The aim is to examine whether this hypothesis can explain the abnormal protuberances near and above 5.5 MeV in the γ spectra of the (n,γ) reactions for the nulei in the mass regions both from 110 to 140 and from 180 to 210 and can be extended to the fair (n,xγ) processes in the same nuclear mass regions. The results agree well with experimental data. Especially the abnormal protuberances near and above 5.5 MeV were improved in the γ energy spectra both for the (n,γ) and (n,n′γ) processes.*

## Introduction

In addition to the practical uses for nuclear energies and other scientific technologies, the γ production data are indispensable for the basic theoretical researches. Because the electromagnetic interaction is well known, the low-exciting state distribution and the high-exciting state wave functions can be studied carefully in terms of the experimental results of the γ production data.

According to the fact[1] that in the nuclear mass regions from 110 to 140 and 180 to 210, there exist abnormal protuberances near and above 5.5 MeV in the γ spectra of the neutron radiative captures, and the locations as well as the strengths of these abnormal protuberances do not change basically at least below 4 MeV of the neutron incident energies. In order to explain this phenomenon quantitatively, references [2] and [3] have supposed that in the primary and cascade γ de-excitation processes of the compound nucleus, there exist the de-excitation processes of the excited states of $^{6}$He, $^{6}$Li, $^{6}$Be, $^{7}$Li and $^{7}$Be particle cliques, and the other de-excitation patterns are still described by means of the giant dipole resonance model. In this way the γ-ray strength function was constructed. The (n,γ) reaction cross sections and the γ spectra were calculated in the neutron incident energy regions from 0.01 MeV to 3 MeV for $^{197}$Au and the results which are in better coincidence with the experiments were obtained. Especially for the γ energy spectra, the abnormal protuberances near and above 5.5 MeV were well reproduced .

As the same with the giant dipole resonance model denoted by GDR model, it is difficult to deduce above hypothesis, denoted by GDR-LPC model, theoretically. The aim of this paper is to test if this hypothesis is available for each nuclide chosen in the nuclear mass regions from 110 to 140 and 180 to 210 and can be extended to the (n,n′γ) reactions. The cross sections of the (n,γ) reactions and the γ spectra both for (n,γ) and (n,n′γ) reactions were calculated in the neutron incident energy regions from 0.01 MeV to 5 MeV for natural Ag and $^{181}$Ta, from 0.01 MeV to 10 MeV for $^{197}$Au. And the comparisons with the experimental values were done. At the same time, some special features of the fast neutron radiative capture cross sections for Au are discussed.

## 1 The Calculation Formulas

The (n,γ) reaction cross sections and the γ spectra both for (n,γ) and (n,n′γ) reactions can be calculated by solving the integral equations that describe the cascade γ de-excitation processes and can be found in reference [2]. As the incident neutron energies are increased and the γ spectra of the (n,n′γ) reactions are also calculated for $^{197}$Au, the calculation formulas of the initial values $\sigma_{i0}$ and $\sigma_{c0}(E,J,\pi)$ are different from that of reference [2].

For the (n,γ) reaction, they are calculated in terms of the following equations:

$$\sigma_{i0} = \sum_f \sigma_{rf} \cdot \frac{S_{dp\,fi}}{S_{dp\,f}} + \sum_{J\pi} \sigma_a^{J\pi} \cdot \frac{T_\gamma^{E_m J\pi, E_i J_i \pi_i}}{T^{E_m J\pi}} \quad (1)$$

$$\sigma_{c0}(E,J,\pi) = \sum_f \sigma_{rf} \cdot \frac{S_{dpfEJ\pi}}{S_{dpf}} \cdot \rho(E,J,\pi) + \sum_{J'\pi'} \sigma_a^{J'\pi'} \cdot \frac{T_\gamma^{E_m J'\pi', EJ\pi}}{T^{E_m J'\pi'}} \cdot \rho(E,J,\pi) \quad (2)$$

Where $S_{dpfi}$ and $S_{dpfEj\pi}$ are the (d,p) reaction spectrum factors of the discrete energy levels and the energy levels of the continues region respectively. $S_{dpf}$ is the (d,p) reaction spectrum factor of one single particle bounded state ($E_f$, $l_f$, $j_f$) and $\sigma_{rf}$ is capture cross section of the direct-semidirect process[4]

$$\sigma_{\gamma f} = \frac{2\pi m e^2 z^2 k_\gamma^2}{3\hbar^2 k^2 A^2} \cdot S_{dpf} \cdot \sum_{ljf} \frac{(2l+1)(2j_f+1)(2J+1)}{2I+1} \cdot \left[C_{l_0 1_0}^{l_f 0} \cdot W(ljl_f j_f; \tfrac{1}{2}1)\right]^2 \cdot \left\{ \left| \int r^2 U_{l_f j_f}(r) \langle U_{lj}^J(r) \rangle \mathrm{d}r \right|^2 + \left| (\alpha - \mathrm{i}\beta) \int r U_{l_f j_f}(r) h(r) \langle U_{lj}^J(r) \rangle \mathrm{d}r \right|^2 + 2\,\mathrm{Re} \cdot \left[ \left( \int r^2 U_{l_f j_f}(r) \langle U_{lj}^J(r) \rangle \mathrm{d}r \right) (\alpha + \mathrm{i}\beta) \left( \int r U_{l_f j_f}(r) h(r) \langle U_{lj}^J(r) \rangle \mathrm{d}r \right) \right] \right\} \quad (3)$$

The definitions of the other symbols can be found in reference [2~4].

For (n,n′γ) reactions:

$$\sigma_{i0} = \sum_{J\pi} \sigma_a^{J\pi} \cdot \frac{T_n^{E_m J\pi, E_i J_i \pi_i}}{T^{E_m J\pi}} \quad (4)$$

$$\sigma_{c0}(E,J,\pi) = \sum_{J'\pi'} \sigma_a^{J'\pi'} \cdot \frac{T_n^{E_m J'\pi', EJ\pi}}{T^{E_m J'\pi'}} \cdot \rho(E,J,\pi) \quad (5)$$

Both for (n,γ) and (n,n′γ) reactions, the γ transmission coefficient can be represented by

$$T_\gamma^{E'J'\pi', EJ\pi} = 2\pi (E' - E)^3 f_\gamma^{E'J'\pi', EJ\pi} \quad (6)$$

and for the sake of the descriptions, the γ-ray strength functions $f_r^{E'J'\pi', EJ\pi}$ are listed as follows:

For GDR model,

$$f_\gamma^{E'J'\pi', EJ\pi} = \frac{1}{6\pi^2 \hbar^2 C^2} \cdot \mathrm{H}(J', J; \pi', \pi) \cdot \sum_{g=1}^{2} \frac{\sigma_g \cdot (E' - E) \cdot \Gamma_g^2}{[E_g^2 - (E' - E)^2]^2 + (E' - E)^2 \Gamma_g^2} \quad (7)$$

For GDR-LPC model,

$$f_\gamma^{E'J'\pi', EJ\pi} = \frac{1}{6\pi^2 \hbar^2 C^2} \cdot \mathrm{H}(J', J; \pi', \pi) \cdot \left\{ \alpha \cdot \sum_{g=1}^{2} \frac{\sigma_g \cdot (E' - E) \cdot \Gamma_g^2}{[E_g^2 - (E' - E)^2]^2 + (E' - E)^2 \Gamma_g^2} + \sum_p \frac{\beta_p \cdot (E' - E)^2 \cdot \Gamma_p^2}{[E_p^2 - (E' - E)^2]^2 + (E' - E)^2 \Gamma_p^2} \right\} \quad (8)$$

## 2 Numerical Calculations

Using the formulas mentioned above, the numerical calculations of the (n,γ) reaction cross sections and γ energy spectra for natural Ag and $^{181}$Ta in the energy region from 0.01 to 5 MeV, for $^{197}$Au in the energy region from 0.01 to 10 MeV, were done. In the calculations the universal optical potential[5] was used to calculate the transmission coefficients and scattering wave functions of the neutrons. Gilbert-Cameron[6] formula was used to calculate the energy level densities. The giant dipole resonance parameters were taken from reference [7]. The excited state energies and decay width of $^6$He, $^6$Li, $^6$Be, $^7$Li and $^7$Be were taken from reference [8]. The discrete energy level data and the γ decay branching ratios were taken from EXFOR.

In the calculations, the optical potential parameters were determined by fitting total, elastic and non-elastic scattering cross sections. Then by adjusting the energy level density parameters of the compound nucleus and α as well as $\beta_p$ in the formula (8) to make the calculated results of the (n,γ) reaction cross sections and the γ energy spectra coincide with the experiments as well as possible. The γ-ray strength function in the formula (7) has also been used to calculate the (n,γ) reaction cross sections and γ energy spectra in order to compare the calculation results obtained by using the two kinds of the γ-ray strength functions.

Table 1 shows the optical potential parameters of the incident neutrons. Table 2 shows the energy level density parameters , the giant dipole resonance parameters and the α values adopted in the calculations both for the GDR model (denoted by I) and the GDR-LPC model (denoted by II). Table 3 shows the experimental values of the excited state energies and the decay widths of $^6$He, $^6$Li, $^6$Be, $^7$Li and $^7$Be as well as the values of $\beta_p$ in formula (8).

Fig. 1 shows the calculation results of the total cross sections and their comparisons with the experimental data taken from EXFOR for the natural Ag. Fig. 2, 3 and 4 show the calculated results of the (n,γ) reaction cross sections and their comparisons with the experimental values taken from EXFOR.

Fig. 5, 6 and 7 show the calculated results of the γ spectra and their comparisons with the experimental data taken from ORNL, where the neutron incident energies are 1.4 MeV, 0.6 MeV and 6.5 MeV for the natural Ag, $^{181}$Ta and $^{197}$Au respectively. It can be seen from Fig. 5, 6 and 7 that the GDR-LPC model is much better than the GDR model for the explanation of the 5.5 MeV abnormal peeks of γ energy spectra. Fig. 7 also shows that for the parts of the energy spectra in which the photon energies are less than or equal to the incident neutron energies, it is mainly coming from (n,n′γ) reactions and the calculation results of the GDR-LPC model are better than GDR model. It also can be seen from Fig. 4 that the GDR-LPC model can obtain better calculated results of the (n,γ) reaction cross sections and that, for $^{197}$Au, it is different from the other heavy nuclei that the direct-semidirect capture cross sections are not much larger than the statistical ones.

# 3 Conclusion

From the calculated results, the following conclusions can be made:

(1) The form of the γ-ray strength function is important for the nuclear reaction statistical theory. This work shows that when the γ-ray strength function is selected reasonably, the statistical theory can completely reproduce the abnormal protuberances near and above 5.5 MeV of the γ spectra.

(2) The hypothesis that in the primary and cascade γ de-excitation processes of the compound nucleus, in addition to the giant dipole resonance model, there exist the de-excitation processes of the excited states of $^{6}$He, $^{6}$Li, $^{6}$Be, $^{7}$Li and $^{7}$Be particle cliques, of which the γ-ray strength function is constructed, i.e., the GDR-LPC model, is available not only for $^{197}$Au but for each nuclide in the nuclear mass regions from 110 to 140 and from 180 to 210 as well.

(3) When the neutron incident energies are larger than 4 MeV, there still exist the abnormal protuberances near and above 5.5 MeV of the γ spectra in the nuclear mass regions mentioned above in the experiments. And it can be explained by extending the GDR-LPC model to (n,n′γ) reactions. In other words, the GDR-LPC model is available for (n,n′γ) cascade γ de-excitation processes.

(4) From the $\alpha$ values in Table 2, it can be seen that the giant dipole resonance takes place in the probability less than 1.0, and in the middle parts of the two mass regions, it is much less than the other parts.

**Table 1 The optical potential parameters of the incident neutrons**

| | $V$/MeV | $r_v$/fm | $a_v$/fm | $w_v$/MeV | $w_D$/MeV | $r_w$/fm | $a_w$/fm | $V_{so}$/fm | $r_{so}$/fm | $a_{so}$/fm |
|---|---|---|---|---|---|---|---|---|---|---|
| $^{107}$Ag | 47.29−0.32E+0.001E$^2$ | 1.25 | 0.71 | −1.56+0.22E | 10.4−0.25E | 1.31 | 0.48 | 8.0 | 1.12 | 0.65 |
| $^{109}$Ag | 47.29−0.32E+0.001E$^2$ | 1.25 | 0.71 | −1.56+0.22E | 10.4−0.25E | 1.31 | 0.48 | 8.0 | 1.12 | 0.65 |
| $^{181}$Ta | 42.85+1.28E−0.006E$^2$ | 1.21 | 0.65 | −1.56+0.22E | 13.74−0.25E | 1.25 | 0.48 | 6.01 | 1.25 | 0.65 |
| $^{197}$Au | 51.23−0.32E+0.001E$^2$ | 1.23 | 0.65 | −1.56+0.22E | 7.20−0.25E | 1.27 | 0.48 | 5.33 | 1.03 | 0.65 |

**Table 2 The energy level density parameters and the giant dipole resonance parameters as well as the α values**

| | | Energy level density parameters | | | | | giant resonance parameters | | | |
|---|---|---|---|---|---|---|---|---|---|---|
| | | $E_x$/MeV | $T$/MeV | $E_0$/MeV | $(P(Z)+P(N))$/MeV | $a$/MeV$^{-1}$ | $\sigma_g$/b | $\Gamma_g$/MeV | $E_g$/MeV | $\alpha$ |
| $^{108}$Ag | I | 3.8901 | 0.6061 | −1.2737 | 0.0 | 16.3679 | 0.3717 | 4.5 | 14.87 | 1.0 |
| | II | 3.8901 | 0.6340 | −1.2737 | 0.0 | 14.9679 | 0.3717 | 4.5 | 14.87 | 0.67 |
| $^{110}$Ag | I | 3.8648 | 0.5890 | −1.3033 | 0.0 | 16.8008 | 0.3775 | 4.5 | 14.82 | 1.0 |
| | II | 3.8648 | 0.6150 | −1.3033 | 0.0 | 15.7408 | 0.3775 | 4.5 | 14.82 | 0.67 |
| $^{181}$Ta | I | 3.3244 | 0.4695 | −0.9900 | 0.0 | 20.4527 | 0.5256 | 4.5 | 13.80 | 1.0 |
| | II | 3.3244 | 0.4695 | −0.9900 | 0.0 | 20.4527 | 0.5256 | 4.5 | 13.80 | 0.39 |
| $^{198}$Ag | I | 4.0876 | 0.6050 | −1.7500 | 0.23 | 18.0000 | 0.5119 | 4.5 | 13.69 | 1.0 |
| | II | 4.0876 | 0.5950 | −1.7500 | 0.23 | 17.9000 | 0.5119 | 4.5 | 13.69 | 0.297 |

**Table 3  The experimental data of $E_p$, $\Gamma_p$ and the values of $\beta_p$**

| | $E_p$/MeV | $\Gamma_p$/MeV | | | $\beta_p$/b | | |
|---|---|---|---|---|---|---|---|
| | | | $^{108}$Ag | $^{110}$Ag | $^{182}$Ta | $^{198}$Au | $^{197}$Au |
| $^{6}$He | 1.80 | 0.113 | 0.0001 | 0.0001 | 0.0001 | 0.0001 | 0.0001 |
| $^{6}$Li | 4.31 | 1.70 | 0.00001 | 0.00001 | 0.00001 | 0.000005 | 0.000055 |
| | 5.37 | 0.54 | 0.0034 | 0.0034 | 0.0019 | 0.0059 | 0.0159 |
| | 5.65 | 1.50 | 0.0109 | 0.0109 | 0.0269 | 0.0209 | 0.1309 |
| $^{6}$Be | 1.67 | 1.16 | 0.0002 | 0.0002 | 0.0002 | 0.0002 | 0.0002 |
| $^{7}$Li | 6.68 | 0.80 | 0.015 | 0.015 | 0.018 | 0.01 | 0.1500 |
| | 7.46 | 0.10 | 0.025 | 0.025 | 0.015 | 0.015 | 0.1900 |
| | 9.85 | 1.80 | 0.01 | 0.01 | 0.01 | 0.01 | 0.1000 |
| $^{7}$Be | 6.73 | 1.20 | 0.02 | 0.02 | 0.02 | 0.015 | 0.1450 |
| | 7.21 | 0.50 | 0.05 | 0.05 | 0.04 | 0.04 | 0.1650 |

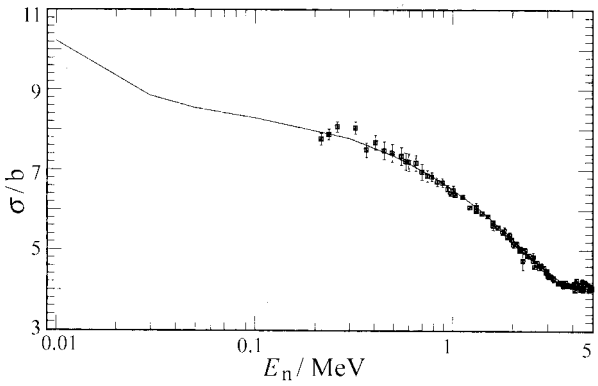


Fig. 1  The total cross sections for natural Ag
(The experimental data are taken from EXFOR)

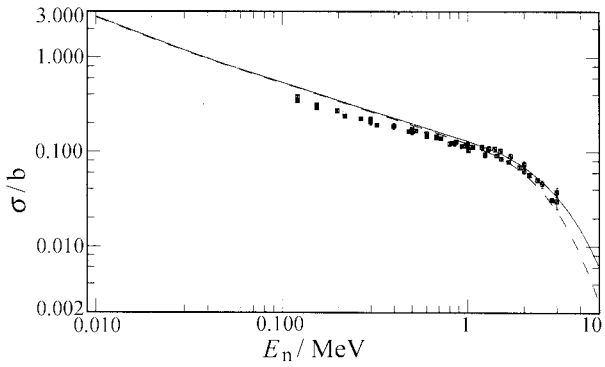


Fig. 3  The same as for Fig. 2 but for $^{181}$Ta

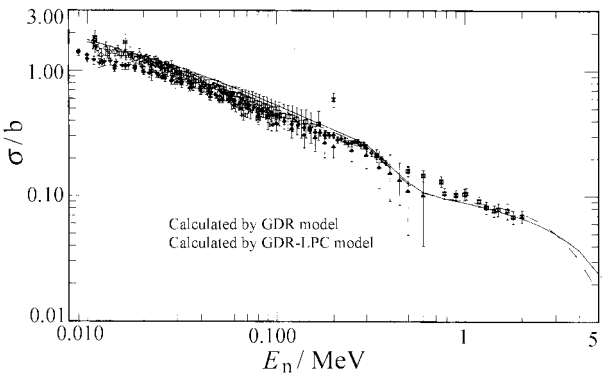


Fig. 2  The (n,γ) reaction cross sections for natural Ag
(The experimental data are taken from EXFOR)

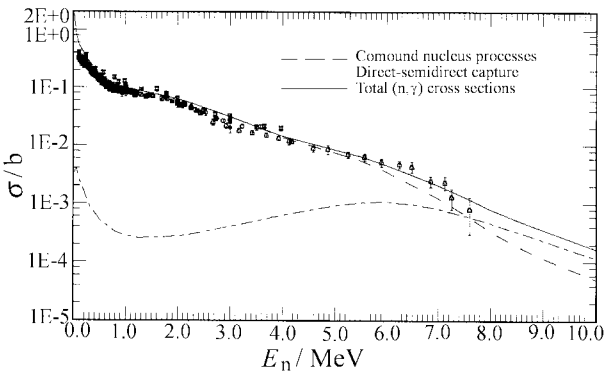


Fig. 4  The (n,γ) reaction cross sections for $^{197}$Au
(The experimental data are taken from EXFOR)

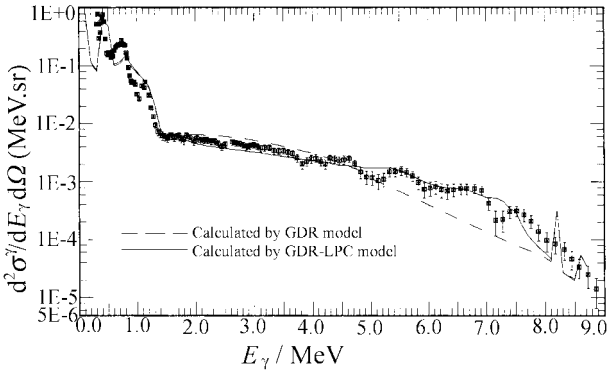


Fig. 5 The γ energy spectrum at $E_n$=1.4 MeV for natural Ag $\theta$=125° (The experimental data are taken from ORNL)

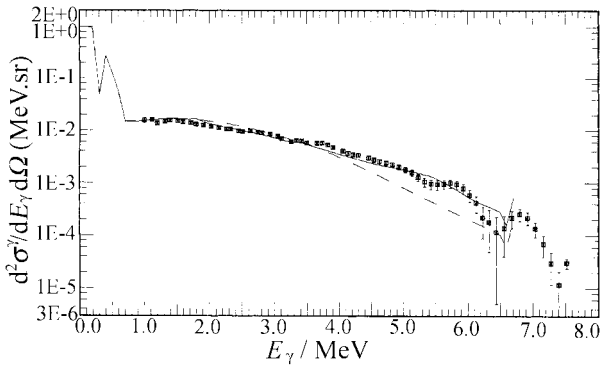


Fig. 6 The same as Fig. 5 but for $^{181}$Ta and $E_n$=0.6 MeV

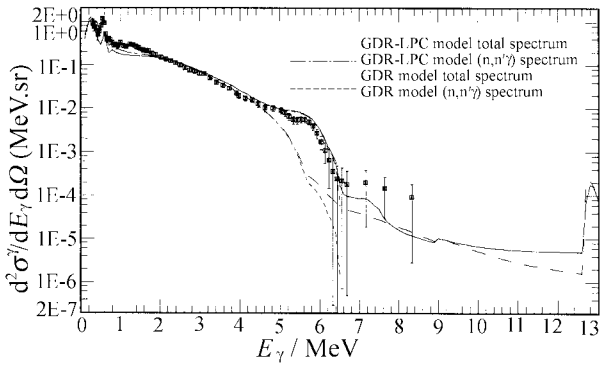


Fig. 7 The γ spectrum at $E_n$=6.5 MeV for $^{197}$Au the $\theta$=125° (The experimental data are taken from ORNL)

## References


[1] DING Dazhao, Progress in Neutron Radiative Capture Stuydy (in Chinese), Nuclear Physics (Material Compilation of the conference in 1978), Atomic Energy Press, 292-306(1979)

[2] LIU Jianfeng et al., CNDP, No.23, 26(2000)

[3] LIU Jianfeng et al., High Energy Phys. and Nucl. Phys. (in Chinese), 10, 994(2001)

[4] LIU Jianfeng et al., Chinese Journal of Nucl. Phys., 2,127(1992)

[5] F. D. Becchetti et al., Phys. Rev., 182,1190(1969)

[6] A. Gilbert, A. G. W. Cameron, Can. J. Phys., 43, 1446(1965)

[7] S. S. Dietrich et al., Atomic Data and Nuclear Data Tables, 38,199(1988).

[8] F. Ajzenberg-selove, Nucl. Phys., A413,1(1984)

# Evaluation of Neutron Reaction Data for $^{Nat, 28, 29, 30}Si$

TANG Guoyou SHI Zhaomin ZHANG Guohui ZHANG Songbai

*Institute of Heavy Ion physics, Peking University, Beijing 100871,China*

**【abstract】** *There are three isotopes for natural silicon,$^{28}Si$,$^{29}Si$ and $^{30}Si$, and their abundance are 92.23% ,4.67% and 3.1%, respectively. The data of each isotope were evaluated.*

## 1 $^{28}Si$

There are a lot of experimental data since the 50's, including $\sigma_{tot}$, $\sigma_{(n,inl)}$, $\sigma_{(n,p)}$, $\sigma_{(n,\alpha)}$, angular distribution for elastic scattering, double differential cross section for (n,nx) reactions. There are also a few experimental data for $\sigma_{(n,n)}$ and $\sigma_{(n,non)}$. Some of the data, especially total cross section, show evident structure.

### 1.1 Theoretic Calculation

1) Adjustment of the optical model parameters for neutron

The optical model parameters are the base of the theoretic calculation. Dr. GE Zhigang from CNDC adjusted neutron optical model parameters by using the APOM code. The experimental data used for the adjustment include the total cross section $\sigma_{tot}$, non-elastic cross sections $\sigma_{(n,non)}$, and elastic angular distributions $\sigma_{n,n}(\theta)$. After fitting the experimental data, there still exist some structure for total cross section. The fitted data were used in adjusting the optical model parameters. There are ten sets of data for elastic angular distribution in the energy range of $E_n$=1~20MeV. There exist experimental data for non-elastic cross section only at 14.0 MeV neutron energy. So we have to get the data in $E_n$=5~8 MeV region by summing up the experimental data of the (n,p), (n,α) and (n,inl) reactions. After the adjustment of the optical parameters, the calculated result of total cross section and non-elastic cross section are plotted in Fig.1. The comparison of the calculated elastic angular distributions and the experimental ones are plotted in Fig.2 (a) to (d).

2) Calculation of the direct inelastic interaction

The direct reaction of the discrete levels were calculated by Prof. WANG Shunuan from CNDC using the ECIS code. Only the first and the second excited states ($E_l$=1.78, 4.62 MeV) were calculated.

3) Calculation of the data for every reaction channels

We used the UNF code (2002-editor) for calculation. The parameters were adjusted to make the calculated data reproduce the experimental data as well as possible. The experimental data include the data of (n,inl), (n,p), (n,α) reactions, and the neutron emission double differential cross section. The main parameters used are given in Table 1 and 2. The exciton model parameter $K$=200 MeV$^3$

The calculated results for (n,inl), (n,p), (n,α) reactions are showed in Fig. 3 (a),(b),(c) and (d).

### 1.2 Evaluation and Recommendation

The cross section of the main reaction channels such as $^{28}$Si(n,tot), $^{28}$Si(n,inl), $^{28}$Si(n,p), and $^{28}$Si(n,α) have complicated structures. Optical model and UNF calculation can not reproduce them. So we have to recommend the data according to the experimental ones.

**Total cross section**: This cross section has complicated structure, especially in the energy range below 10 MeV, there are obvious resonance structures. We utilized the two sets of data[1,2] measured by GEL laboratory in 1978 with LINAC white spectrum neutron source. To reduce amount of data, we fitted the experimental data, keeping the structures as complete as possible, then more than 300 data points were taken.

**(n,p) Reaction**: In the energy range above 12 MeV, the theoretical results are in good agreement with the data newly measured[3~6] in 1999 and 2000. But in the energy range below 9 MeV, the calculated results can't reproduce the structure of the experimental data[7~9]. So, the fitted experimental data were recommended data from the threshold to 9 MeV, while above 9 MeV the theoretical data were adopted.

**(n,α) Reaction**: This reaction is similar to the (n,p) reaction . From the threshold to 9 MeV, the fitted experimental data [10,11] are recommended, while above 9 MeV, the theoretical data were adopted.

**(n,inl) Reaction**: There are structures for total inelastic cross sections below 6 MeV. The inelastic cross sections to excited state $E_l$=1.78 MeV shows the same structure as total inelastic cross section below 6 MeV, which means the total inelastic cross section's structures come from the excited state $E_l$=1.78 MeV. The theoretical calculation could not reproduce these structures. So for inelastic cross section to $E_l$=1.78 excited state, from threshold to 6 MeV, the data of the measurements[12~14] were fitted and recommended. In other energy range, the calculated data, which are in agreement with the measurements[15~18], were recommended. The total inelastic cross section were given by adding the cross sections of above first excited state and other excited states calculated by the theoretical calculation.

**(n,2n) Reaction**: There is a unique set of data[20], which were recommended.

**(n,γ), (n,np) and (n,nα) Reactions**: There is no measured data, so the theoretical results were recommended.

For the resonance region, the JENDL-3.2 data were adopted. Other files (4,6,12,14,15) were taken from theoretical calculations.

## 2 $^{29}$Si

Because of the valuables and difficulty of the target preparation, there are no experimental data of total, elastic scattering and non-elastic cross sections. The data were calculated by using the same optical parameters as $^{28}$Si. The direct inelastic scattering data were calculated with the ECIS code for three states, $E_l$=2.462, 4.741, 5.2855 MeV. Using a few $^{29}$Si(n,p) experimental data, some parameters for UNF code were adjusted. The exciton model parameter $K$ is 200 MeV$^3$. The energy level density and pair correction parameters are given in Table 3.

In Fig.4, the calculated results for (n,p) cross section are given compared with experimental data.

**Table 1 $^{28}$Si optical parameters for neutron**

| | | | | | | | | | |
|---|---|---|---|---|---|---|---|---|---|
| AR | 0.4051 | AS | 0.5769 | AVV | 0.7000 | AS0 | 0.4051 | XR | 1.1939 |
| XS | 1.3371 | XV | 1.1100 | XS0 | 1.1939 | XC | 1.2500 | U0 | 0.0000 |
| U1 | 0.0200 | U2 | 0.0003 | V0 | 48.0000 | V1 | -0.0516 | V2 | 0.0597 |
| V3 | -24.0000 | V4 | 0.0000 | VS0 | 6.2000 | W0 | 7.5812 | W1 | 0.1589 |
| W2 | -12.0000 | | | | | | | | |

**Table 2 Level density and pair correction parameter *a*, *Δ* for $^{28}$Si**

| reaction | n,γ | n,n | n,p | n,α | n,$^3$He | n,d | n,t | n,2n | n,nα | n,2p | n,3n |
|---|---|---|---|---|---|---|---|---|---|---|---|
| *a* | 3.388 | 2.3215 | 3.3784 | 3.3825 | 3.900 | 6.94 | 3.539 | 5.9181 | 5.39668 | 4.39105 | 3.958 |
| *Δ* | 2.090 | 1.100 | 0.000 | 1.000 | 1.150 | 1.080 | 0.000 | 0.390 | 0.0670 | 0.000 | 1.760 |

**Table 3 The level density and pair correction parameters *a*, *Δ* for $^{29}$Si**

| reaction | n,γ | n,n | n,p | n,α | n,$^3$He | n,d | n,t | n,2n | n,nα | n,2p | n,3n |
|---|---|---|---|---|---|---|---|---|---|---|---|
| *a* | 3.671 | 3.45088 | 4.080 | 3.20900 | 4.105 | 3.784 | 3.594 | 2.30215 | 3.825 | 4.412 | 3.181 |
| *Δ* | 1.760 | 1.090 | 1.170 | 1.800 | 2.000 | 0.000 | 2.800 | 2.890 | 2.000 | 1.670 | 2.090 |

The resonance parameters for the resonance region were taken from JENDL-3.2 library. Above the resonance region, all cross sections and other files (4, 6, 12, 14, 15) were taken from the UNF calculation.

## 3 $^{30}$Si

There is no experimental data. The complete set of data was theoretically calculated by using the same optical parameters as $^{28}$Si. The direct inelastic scattering data for state $E_l$=2.23535 MeV were calculated by using the ECIS code. Most of the parameters used in the UNF calculation were taken from the RIPL parameter library. The exciton model parameter $K$ is 600 MeV$^3$. The energy level density and pair correction parameters are given in Table 4.

Since there is no experimental data for this isotope, the data calculated with UNF were adopted in the energy region above the resonance region. The data in resonance region were taken from JENDL-3.2.

# 4 Natural Si

The data of $^{Nat}$Si are mainly dominated by that of $^{28}$Si, since its abundance is 92.23%. Above resonance region ($E_n$>1.81 MeV), the cross section of all reactions were derived from summing the cross sections of $^{28}$Si, $^{29}$Si and $^{30}$Si with their abundances as weight. Codes for summing up are CABEI[21], developed by Prof. LIU Tingjin et al. from CNDC.

The resonance parameters for the resonance region were taken from JENDL-3.2.

Other files (4, 6, 12, 14, 15) were calculated with code UNF using the adjusted parameters for $^{28}$Si,$^{29}$Si and $^{30}$Si isotopes.

The authors thank Profs. ZHANG Jingshang, WANG Shunuan and LIU Tingjin and Dr. GE Zhigang, for their helps with this work.

**Table 4 The energy level and pair correction parameters *a*, *Δ* for $^{30}$Si**

| reaction | n,γ | n,n | n,p | n,α | n,$^3$He | n,d | n,t | n,2n | n,nα | n,2p | n,3n |
|---|---|---|---|---|---|---|---|---|---|---|---|
| *a* | 4.075 | 4.671 | 4.0492 | 5.7505 | 4.412 | 4.080 | 3.784 | 3.388 | 3.900 | 4.833 | 3.215 |
| *Δ* | 2.090 | 1.760 | -0.5000 | 1.000 | 1.170 | 1.170 | 0.000 | 2.090\ | 1.800 | 2.000 | 1.890 |

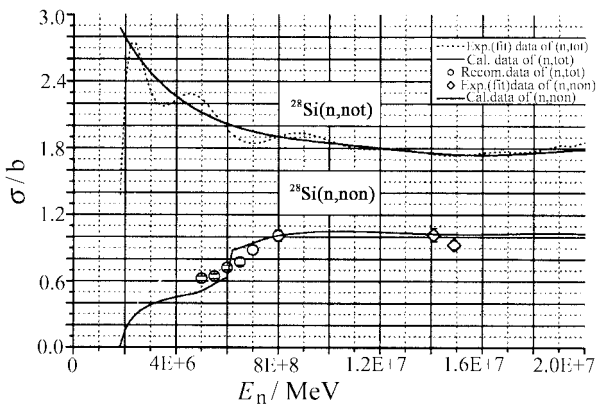


Fig. 1 Total cross sections and the non-elastic cross sections

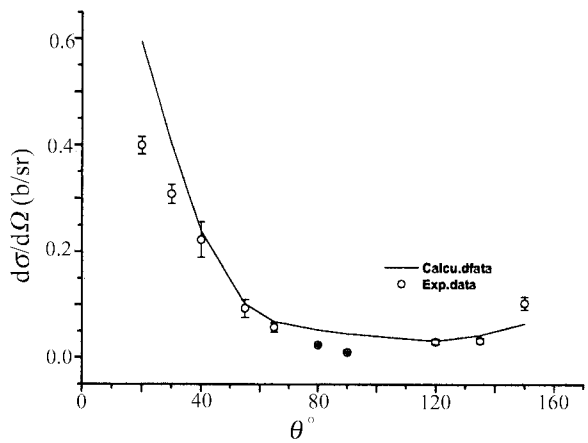


Fig. 2 (b) Angular distribution of $^{28}$Si(n,n) at 6.0 MeV

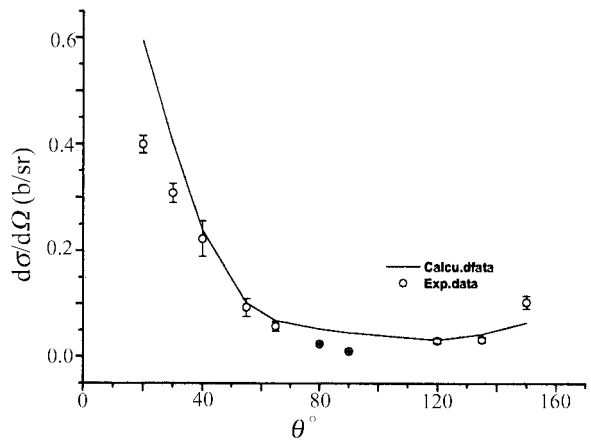


Fig. 2 (a) Angular distribution of $^{28}$Si(n,n) at 5.0 MeV

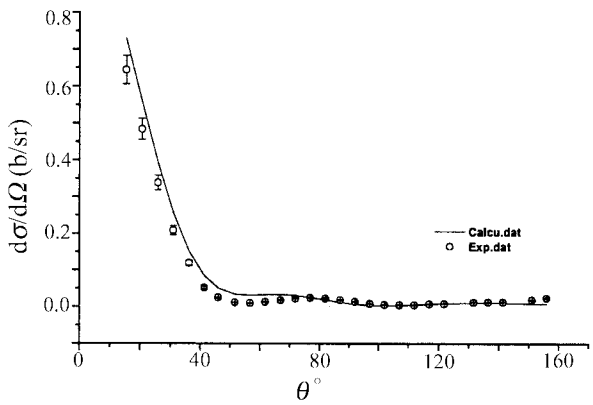


Fig. 2 (c) Angular distribution of $^{28}$Si(n,n) at 10.0 MeV

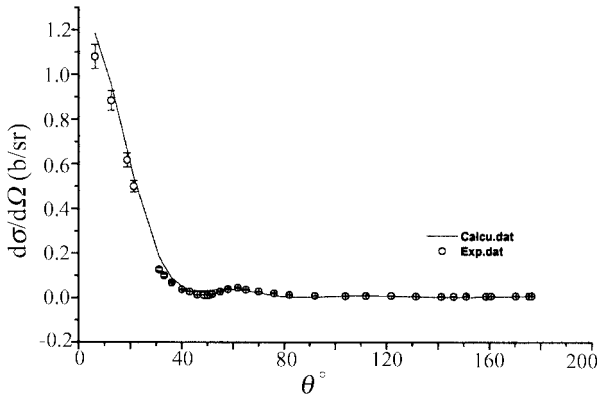


Fig. 2 (d) Angular distribution of $^{28}$Si(n,n) at 14.0 MeV
Fig.2 Elastic angular distributions

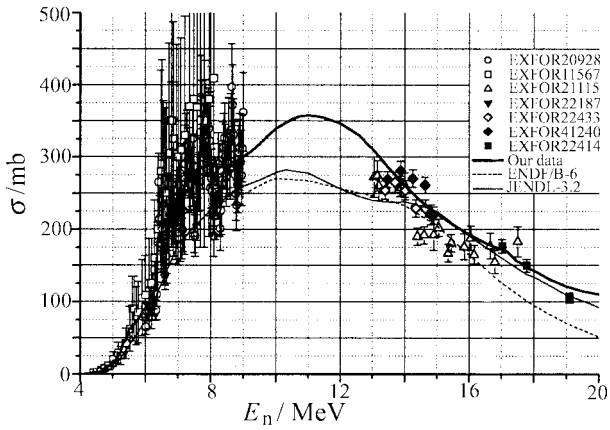


Fig. 3 (a) $^{28}$Si(n,p) cross section

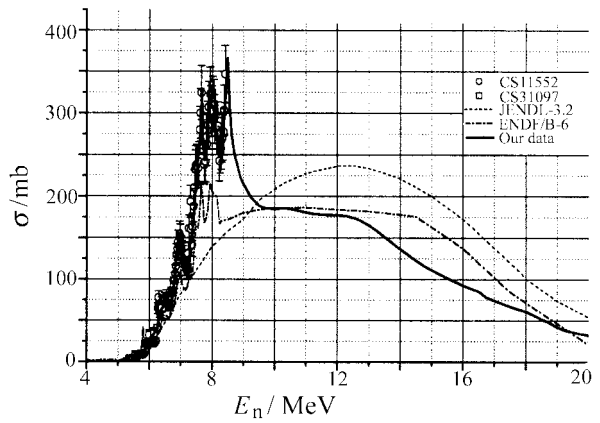


Fig. 3 (b) $^{28}$Si(n,α) cross section

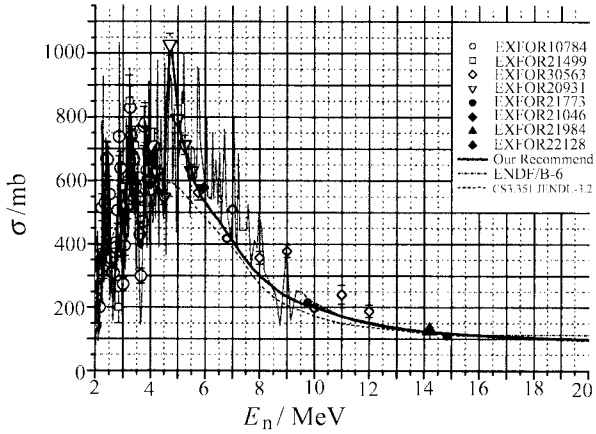


Fig. 3 (c) $^{28}$Si(n,inl) cross section for $E_1$=1.78 MeV

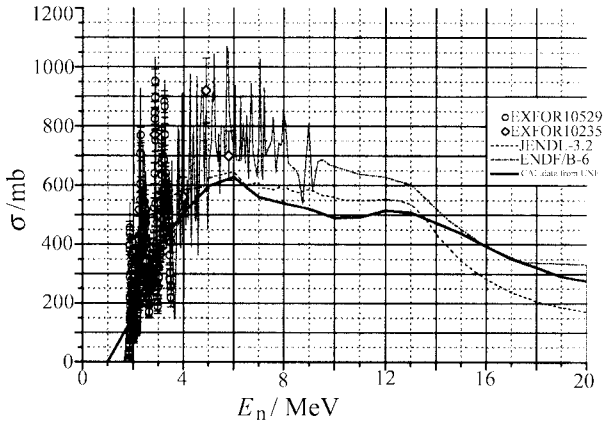


Fig.3 (d) $^{28}$Si(n,inl) total cross section
Fig. 3 The comparison betweene UNF calculation and experimental data

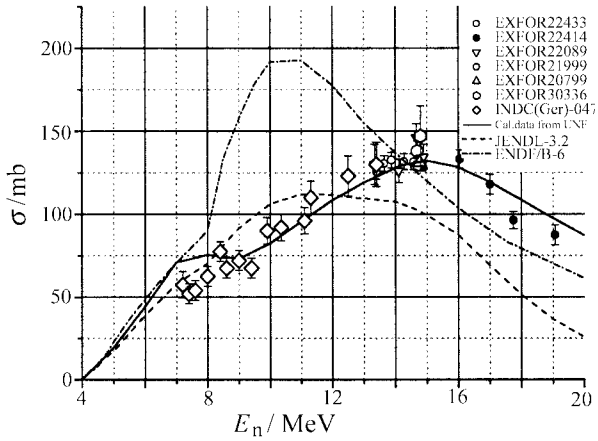


Fig. 4 The comparison of theoretical calculation with the experimental data for $^{29}$Si(n,p) reaction

## References


[1] R.Koehler, et al. J.PR/C ,35,1946,(1987)

[2] H.Weigmann et al. J.PR/C ,36,585(1987)

[3] Y.Kasugai et al. J.ANE, 25(1-3),23(1998)

[4] K.Kawade et al. R.JAERI-M-90-171(1990)

[5] A.Filatenkov et al. R.RI-252(1999)

[6] A.Fessler et al. J.NSE,134(2),171(2000)

[7] R.Bass et al. R.EANDC(E)-66,64(1966)
[8] J.B.Marion et al. J.PR,101,247(1956)
[9] A.V.Cohen et al. J.NP,1,73(1956)
[10] R.Mainsbridge et al. J.NP,49,83(1963)
[11] J.A.Shannon, et al. J.NIM,41,255(1966)
[12] N.B.Sullvan et al. J.NSE,70,294(1979)
[13] U.Fasoli et al. R.INFNIBE-65,6(1965)
[14] H.H.Knitter et al. J.ZP,207,56,(1967)
[15] A.Virdis et al. R.CEA-R-5144(1981)
[16] J.Martin et al. J.NP/A,113,564(1968)
[17] W.Chiba et al. C.85SANTA,1,223(1985)
[18] W.Pilz et al. J.NP/A 460,265(1986)
[19] G.Boerker et al. C.88Mito,193(1988)
[20] D.Aronold. et al. J.DA.26,3425(1965)
[21] LIU Tingjin et al. CNDP, 20, 110(1998)

# The Evaluation of the Mass Distribution Data for $^{238}$U, $^{239}$Pu and $^{242}$Pu Fission

LIU Tingjin

*China Nuclear Data Center, CIAE, Beijing 102413, China tjliu@iris.ciae.ac.cn*

【**abstract**】 *The mass distribution data for $^{238}$U at $E_n$=1.5, 5.5, 8.3, 11.3 14.9, 22.0, 27.5 ,50.0 ,99.5, 160.0 MeV, $E_p$=20.0, 60.0 MeV and $^{242}$Pu at $E_n$=15.1 MeV were evaluated and recommended based on the main available experimental data up to now. The experimental data were make necessary corrections and their errors were also made necessary adjustments. The problems concerned were discussed.*

## Introduction

The mass distribution data are very important for both practical application and physical investigation of fission mechanism, especially for the developing systematics of the fission product yield. As well known that the dependence of fission product yield on incident particle energy is still an open problem in terms of both microscopic theory and experimental measurement. The existing data can be used as base for both microscopic and systematics research.

There are some definitions concerning the “mass distribution”. “Cumulative yield” is the total number of the nuclide produced over all time after one fission, including produced in the fission and decayed from its precursor. “Chain yield” is the total of the independent yields of all products for a given mass chain (if there is no shielding nuclide). “Mass yield” is the total number of all nuclides in a given mass chain produced in one fission. If a product nuclide is stable, its cumulative yield is equal to the chain yield of the mass chain, where it is in. When a product nuclide is radioactive with very long half-life, its cumulative is approximately equal to the chain yield of it mass chain. The difference between chain yield and mass yield for a mass chain is after delayed neutron emission for the former and is before delayed neutron emission for the latter. Also the measured data by recording prompt fragment are concerning a concept “pre” and “post” neutron emission, in this case, it means prompt neutron emission, including from compound nucleus and fragments by evaporation of neutrons prior to and after scission.

In this paper, the mass distribution data for $^{238}$U at $E_n$=1.5, 5.5, 8.3,11.3, 14.9, 22.0, 27.5, 50.0, 99.5, 160.0 MeV, $E_p$=20.0, 60.0 MeV, $^{239}$Pu at $E_n$=0.17, 7.9, 14.5 MeV and $^{242}$Pu at $E_n$=15.1 MeV were evaluated and recommended on the basis of the main available experimental data up to now.

## 1 Data Collection and Selection

The experimental data were collected from EXFOR Library as well as some recent publications.

As mentioned above, the mass distribution data may refer to the data of “chain yield”, “cumulative yield” and “fragment mass yield”. At the beginning, as the data collection, all these kinds of data, even “pre fission yield” data, were collected. More than 200 subentries were retrieved from the EXFOR Master Library.

The valuable data were received from private communication, which were not compiled into EXFOR library or published, including the data of F.Vives, C.M.Zoller, J.H. Hamilton and I.Winkelman for $^{238}$U and $^{242}$Pu respectively.

Also some valuable data, which were not compiled into the EXFOR Library, were collected from the publications, including LIU Conggui’s and LIU Yonghui’s data in CIAE, the latter were just measured and published in INDC(CRP-056/L) in December of 2001.

The collected data were selected according to the following principles:

**a.** As the data are for “mass distribution”, the data were taken in first priority, for which there are enough nuclides, whose yields were measured. Only in the case that there are no this kind of data, the data including less nuclides have to be taken.

**b.** According to the definition, only the "chain yield" or "mass yield" data can be used. But if there are no these kinds of data, the "cumulative yield" data were also taken. In this case, only the data in the data table, whose differences with the corresponding chain yields are smaller than the experimental data error bar, were used, namely in the case that the cumulative yield is equal to the corresponding chain yield within error bar.

**c.** The data measured later and with reliable method were taken with high priority. If there are more data available, the data measured in earlier years and with outmoded method were abandoned.

**d.** In the case that there are no enough data available, some data marked by "pre, FY" in EXFOR library were also taken at beginning, and then they were decided if they were used in the evaluation process through analyzing the data and comparing them with others.

## 2 Data Analysis and Evaluation

According to the principles mentioned above, the following data were taken at last. Some information about them, evaluation and processing of them are as follows.

1) **F.Vives et al**[1] The pre-neutron emission mass, kinetic energy and fission fragment angular distributions were measured with a double Frisch-gridded ionization chamber. The $^{238}$U samples were mounted in the center of the common cathode. The information about the fission fragment properties was obtained from anode and the sum of the anode and grid signals of the ionization chamber. The kinetic energy of the fission fragments was obtained from the anode signal, whereas the emission angle was provided by the sum signal. The mass resolution of the chamber was about 2 mass units. The mono-energy neutrons were produced by Van de Graaff Accelerator in the energy range from 1.2 to 5.8 MeV through different neutron source reactions. The prompt neutron emission was corrected to get the pre-emission mass distribution data.

The measurements were completed simultaneously for all nuclides in the measured mass range, so more complete nuclides were included and there is no systematical error among the data of different product nuclides, the main error is statistical one. Due to the mass resolution, the measured yield for a mass number is not exact one, but its Gaussian extension with the corresponding width 2 mass units. So the measured mass distribution is also not exact one, but a summation over all Gaussian extensions of each mass number.

There is no data given in the paper. The data were provided by Dr. M. Duijvestijn[2]. The pre neutron emission fragment mass distribution data at $E_n$=1.6, 5.5 MeV were used. The data were renormalized to 200% (originally, they were normalized to 100%). There are no errors given by author, they were assigned based on the method and the estimation from the figure in the paper (Fig. 9) as 2% for the yields larger than and equal to 4%, 6% for the yields less than 4% and larger than and equal to 1%, and 8% for the yields less than 1%.

2) **C.M.Zoller**[3] The measurements were performed with LANL spallation neutron source WNR fed by 800 MeV protons from the LAMPF accelerator. The fragments were identified by a double energy measurement, using 38 silicon PIN diodes assembled to two detector arrays of 171cm$^2$ area each. The corrections were made for detector pulse-height defect, energy losses in target material and backing, and for linear momentum transferred to the compound nucleus. The corrections were also made to consider the average mass losses of both the compound nucleus and the fragments by evaporation of neutrons prior to and after scission to get pre-neutron emission mass distributions. The mass resolutions are 3.5 mass units at neutron energy 13 MeV and 4 mass units at neutron energy 22 MeV. The fragment mass and kinetic energy distributions for $^{238}$U were measured in the energy range from 2.0 to 450 MeV.

This is the same kind of measurement and has the same advantage and disadvantage as F.Vives. In addition, this measurement was performed with white neutron source, the data were averaged over the given energy bins with the corresponding neutron spectra in the bins as weight.

The fragment mass distribution of pre and post neutron emission data were taken at neutron energy 13(11.5~14.5), 20(18~22), 27.5(22~33), 50(45~55), 99.5(89~110), 160(145~175) MeV. The data were provided by Dr. M.Duijvestijn[2]. To compare, the data at neutron energy 5.0(4.5~6.5) were also used, take from Zoller's thesis[3].

3) **S.Nagy**[4] The chain yields of 44 mass chains were determined with Ge(Li) γ-spectrometry and radiochemical separation of the fission products followed by β counting and/or γ-spectrometry. The data were measured absolutely by recording the fission rates and normalized to 200%. The mono-energy neutrons at 1.5, 2.0, 3.9, 5.5, 6.9, and 7.7 MeV were produced through $^7$Li(p,n) and D(d,n) reactions with ANL Fast Neutron Generator.

This one and the measurements hereafter (except for J.H.Hamilton[11]) are another different kind of method from above. The radioactivity of the fission products was measured one by one at sometime after

the fissile nucleus was irradiated. So the yields measured are not prompt ones, but "delayed" ones, not only the prompt neutrons were emitted, but also the radioactive products decayed. The yields become "cumulative" (although they can be corrected to the "zero" time). There is no mass resolution problem for this kind of measurement. Due to the measurements are performed one by one, there are possibly systematical errors among the different nuclide yields, and in general, the product nuclides can not be measured as complete as "prompt fragment" method as described above.

The data at neutron energy 1.5 and 5.5 MeV were used. The yield of mass number 107 at $E_n$=1.5 MeV was abandoned due to it is too small and not consistent with others.

4) **T.C.Chapman**[5] The cumulative yields were measured with radiochemistry separation followed by β counting and Ge(Li) γ-spectrometry at neutron energy 6.0, 7.1, 8.1, 9.1 MeV for $^{235,238}$U fission. The neutrons were produced through D(d,n) reaction with Van de Graaff Accelerator.

The data at $E_n$=8.1 MeV were used. Due to the measured yields were cumulative ones, the data of 7 product nuclides, whose difference with the corresponding chain yields are larger than the experimental error bar, were abandoned. Also the data for mass 137, 142 were abandoned for there is something wrong with the data (for the former) and the error is too larger (for the latter).

5) **LI Ze**[6,7] The chain yields of more than 30 product nuclides for $^{238}$U fission were measured with HPGe γ spectrometry and/or radiochemical method (followed by β or γ counting) absolutely by recording fission rates. The measurements were performed at neutron energy 8.3 and 11.3 MeV at CIAE Cyclotron and Tandem Accelerator, respectively. The corrections were made for the recorded γ spectra and for the difference between the measured cumulative yield and corresponding chain yield.

The two sets of data were all used. The yields at 11.3 MeV were taken from the paper[7] and the average with weight was made for 5 yields, which were measured by using both methods at the same time.

6) **LIU Conggui**[8] The mass distribution for 14.9 MeV neutron-induced fission of $^{238}$U was measured by using Ge(Li) γ spectrum method. The fission rate was absolutely measured by double ionization chamber. 39 chain yields and 1 cumulative yield were determined in the mass region *A* from 84 to 151. Among them, 13 yields were measured relatively to the yields of $^{132}$Te or $^{140}$Ba. A fine structure was observed in the vicinity of the mass number 134.

The data were used and taken from the paper. The yield for product nuclide $^{130}$Sb is cumulative one and is not equal to the corresponding chain yield, so it was abandoned.

7) **S.Daroczy**[9] The cumulative yield were measured by using Ge(Li) γ spectrometry at neutron energy 14.5 MeV relatively to $^{27}$Al(n,α) and $^{62}$Cu(n,2n) reactions. The three sets of data measured separately were given respectively and were averaged with weight. To deduce chain yield, the averaged data were corrected by using charge distribution data and branching ratios for the formation of the measured nuclides from β decay of their precursors. The obtained chain yield data were used.

8) **LIU Yonghui**[10] The chain yields of 32 mass chain were determined for the $^{238}$U fission induced by 22 MeV mono-energy neutrons, produced through T(d,n) reaction with CIAE HI-13 Tandem. The product activities were measured with HPGeγ spectrometry without radio-chemical separation. Absolute fission rate was monitored with a double-fission chamber. The data at this neutron energy were measured firstly.

The data were used, but the yield of mass number *A*=128 was abandoned due to it's too large error (checked with the author).

9) **J.H.Hamilton**[11] The pre-neutron emission fragment mass distribution from $^{238}$U fission induced by proton at $E_p$=20.0, 60.0 MeV were measured by recording prompt fragment method. The mass resolution of recording fragments is about 4 mass units. The main error is statistical one, but was not given by the author. The relative errors were assigned as 1% for the yields larger than and equal to 4%, 3% for the yields lager than and equal to 1% and less than 4%, 5% for the yields less than 1%. The data were provided by Dr. M.C.Duijvestijn[2] and were used.

10) **J.E.Gindler**[12] The cumulative yields for $^{239}$Pu fission were measured absolutely by using Ge(Li) γ spectrometry and radio-chemistry separation followed by β counting with proportional counter at the neutron energies 0.17, 1.0, 2.0, 3.4, 4.5, 6.1, 7.9 MeV. The neutrons were produced with ANL Fast Neutron Generator through $^{7}$Li(p,n) reaction for neutron energy less than 5 MeV and D(d,n) reaction for $E_n$ larger than 5 MeV. The nuclides measured are not so many, but the data are only ones available in this energy range.

The data at neutron energy $E_n$=0.17, 7.9 MeV were used. Only the yields, whose differences with the corresponding chain yields were smaller than experimental error bar, were taken. As a result, the yields of 4 nuclides at $E_n$=0.17 MeV and 3 at $E_n$=7.9 MeV were abandoned. Also the data table was processed technically.

11) **G.P.Ford**[13] The cumulative yields for $^{239}$Pu fission were measured with radiochemistry method relatively. The $^{99}$Mo cumulative yield of $^{239}$Pu fission or corresponding cumulative yield from $^{235}$U fission was used as monitors. The 14 MeV neutrons were produced through T(d,n) reaction with Cockcroft-Walton Accelerator.

There are two sets of data measured by same method and at same neutron energy but for the different product nuclides in the same paper[13] and in different EXFOR entries. Two sets of data were combined together, and the data were arithmetically averaged, if there are yield data for same product nuclide ($^{111}$Ag) in both sets of data. There are no errors given by author. Considering the data measured by radiochemistry method and in the earlier year, also taking into account of the error given by author for R value, the relative errors were assigned as 10% for all product nuclides. Also the data tables were processed technically.

12) **J.Laurec**[14] The cumulative yields from $^{233,235,238}$U and $^{239}$Pu fission induced by fission spectrum and 14.7 MeV neutrons were measured by radiochemistry method. The γ spectra were measured by Ge(Li) spectrometry and fission numbers were determined with plane ionization chamber.

The data for $^{239}$Pu fission at 14.9 MeV were taken. Although the measured yields are cumulative ones, the differences between the yields of the measured nuclides and the corresponding stable nuclides are all within the experimental error bar, so all data were used except for nuclide $^{136}$Xe, whose yield is too small, possibly there is something wrong with it.

13) **I.Winkelmann**[15] The cumulative yields from the $^{242}$Pu fission induced by 15.1 MeV neutrons were measured for 65 fission product nuclides from $^{85}$Kr to $^{151}$Pm. The fission product activities were measured by Ge(Li) γ spectrometry and chemical separation of the fission product elements Pd, Ag, Cd, Sn, Sb and Ce followed by β counting or γ spectrometry. The chain yields of 43 mass chains were obtained by dividing the measured cumulative yields by a correction factor, which is a ratio of cumulative yield of the measured product nuclide to the corresponding chain yield.

The data were used after following processing:

**a.** Some chain yields were obtained from 2 or more than 2 cumulative yields. In this case, they were averaged with weight to get the recommended chain yield.

**b.** The data of product nuclides $^{126g}$Sb, $^{111m}$Pm were abandoned. It is an independent yield for the former, and is partial isomeric yield for the latter.

**c.** The data of product nuclides $^{130g}$Sb, $^{131}$Sb, $^{131m}$Te were also abandoned. The chain yields obtained from the cumulative yields of these nuclides are too small. The fractions of the measured cumulative yields to the corresponding chain yields are too small, which could introduce large error into the obtained chain yields. In addition, there are large differences for the correction factors of these nuclides between the values given in the paper and calculated by us with the data from ENDF/B-6.

# 3 Results, Recommendation and Discussion

Based on the selected data of the collected experimental data available, and after their evaluation and processing as described above, the following evaluated mass distribution data for $^{238}$U, $^{239, 242}$Pu fission are recommended as given in Table 1.

The recommended data are shown in Figs.1~4 for $^{238}$U fission induced by neutron, proton and $^{239,242}$Pu fission induced by neutron respectively.

As mentioned above that the data were measured by two kinds of measurement method for the mass distributions. One is the data measured by recording prompt fission fragments (data type 1 in Table 1) with double Frisch-gridded ionization chamber, silicon PIN diode detector arrays etc, as reported by Vives[1], Zoller[3] and Hamilton[11]. Another is the data measured by recording the radioactivity of fission product nuclides (data type 2 in Table 1) with Ge(Li), HPGe γ spectrometry and radio-chemistry method, as reported by Nagy[4], Chapman[5], LI Ze[6], LIU Conggui[8], Daroczy[9], LIU Yonghui[10], Gindler[12], Ford[13], Laurec[14], Winkelmann[15]. In general, the data measured by different laboratories but with the same kind of method, like data type 2, are in good agreement within the experimental error, as shown in Figs. 5, 6 for the data type 2. But there is systematical error between the two types of data (see Fig. 6). The reason is in physics and the measurement techniques.

The essential difference of the two kinds of measurements is the time (days, hours, seconds etc.) delayed for data type 2, so the radioactive products decay (although which can be corrected to a certain time), and is “prompt” for the data type 1. Even though for the data type 1, the fragments measured are still ones after “prompt neutron emission”, so called post neutron emission, while to get the fragments before the prompt emission, so called pre neutron emission, must make necessary correction, which was described in the Vives's[1] and Zoller's[3] papers. So in the data file, the “post” and “pre” mean the prompt neutron for the data type 1. In Fig.7 is shown the difference between these two kinds of yields. Regards as the data type 2, the data are all ones of not only “post neutron emission” but also “delayed neutron emission”. As well know that in

**Table 1 Recommended mass distribution data**

| Fissile nuclide | Energy point / MeV | Data(author) | Ref. | Data type |
|---|---|---|---|---|
| $^{238}$U | $E_n$ around 1.5 | Vives(1.6), Nagy(1.5) | 1, 4 | 1, 2 |
| | $E_n$ at 5.5 | Vives, Nagy | 1, 4 | 1, 2 |
| | $E_n$ around 8.2 | LI Ze(8.3), Chapman(8.1) | 6, 5 | 2 |
| | $E_n$ around 11.3 | LI Ze(11.3), Zoller(11.5~14.5) | 7, 3 | 2, 1 |
| | $E_n$ around 14.5 | LIU Conggui(14.9), Daroczy (14.5) Zoller(11.5~14.5) | 8, 9, 3 | 2, 1 |
| | $E_n$ around 22.0 | LIU Yonghui(22), Zoller(18~22) | 10, 3 | 2, 1 |
| | $E_n$ around 27.5 | Zoller(22~33) | 3 | 1 |
| | $E_n$ around 50.0 | Zoller(45~55) | 3 | 1 |
| | $E_n$ around 100 | Zoller(89~110) | 3 | 1 |
| | $E_n$ around 160 | Zoller(145~175) | 3 | 1 |
| | $E_p$ at 20.0 | Hamilton | 11 | 1 |
| | $E_p$ at 60.0 | Hamilton | 11 | 1 |
| $^{239}$Pu | $E_n$ at 0.17 | Gindler | 12 | 2 |
| | $E_n$ at 7.9 | Gindler | 12 | 2 |
| | $E_n$ around 14.5 | Ford(14.0), Laurec(14.7) | 13,14 | 2 |
| $^{242}$Pu | $E_n$ at 15.1 | Winkelmann | 15 | 2 |

addition to β decay of the radioactive fission product nuclides, some of them also decay by emitting neutron, so called delayed neutron. For the data type 2, the delayed neutrons are emitted, but for the data type 1 not, even the data are “post-neutron” emission ones.

Another essential difference of the two kinds of measurements is mass resolution, which is more important for using the data to compare with the calculation ones. For second type of data, there is no this problem, but for first type of data, as mentioned above, the measured mass distribution is not exact one, but is a summation over all Gaussian extensions with the mass resolution width of each mass number. To confirm the point, the second type of data were “corrected” by following steps:

a) The data were linearly interpolated for the mass number, where there is no measured data, so that there are the yields for all each mass A in the mass range measured.

b) The data were made Gaussian extension with the width of 3 or 4 mass unit, which is the width of Vives or Zoller's measurement at the given energies, for the yields of each mass A.

c) The all yields were summed over all mass number in the mass range measured.

The results are shown in Figs. 8~9, marked “corrected”. It can be seen that the “corrected” second type of data are consistent with the fist type of data, e.g. Nagy corrected with Vives and Zoller in Fig. 8, LIU Conggui corrected and Daroczy corrected with Zoller in Fig. 9.

## 4 Conclusion Remarks

The mass distribution data were evaluated and recommended on the basis of available experimental data at the energies $E_n$=1.5, 5.5, 8.2, 11.3, 14.5, 22, 27.5, 50, 100, 160 MeV and $E_p$=20, 60 MeV for $^{238}$U fission, $E_n$=0.17, 7.9, 14.5 MeV for $^{239}$Pu fission, $E_n$=15.1 MeV for $^{242}$Pu fission, respectively. The data measured by different laboratories but with the same kind of method, like data type 2, are in good agreement within the experimental error. Considering the difference between the two types of data in physics and measurement technique and make some corresponding corrections, the two types data are also consistent with each other within errors. The data are recommended to use as base for both microscopic and systematics research.

The difference between the two types of data must be paid attention to. The calculated data should be made Gaussian extension with the corresponding experimental width when they are compared with the first type of data. There is no this problem when the second type of data are used to compare.

## Acknowledgement

The authors are indebted to Dr. M.C.Duijvestijn, Prof. M.Mutterer for their offering the experimental data and papers, and to Dr. M.Lammer for his supporting to the work and some translations of Zoller's thesis.

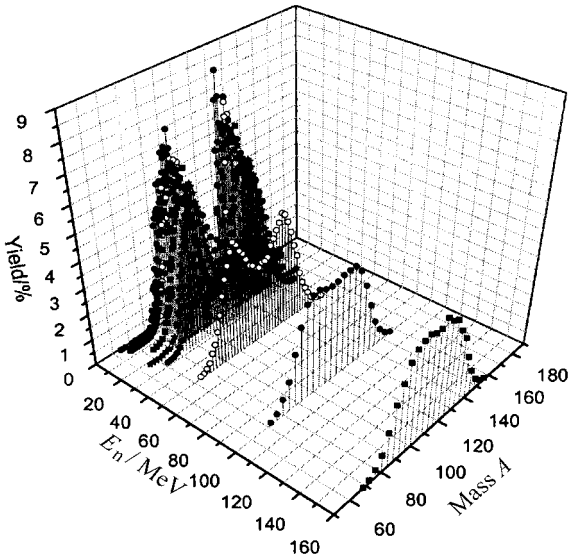


Fig. 1 The mass distribution of $^{238}$U fission induced by neutron

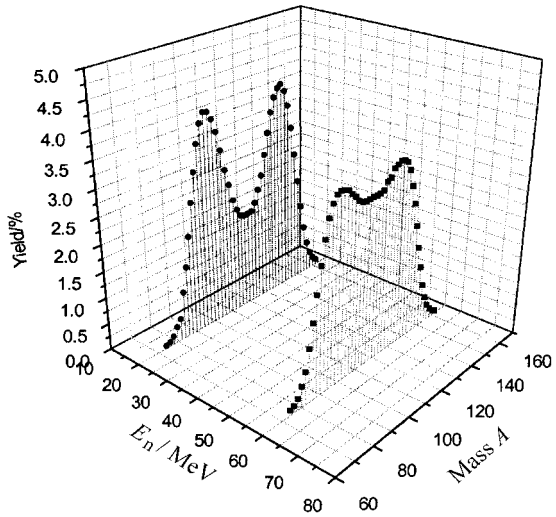


Fig. 2 Mass distribution of $^{238}$U fission induced by proton

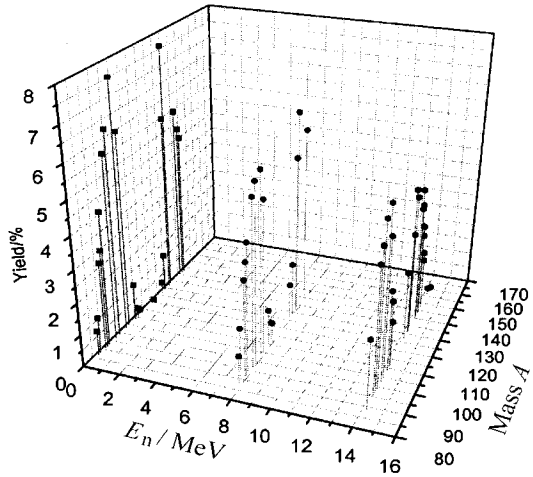


Fig. 3 Mass distribution of $^{239}$Pu fission

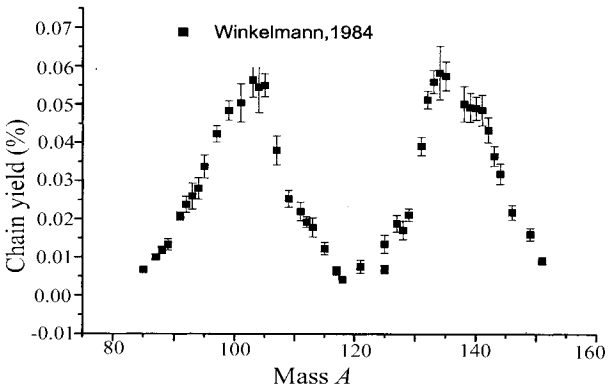


Fig. 4 Mass distribution from $^{242}$Pu fission at $E_n$=15.1 MeV

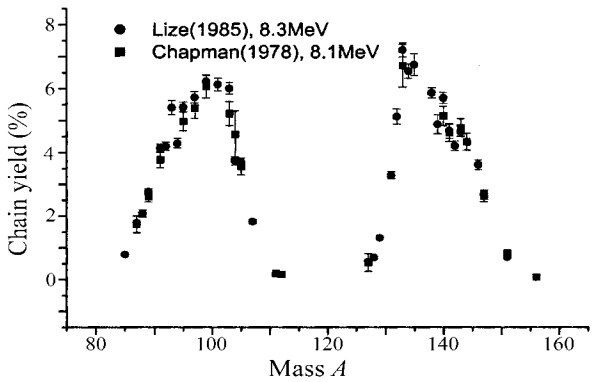


Fig. 5 Mass distribution from $^{238}$U fission at $E_n$ around 8.2 MeV

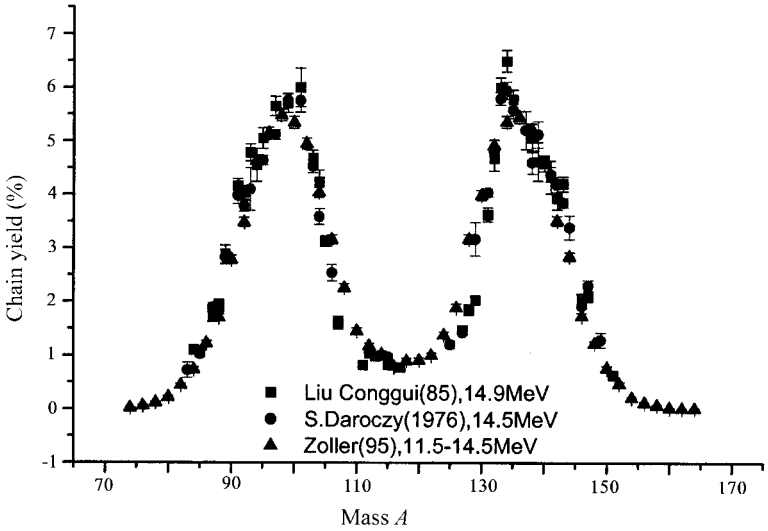


Fig. 6 Mass distribution from $^{238}$U fission at $E_n$ around 14.5 MeV

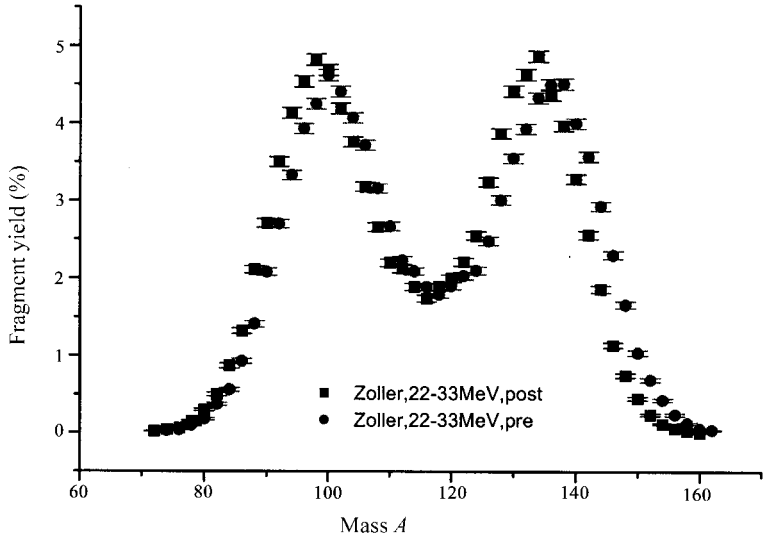


Fig. 7 Fragment mass distribution from $^{238}$U fission at $E_n$ around 27.5MeV

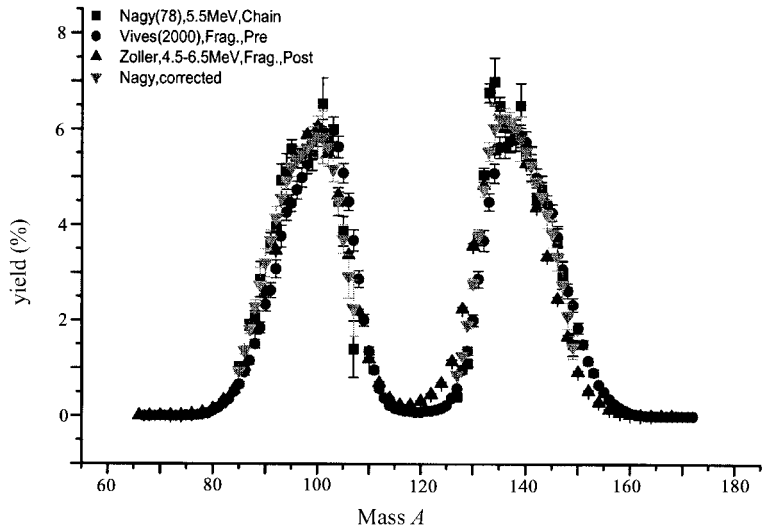


Fig. 8 The comparison of mass distribution of $^{238}$U fission around 5.5 MeV measured with different method

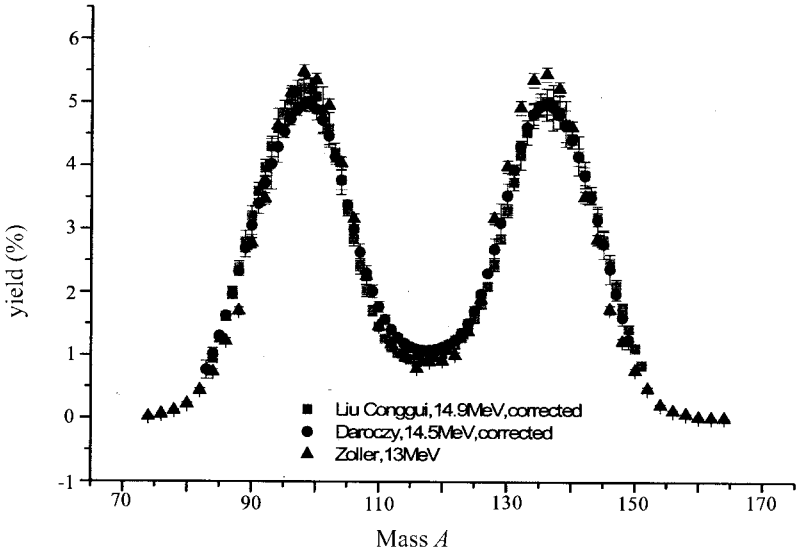


Fig. 9 Comparison of mass distribution of $^{238}$U fission at $E_n$ around 14 MeV measured with different method

## References


[1] F.Vives et al, Nucl. Phys., A662, 63(2000)

[2] M.C.Duijvestijn, Private communication(2002)

[3] C.M.Zoller, Ph. D. Thesis, TU Darmstadt 1995

[4] S.Nagy et al, Phys. Rev., C17, 163(1978)

[5] T.C.Chapman, Phys. Rev. C17(3), 1089(1978)

[6] LI Ze et al, Chinese Nucl . Phys., 7(2), 97(1985)

[7] LI Ze et al, Radiochimica Acta, 64, 95(1994)

[8] LIU Conggui et al, Chinese Nucl. Phys7(3),235(1985)

[9] S.Daroczy et al, Atomki Kozlemenyek, 18, 317(1976)

[10] LIU Yonghui et al, INDC(CPR)-056/L, 2(2001)

[11] J.H. Hamilton et al, Aysto97-Aysto, Proc, Int. Conf. on Fission and Properties of Neutron Rich Nuclei, Florida, USA, 457 (1997)

[12] J.E.Gindler et al, Phys. Rev., C27, 2508(1983)

[13] G.P.Ford, LA-6129(1976)

[14] J.Laurec et al, CEA-R-5147(1981)

[15] I.Winkelmann et al, Phys. Rev.,C30(3), 934(1984)

# Evaluation of Neutron Data of $^{197}$Au

FAN Sheng[1] ZHANG Hongzhou[1,2] WANG Shunan[1] YU Baosheng[1] LIU Tingjing[1]

*1 China Nuclear Data Center, CIAE Beijing 102413*

*2 Physics Department, Northwest University, Xi'an 710000*

**【abstract】** *The evaluation of neutron data of $^{197}$Au in the energy range from $10^{-5}$eV to 20 MeV was carried out. Based on the available measured data, the parameters for neutron optical potential in the energy region from 5 keV to 20 MeV were adopted. The ECIS code was used to investigate the cross section for neutron direct inelastic scattering. The resonance parameters were directly taken from ENDF/B-6. The re-evaluated neutron data is based on the available measured data and theoretic program UNF, compared with the data of ENDF/B-6 and CENDL-2.*

## Introduction

The experimental data of $^{197}$Au from neutron-induced reaction with energy lower than 20 MeV were collected from EXFOR and current publications. The resonance parameters were directly taken from ENDF/B-6. According to the experimental data and theoretic program, UNF[1] code, the neutron data were re-evaluated, compared with the data of ENDF/B-6 and CENDL-2.

## 1 Theoretic Calculations and Parameters

The parameters of the neutron optical potential is also employed as input data for the ECIS[2] code in order to get the cross section for neutron direct inelastic scattering.

The code APMN[3] is used to get the neutron optical potential parameters with energy region from 5 keV to 20 MeV based on the available measured data, such as total cross sections, non-elastic scattering cross sections and elastic angular distributions. Fig.1 shows the result fitting for the experimental data[4~8] on total cross section and the comparison with the ENDF/B-6 and CENDL-2. It can be seen that they are in agreement basically, the deviation with ENDF/B-6 is shown at energy around 1 MeV and below 2.5 MeV. The data of ENDF/B-6 is lower than present result and the measured data around 1 MeV and higher than the one below 2.5 MeV.

Fig. 2 gives the comparisons of the calculated results with the experimental data[9~14] of $^{197}$Au for elastic differential cross section at 0.5, 2.5, 4.1, 5.0, 7.0, and 8.0 MeV. It is clear that good agreement are at energies of 0.5, 2.5, 4.1, 5.0 MeV, the deviation is shown at energies of 7.0 and 8.0 MeV around 60 degree.

From fitting the total, non-elastic scattering cross sections and elastic angular distributions, the parameters of neutron optical potential were obtained, shown in Table 1.

In order to adjust the exciton model parameter *K*, the double differential cross section of neutron emission was compared with the experimental data [15,16]. Fig. 3 shows the comparisons at energies of 14.1 and 20 MeV and at angle of 90 degree. The reasonable agreements was obtained. Exciton model parameter *K* was taken as 1500 MeV$^3$ .

The code UNF is used to calculate the neutron data of files 3, 4, 6, 12, 13 and 15 in energy region from 5 keV to 20 MeV. The parameters of density level, giant dipole resonance, the nuclear level scheme, pair corrections, binding energy were taken from RIPL[17].

## 2 Evaluation and Recommendation

### 2.1 Resonance Parameters

The resonance parameters were directly taken from ENDF/B-6 in the energy region of $10^{-5}$eV to 5 keV.

### 2.2 (n,γ) Cross Section

The cross section of (n,γ) for $^{197}$Au was also directly taken from ENDF/B-6, because they are standard cross section, internationally accepted.

### 2.3 (n,2n) Cross Section

The cross section of $^{197}$Au(n,2n)$^{196}$Au was evaluated carefully[18] in neutron energy range from 8.12 to 30 MeV and compared with experimental data, ENDF/B-6, CENDL-2 and Yu Baosheng's evaluation.

**Table 1 Optical potential parameters**

| | N | P | α | $^3$He | D | T |
|---|---|---|---|---|---|---|
| $A_R$ / fm | 0.82233900 | 0.30 | 0.52 | 0.72 | 0.81 | 0.75 |
| $A_S$ / fm | 0.38018462 | 0.31 | 0.49 | 0.88 | 0.68 | 0.75 |
| $A_V$ / fm | 0.46904564 | 0.31 | 0.49 | 0.88 | 0.68 | 0.75 |
| $A_{S0}$ / fm | 0.82233900 | 0.30 | 0.51 | 0.72 | 0.81 | 0.75 |
| $X_R$ / fm | 1.17438900 | 1.13 | 1.20 | 1.20 | 1.15 | 1.20 |
| $X_S$ / fm | 1.28589952 | 1.13 | 1.20 | 1.20 | 1.34 | 1.20 |
| $X_V$ / fm | 1.54957497 | 1.13 | 1.20 | 1.20 | 1.34 | 1.20 |
| $X_{S0}$ / fm | 1.17438900 | 1.13 | 1.20 | 1.20 | 1.15 | 1.20 |
| $X_C$ / fm | 1.25000000 | 1.25 | 1.30 | 1.30 | 1.15 | 1.30 |
| $U_0$ / MeV | –1.44621181 | –2.7 | 0.0 | 0.0 | 0.0 | 0.0 |
| $U_1$ / MeV | 0.24428833 | 0.22 | 0.0 | 0.0 | 0.0 | 0.0 |
| $U_2$ / MeV | 0.00257329 | 0.0 | 0.0 | 0.0 | 0.0 | 0.0 |
| $V_0$ / MeV | 54.48585510 | 54.0 | 151.9 | 151.9 | 81.00 | 165.0 |
| $V_1$ / MeV | –0.28320849 | –0.32 | –0.17 | –0.17 | –0.22 | –0.17 |
| $V_2$ / MeV | 0.02015233 | 0.0 | 0.0 | 0.0 | 0.0 | 0.0 |
| $V_3$ / MeV | –24.000000 | 24.0 | 50.0 | 50.0 | 0.0 | –6.4 |
| $V_4$ / MeV | 0.00000000 | 0.4 | 0.0 | 0.0 | 2.0 | 0.0 |
| $V_{S0}$ / MeV | 6.20000000 | 6.2 | 2.5 | 2.5 | 7.0 | 2.5 |
| $W_0$ / MeV | 11.28027630 | 11.8 | 41.7 | 41.7 | 14.4 | 46.0 |
| $W_1$ / MeV | –0.60000002 | –0.25 | –0.33 | –0.33 | 0.24 | –0.33 |
| $W_2$ / MeV | –12.0000 | 12.0 | 44.0 | 44.0 | 0.0 | –110.0 |

A2S = 0.7 fm A2V= 0.7 fm

Note: $V_r(E) = V_0 + V_1E + V_2E(2) + V_3(A\text{-}2Z)/A + V_4Z/A^{1/3}$; $Ws(E) = W_0 + W_1E + W_2(A\text{-}2Z)/A$; $U_V(E) = U_0 + U_1E + U_2E(2)$;

## 2.4 (n,3n) Cross Section

Fig.4 shows the comparison of the UNF calculation, measured data with ENDF/B-6 and CENDL-2. The experimental data was measured by A.K.Hankla[19] at 14.4 MeV, L.R.Veeser[20] in energies from 16 to 24 MeV, B.P.Bayhurst[21] in energies from 17.73 to 24.48 MeV, E.T.Bramlitt[22] at 14.7 MeV, LU Hanlin[23] in energies from 16.25 to 18.63 MeV, G.A.Prokopets[24] at 20.06 MeV, C.Philis[25] in energies from 14.82 to 30 MeV, respectively. The above data were corrected and normalized by using nuclear decay data and standard cross section. LU Hanlin and E.T.Bramlitt's measured data are consistent each other within the errors. From Fig. 4, it can be seen that UNF calculation is in good agreement with the experimental data , ENDF/B-6 and CENDL-2.

## 2.5 (n,p) Cross Section

The experimental data of (n,p) reaction on $^{197}$Au were measured by B.P.Bayhurst[26] in energy region from 12.13 to 19.76 MeV, H.A.Tewes[27] in energies from 11.8 to 13.851 MeV, R.A.Peck[28] at 14.1 MeV, R.F.Colemen[29] at 14.5 MeV, and V.K.Maidanyuk[30] at 14.7 MeV, respectively. Most of ratio measurements and relative measurement to the reference reactions such as $^{196}$Au(n,2n) were renormalized. B.P.Bayhurst's measured data are consistent with other measured ones within the errors in energy region of 12.13 to 19.76 MeV. The evaluated data were from the least squares fitting for all experimental data, compared with the results of ENDF/B-6. The comparison is shown in Fig. 5.

## 2.6 Elastic Cross Section

All experimental data[12,14,31,32] were measured before 1980's. The UNF calculation is not in good agreement with the measured data. The measurements were corrected by using the standard cross section of H(n,n) from ENDF/B-6 to the reference reaction. The cross section is derived by subtracting the non-elastic cross sections from the total cross sections. Fig.6 shows the comparison of the present work with the measured data and results of ENDF/B-6.

### 2.7 (n,α) Cross Section

Comparing with the data of (n,2n) and (n,3n) reactions, the cross section of (n,α) is the same as the data of (n,p) reaction. It is much lower. The experimental data were measured by B.P.Bayhurst[26] in energy range from 7 to 19.6 MeV, R.F.Coleman[29] at 14.5 MeV, V.K.Maidanyuk[30] at 14 MeV, J.C.Hill[25] at 18.7 MeV, respectively. B.P.Bayhurst's measured data are consistent with other ones within the errors. The evaluated data were from least squares fitting for experimental data. The Fig. 7 shows the comparison of the evaluation data with the experimental data and ENDF/B-6.

### 2.8 (n,d) and (n, t) Cross Sections

There are no measured data for cross sections of (n,d) and (n,t) reactions, and the two reaction data is not included in ENDF/B-6. The evaluated data were taken from UNF calculation. Fig. 8 shows the result compared with CENDL-2.

### 2.9 Non-Elastic Scattering Cross Section

The cross section was obtained by summing all the reaction cross section.

## Summary

The neutron data for $^{197}$Au were evaluated and recommended in energy range from $10^{-5}$eV to 20 MeV by fitting the measured data and UNF calculations.

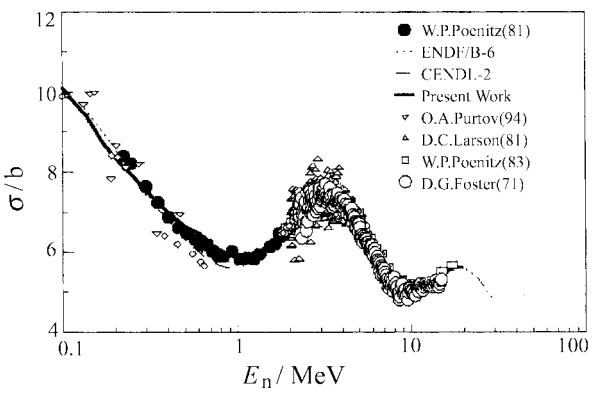


Fig. 1 Comparison of neutron total cross section

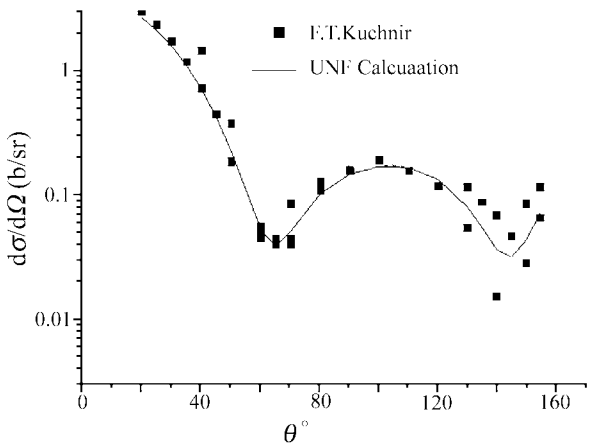


Fig. 2 (b) $^{197}$Au elastic differential cross section

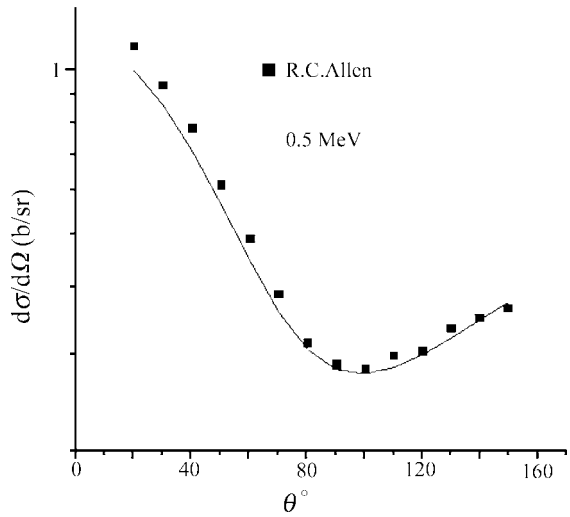


Fig. 2 (a) $^{197}$Au elastic differential cross section

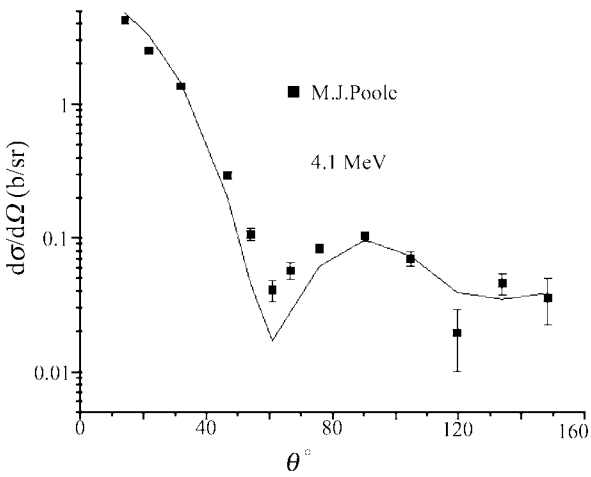


Fig. 2 (c) $^{197}$Au elastic differential cross section

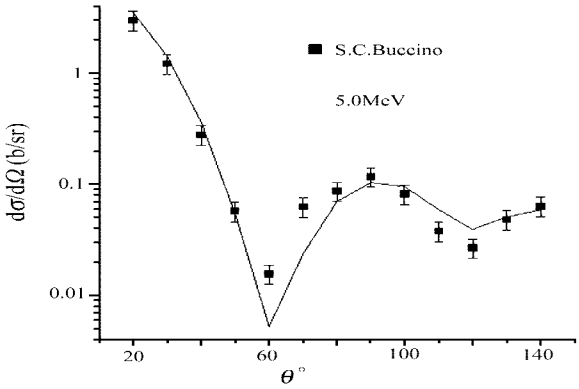


Fig. 2 (d) $^{197}$Au elastic differential cross section

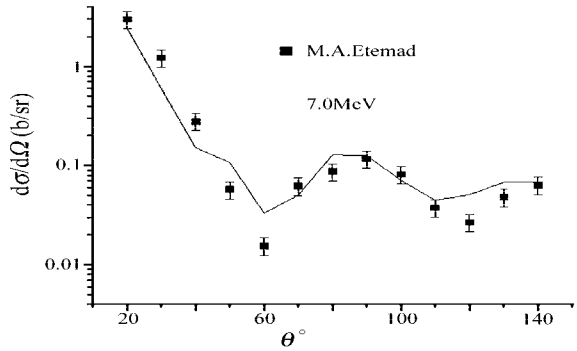


Fig. 2 (e) $^{197}$Au elastic differential cross section

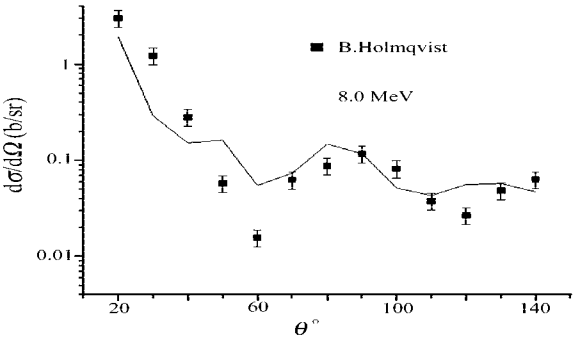


Fig. 2 (f) $^{197}$Au elastic differential cross section

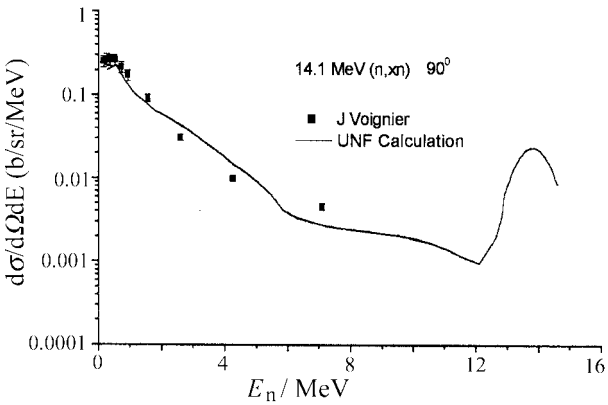


Fig. 3 (a) Double differential cross section of neutron emission at 14.1 MeV and 90° angle

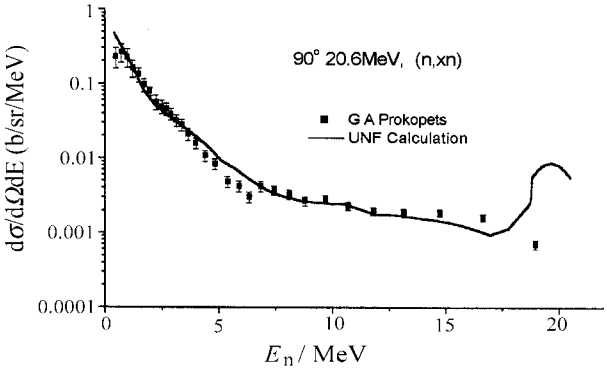


Fig. 3 (b) Double differential cross section of neutron emission at 20 MeV and 90° angle

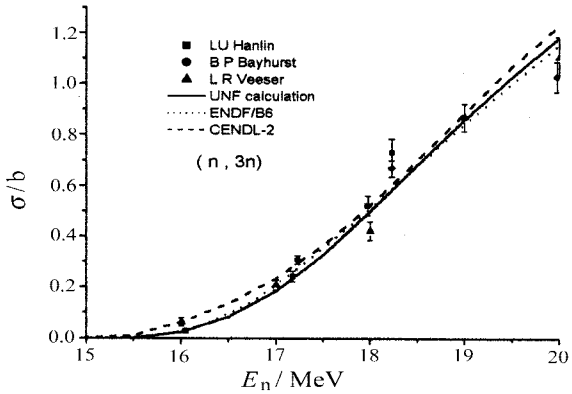


Fig. 4 Cross section of $^{197}$Au(n,3n) $^{195}$Au

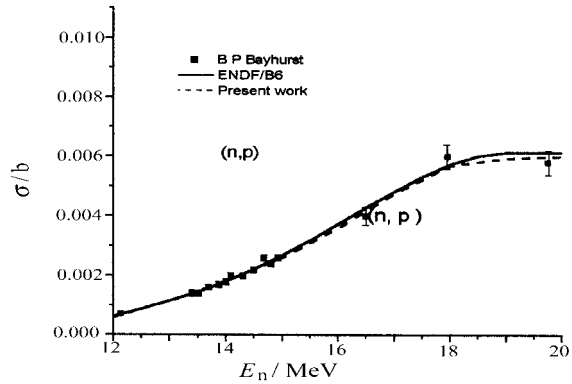


Fig. 5 The cross section of (n, p) for $^{197}$A

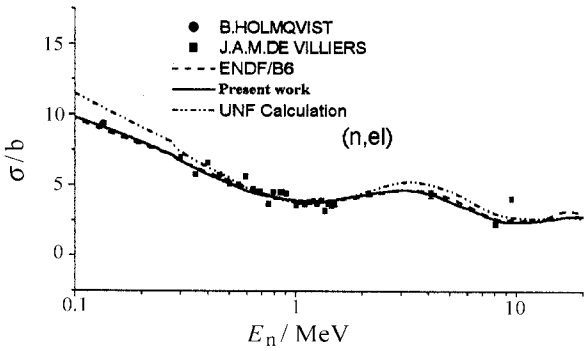


Fig. 6 The elastic cross section of n + $^{197}$Au reaction

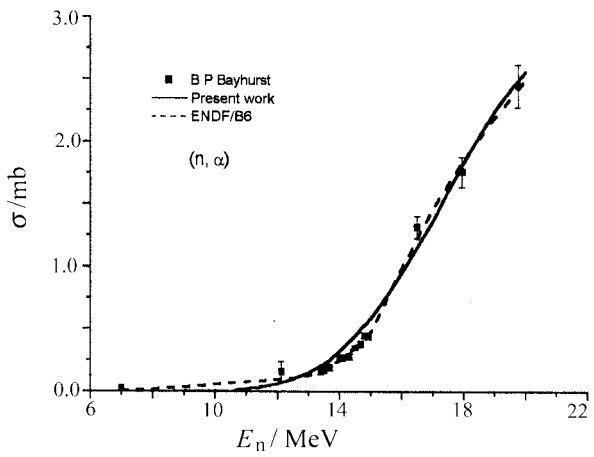


Fig. 7  The cross section of (n,α) for $^{197}$Au

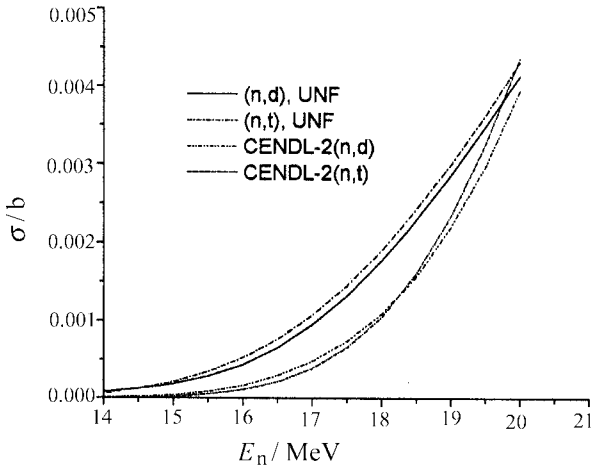


Fig. 8  The cross section of (n,D) and (n,T) for $^{197}$Au

## References


[1] ZHANG Jingshang, CNIC-01616, CNDC-0032, 2001

[2] J Raynal, note on ECIS94, note CEA-N-2772, 1994

[3] SHEN Qingbiao, CNDP, 7, 43, 1992

[4] W P Poenitz et al., Nucl. Sci. and Eng., 78,333, 1981

[5] D A Purtov et al., AE, 77(1), 44, 1994

[6] D C Larson et al., BNL-277, 1980

[7] W P Poenitz et al., ANL-NDM-80, 1983

[8] D G Foster et al., Phys. Rev., C3, 576, 1971

[9] M.Walt et al., Phys. Rev., 98,677,55

[10] S.C.Buccino et al., Z. Phys., 196, 103, 1966

[11] R.C.Allen et al., Phys. Rev., 104, 731, 1956

[12] B.Holmqvist et al., AE-430, 1971

[13] B.Holmqvist et al., AE-485, 1974

[14] B.Holmqvist et al., AE-482, 1973

[15] J.Voignier et al., CEA-R-4279, 1972

[16] G.A.Prokopets, 80KIEV, 2, 54, 1980

[17] P Oblozinsky et al., IAEA-TECDOC-1034, 1998

[18] FAN Sheng et al., INDC(CPR)-058/L, 27, 19, 2002/10/30

[19] A.K.Hankla et al., Nucl. Phys., A180, 157, 1972

[20] L.R.Veeser et al., Phys. Rev., C16, 1792, 1977

[21] B.P.Bayhurst et al., Phys. Rev., C12, 451, 1975

[22] E.T.Bramlitt et al., Phys. Rev., 131, 2649, 1963

[23] LU Hanlin et al., INDC(CPR)-16, 1989

[24] G.A.Prokopets, YF, 32, 37, 1980

[25] C.Philis et al., CEA-R-4826, 1977

[26] B.P.Bayhurst et al., JIN, 23, 173, 1961

[27] H.A.Tewes et al., UCRL-6028-T, 1960

[28] R.A.Peck et al., Phys. Rev., 106, 965, 1957

[29] R.F.Coleman et al., PPS, 73, 215, 1959

[30] V.K.Maidanyuk et al., 94PETRBG, 194, 1994

[31] J.Tittman et al., Phys. Rev., 83, 746, 1951

[32] J.A.M.Devilliers et al., Z. Phys., 183, 323, 1965

# Consistent Evaluation of the Complete Sets of Nuclear Data for n + $^{85,87,Nat}$Rb in the Energy Region 0~20 MeV

CAI Chonghai

*Department of Physics, Nankai University, Tianjin 300071, P.R.China*

【**abstract**】*The complete sets of nuclear data, including all kinds of cross sections, especially for some reactions leaving the residual nuclei in metastable (isomeric) states, angular distributions of elastic scattering, energy spectra and/or double-differential cross sections of all emitted particles, gamma production data (production cross sections and multiplicity, energy spectra) for all kinds of reactions, for n + $^{85,87,Nat}$Rb below 20 MeV were calculated and evaluated. In most cases, the calculated cross sections are in good accordance with the experimental data.*

## Introduction

$^{85,87}$Rb are the only two stable isotopes for the element rubidium, which are the important fission products. The existed evaluation files for these two isotopes are included in ENDF/B-6, JEF-2, JENDL-3.2 and CENDL-3. We found that in JEF-2 there are no (n,2n) reaction data, the inelastic cross sections are without good shape. So we only compared ENDF/B-6, JENDL-3.2 and CENDL-3 with each other and with experimental data in Figs. 1 to 7. All the experimental data in these figures were taken from EXFOR, in this paper we do not give the references indicated in EXFOR for each set of data respectively. In some cases we indicate the first author and the publishing year.

The complete sets of neutron nuclear data of $^{85}$Rb and $^{87}$Rb in ENDF/B-6 and JENDL-3.2 were evaluated before 1990. The experimental data after 1988 were not used in their evaluation. The calculations of $^{85}$Rb and $^{87}$Rb for CENDL-3 were made by us in 1997. But at that time we did not carefully analyze the experimental data from different authors and at different years, simply dealing with them equally. So the data in CENDL-3 were improved little in comparison with JENDL-3.2. Furthermore, for $^{85}$Rb and $^{87}$Rb, there are no neutron double differential cross sections and gamma production data in ENDF/B-6, JENDL-3 and CENDL-3. Later on we realized that the experimental data given by YUAN Xialin et al. in 1990 are much more reliable. The new version 2001 of program UNF[1] was much improved in comparison with version 1997, especially it can calculate the reaction cross section leaving the residual nucleus in a metastable (isomeric) state. Considering the newer reliable experimental data and those of isomeric state, we recalculated and gave better complete sets of neutron nuclear data for $^{85}$Rb, $^{87}$Rb and natural rubidium, including double-differential cross sections and gamma production data in B-6 format output. In this paper we give the methods, parameters and part calculated cross sections in comparison with experimental data and three evaluation files above mentioned.

## 1 Optical Potential Parameters and Direct Inelastic Contribution

There are no experimental data of total and non-elastic cross sections as well as elastic scattering angular distributions for $^{85,87}$Rb, only experimental total cross sections of natural rubidium. So we use the program APMN[2] to automatically search for the optimal optical potential parameters of $^{85}$Rb and $^{87}$Rb in neutron channel based on the experimental total cross sections of natural rubidium given by D.G.Forster in 1971 and E.Barnard in 1969. Because there are no elastic and/or non-elastic experimental cross sections, in practical operation we need to do a few recursion to adjust the non-elastic cross sections in keeping later calculated cross section in accordance with experimental data in every reaction channel. In order to make the calculated (n,p) and (n,$\alpha$) reaction cross sections in agreement with experimental data, we also need adjusting the optical potential parameters in proton and alpha channels by hand. The meaning of all the parameters is explained in Eqs. (1), (2), (6) and (7) of Ref. [2]. The optical potential parameters used in our final calculations are given in Table 1 (a) and (b) for $^{85}$Rb and

$^{87}$Rb, respectively. The same set of optimal optical potential parameters in neutron channel are also used in calculations of the direct inelastic cross sections as well as the Legendre coefficient of their angular distributions with DWUCK4[3]. Levels and their deformation parameters $\beta_2$ used in direct inelastic calculation are given in Table 2.

The optical potential parameters in Table 1 and the direct inelastic cross sections as well as the Legendre coefficients of their angular distributions were used as a part of input data for the main code UNF.

## 2 Other Parameters Used in UNF Calculations

In UNF, Gilbert-Cammeron formula is employed for calculation of the level density. The level density parameter $a$, the pair energy correction $\Delta$ and the two peak giant resonance parameter for gamma emission were taken from the Parameters Library at CNDC. The data of levels and their spin, parity and the branch ratio of gamma emission were taken from the Parameters Library at CNDC and/or the Web of NNDC at BNL, USA. In practical calculation, in order to make the calculated cross sections in better accordance with experimental data, we often adjust some of the level density parameters $a$ and the pair energy corrections $\Delta$ by hand in some ranges.

In addition to above mentioned parameters, there is adjustable Kulbach parameter in exciton model CK=920.0 for both $^{85}$Rb and $^{87}$Rb, the adjustable factor in (n,γ) cross section calculation CE1=3.2 for $^{85}$Rb and 14.0 for $^{87}$Rb, the adjustable parameter in direct (n,γ) calculation DGM=0.43 for $^{85}$Rb and 2.2 for $^{87}$Rb.

## 3 Evaluation and Discussion on Some Calculated Results

With above mentioned parameters and the calculated direct inelastic data by DWUCK4 as the input data, we calculated the complete sets of neutron nuclear data of $^{85}$Rb, $^{87}$Rb and natural rubidium with the code UNF.

The resonance parameters were taken from JENDL-3, only the data in 0.1~20 MeV energy region were calculated and evaluated. In Figs.1~7, “this work” means our evaluated value, it is just the calculated value in most cases. Only the (n,γ) cross sections of $^{87}$Rb is taken from CENDL-3 because it is in better accordance with experimental data than our

**Table 1(a) Optical potential parameters of $^{85}$Rb used**

| Channel | n | p | alpha | $^3$He | d | t |
|---|---|---|---|---|---|---|
| $a_r$ | 0.6236157 | 0.55 | 0.78 | 0.72 | 0.71 | 0.72 |
| $a_s$ | 0.6028041 | 0.55 | 0.78 | 0.88 | 0.78 | 0.84 |
| $a_v$ | 0.6965684 | 0.55 | 0.78 | 0.88 | 0.78 | 0.84 |
| $a_{so}$ | 0.6236157 | 0.55 | 0.78 | 0.72 | 0.71 | 0.72 |
| $r_r$ | 1.2491100 | 1.20 | 1.40 | 1.20 | 1.17 | 1.20 |
| $r_s$ | 1.3112580 | 1.20 | 1.39 | 1.40 | 1.30 | 1.40 |
| $r_v$ | 1.0819450 | 1.20 | 1.39 | 1.40 | 1.30 | 1.40 |
| $r_{so}$ | 1.2491100 | 1.01 | 1.40 | 1.20 | 0.64 | 1.20 |
| $r_c$ | 1.2500000 | 1.25 | 1.25 | 1.30 | 1.30 | 1.30 |
| $W_{v0}$ | 2.3493840 | -2.70 | 22.4 | 0.0 | 0.0 | 0.0 |
| $W_{v1}$ | -.0169647 | 0.22 | 0.0 | 0.0 | 0.0 | 0.0 |
| $W_{v2}$ | 0.0221148 | 0.0 | 0.0 | 0.0 | 0.0 | 0.0 |
| $V_0$ | 52.6595600 | 54.0 | 164.7 | 151.9 | 90.6 | 165.0 |
| $V_1$ | -.1336608 | -0.32 | 0.0 | -0.17 | 0.0 | -0.17 |
| $V_2$ | -.0102717 | 0.0 | 0.0 | 0.0 | 0.0 | 0.0 |
| $V_3$ | -24.00000 | 24.0 | 0.0 | 50.0 | 0.0 | -6.4 |
| $V_4$ | -.0378085 | 0.4 | 0.0 | 0.0 | 0.0 | 0.0 |
| $V_{so}$ | 6.200000 | 6.2 | 0.0 | 2.5 | 7.13 | 2.5 |
| $Ws_0$ | 2.6253160 | 11.8 | 0.0 | 41.7 | 12.0 | 46.0 |
| $Ws_1$ | 0.00645436 | -0.25 | 0.0 | -0.33 | 0.0 | -0.33 |
| $Ws_2$ | -12.00000 | 12.0 | 0.0 | 44.0 | 0.0 | -110.0 |

$a_{s1}$=0.7, $a_{v1}$=0.7 for p channel.

**Table 1 (b) Optical potential parameters of $^{87}$Rb used**

| Channel | n | p | alpha | $^3$He | d | t |
|---|---|---|---|---|---|---|
| $a_r$ | 0. 6236157 | 0.47 | 0.62 | 0.72 | 0.71 | 0.72 |
| $a_s$ | 0. 6031808 | 0.45 | 0.62 | 0.88 | 0.78 | 0.84 |
| $a_v$ | 0. 6973935 | 0.45 | 0.62 | 0.88 | 0.78 | 0.84 |
| $a_{so}$ | 0. 6236157 | 0.47 | 0.62 | 0.72 | 0.71 | 0.72 |
| $r_r$ | 1.2491100 | 1.15 | 1.30 | 1.20 | 1.17 | 1.20 |
| $r_s$ | 1. 3115620 | 1.15 | 1.34 | 1.40 | 1.30 | 1.40 |
| $r_v$ | 1. 0822300 | 1.15 | 1.34 | 1.40 | 1.30 | 1.40 |
| $r_{so}$ | 1.2491100 | 1.01 | 1.30 | 1.20 | 0.64 | 1.20 |
| $r_c$ | 1.2500000 | 1.25 | 1.25 | 1.30 | 1.30 | 1.30 |
| $W_{v0}$ | 2.3528460 | -2.70 | 22.4 | 0.0 | 0.0 | 0.0 |
| $W_{v1}$ | -. 0387146 | 0.22 | 0.0 | 0.0 | 0.0 | 0.0 |
| $W_{v2}$ | 0. 0370749 | 0.0 | 0.0 | 0.0 | 0.0 | 0.0 |
| $V_0$ | 52.6598400 | 54.0 | 164.7 | 151.9 | 90.6 | 165.0 |
| $V_1$ | -. 1411178 | -0.32 | 0.0 | -0.17 | 0.0 | -0.17 |
| $V_2$ | -. 0105710 | 0.0 | 0.0 | 0.0 | 0.0 | 0.0 |
| $V_3$ | -24.00000 | 24.0 | 0.0 | 50.0 | 0.0 | -6.4 |
| $V_4$ | -. 0374564 | 0.4 | 0.0 | 0.0 | 0.0 | 0.0 |
| $V_{so}$ | 6.200000 | 6.2 | 0.0 | 2.5 | 7.13 | 2.5 |
| $W_{s0}$ | 2.6266940 | 11.8 | 0.0 | 41.7 | 12.0 | 46.0 |
| $W_{s1}$ | 0.00611578 | -0.25 | 0.0 | -0.33 | 0.0 | -0.33 |
| $W_{s2}$ | -12.00000 | 12.0 | 0.0 | 44.0 | 0.0 | -110.0 |

$a_{s1}$=0.7, $a_{v1}$=0.7 for p channel.

**Table 2 levels and deformation parameters $\beta_2$ used in direct inelastic calculation**

| $^{85}$Rb | | | | $^{87}$Rb | | | |
|---|---|---|---|---|---|---|---|
| Level / MeV | $J$ | $\pi$ | $\beta_2$ | Level / MeV | $J$ | $\pi$ | $\beta_2$ |
| 0.1512 | 1.5, | -1 | 0.08 | 0.40259 | 2.5 | -1 | 0.085 |
| 0.2810 | 0.5 | -1 | 0.08 | 0.84544 | 0.5 | -1 | 0.085 |
| 0.7318 | 1.5, | -1 | 0.08 | 1.46300 | 0.5 | -1 | 0.085 |
| 0.8690 | 3.5 | -1 | 0.08 | 1.57801 | 0.5 | -1 | 0.085 |
| 0.8858 | 0.5 | -1 | 0.08 | 1.89300 | 0.5 | -1 | 0.085 |
| 0.9197 | 0.5 | -1 | 0.08 | | | | |
| 1.1755 | 1.5 | -1 | 0.08 | | | | |
| 1.2959 | 1.5 | -1 | 0.08 | | | | |

calculated value. The calculated values below 0.6 MeV were changed a little for total, elastic scattering and (n,γ) cross sections to make them smoothly connecting with those calculated from resonance parameters. "ms" means this reaction to leave the residual nucleus in metastable (isomeric) state. All the calculated and/or evaluated data of natural rubidium were combined from the values of $^{85}$Rb and $^{87}$Rb with their abundances as weights, so the data for $^{85}$Rb, $^{87}$Rb and natural rubidium are consistent.

From Fig.1(a) and (b) we can see that the calculated $\sigma_{tot}$ for both $^{85}$Rb and $^{87}$Rb are in better agreement with experimental data than JENDL-3.2 and CENDL-3, still not good as ENDF/B-6 in the energy region 0.7~1.2 MeV. It seems to us from Fig.2(a) and (b) that the calculated lines of $\sigma_{non}$ for both $^{85}$Rb and $^{87}$Rb are of smooth shape without sharp structure, it should be reasonable. From Fig.3(a) we can see that for $^{85}$Rb, not only the calculated $\sigma_{n,\gamma}$ are in good accordance with experimental data, the part of calculated $\sigma_{n,\gamma}$ leaving the residual nucleus $^{86}$Rb in the metastable (isomeric) state (0.5661 MeV, $J^{\pi}=6^{-}$, $T_{1/2}$=1.017 minute) are also in good agreement with experimental data. For $^{87}$Rb, the calculated $\sigma_{n,\gamma}$ are in good accordance with experimental data when $E_n$ is less than 1.1 MeV, but worse in the energy region 1.2~3.5 MeV, so we used the value from CENDL-3 as our evaluation value in Fig.3(b). Fig.3(c) shows that our evaluated $\sigma_{n,\gamma}$ of natural rubidium combining from the calculated values of $^{85}$Rb and the evaluated values of $^{87}$Rb are also in rather good agreement with experimental data.

There are experimental data only for the reaction $^{85}$Rb(n,p)$^{85}$Kr(ms), not for $^{85}$Rb(n,p)$^{85}$Kr(gs) because of the ground state ($J^{\pi}=4.5^{+}$) of $^{85}$Kr with very long life ($T_{1/2}$=3934.4 day) and its metastable state (0.30487 MeV, $J^{\pi}=0.5^{-}$) with moderate life ($T_{1/2}$=4.48 hour). The activation measurement method is suitable for the reaction $^{85}$Rb(n,p) $^{85}$Kr(ms), but can not be used for the reaction $^{85}$Rb(n,p) $^{85}$Kr(gs). So in this work we make the calculated cross sections of the reaction $^{85}$Rb(n,p) $^{85}$Kr(ms) by adjusting some optical potential parameters, the level density parameter and the pair energy correction in p channel in accordance with their experimental data. From Fig.4(a) we can see that this agreement is good. Then we naturally obtained the (n,p) reaction cross sections. There is one point needed to indicate that the level scheme do not give the $J^{\pi}$ value for the level 1.16669 MeV, we assigned a value $0.5^{-}$ for it. If we change this $J^{\pi}$ from $0.5^{-}$ to $2.5^{-}$, the values of (n,p) reaction cross sections are unchanged much and the fractions of $^{85}$Rb(n,p) $^{85}$Kr(ms) in (n,p) reaction increases from 12.8%~23.6% to 15.9%~26.4%. If this $J^{\pi}$ changes to $4.5^{+}$, then these fractions change to 16.6%~25.9%. From Fig. 4 (b) we can see that the calculated (n,p) reaction cross sections of $^{87}$Rb are in good accordance with the experimental data given by YUAN Xialin in 1990, which we think are the better measurement values. From the calculated (n,p) and (n,pn) cross sections of $^{85}$Rb and $^{87}$Rb, we obtained the inclusive (n,p) reaction cross sections of $^{85}$Rb, $^{87}$Rb and natural rubidium. From Fig. 4 (c) we can see that the calculated inclusive (n,p) reaction cross sections of natural rubidium are also in very good agreement with experimental data.

Fig.5 (a) tells us that the calculated (n,α) reaction cross sections of $^{85}$Rb are in good accordance with the most reliable experimental data given by YUAN Xialin in 1990. There are four discrepant experimental data obtained by different authors for (n,α) reaction cross sections of $^{87}$Rb. There is a group of newer reliable measurement values on $^{87}$Rb(n,α) $^{84}$Br(ms) given by K.Kawade in 1992. Based on them we got calculated (n,α) reaction cross sections of $^{87}$Rb and the part corresponding to $^{84}$Br lain in the isomeric state (0.320 MeV, $J^{\pi}=6^{-}$, $T_{1/2}$=6.0 minutes), which are shown in Fig. 5 (b). From the calculated (n,α) and (n,αn) cross sections of $^{85}$Rb and $^{87}$Rb, we obtained the inclusive (n,α) reaction cross sections of $^{85}$Rb, $^{87}$Rb and natural rubidium. From Fig. 5 (c) we can see that the calculated inclusive (n,α) reaction cross sections of natural rubidium are lower than the experimental data given by V.Koenig in 1965 by a factor of about two. This shows that for (n,α) reaction cross sections, the measurement values of natural rubidium are not consistent with the experimental data of its isotopes. We think that the experimental data given by YUAN Xialin in 1990 for $^{85}$Rb and those given by K.Kawade in 1992 for $^{87}$Rb(n,α) $^{84}$Br(ms) are better and more reliable than the measured inclusive (n,α) reaction cross sections of natural rubidium given by V.Koenig in 1965, so we gave up the measured values given by V.Koenig in 1965 in our consistent calculations and evaluations.

Fig. 6 (a) and (b) give the calculated and experimental (n,2n) reaction cross sections for $^{85}$Rb and $^{87}$Rb, from which we can see that the calculated (n,2n) cross sections are in good accordance with the experimental data given by YUAN Xialin in 1990, which we think are more reliable measured values for both $^{85}$Rb and $^{87}$Rb. There are no experimental data of (n,n') cross sections for both $^{85}$Rb and $^{87}$Rb. Fig. 7 (a) and (b) give the calculated (n,n') cross sections in comparison with ENDF/B-6, JENDL-3.2 and CENDL-3 for $^{85}$Rb and $^{87}$Rb, respectively. It seems that our calculated values are both reasonable in shapes and in physics, which include direct inelastic contributions.

In addition to cross sections, we also in a consistent way calculate the angular distributions of elastic scattering, energy spectra and/or double-differential cross sections of all emitted particles, gamma production data (production cross sections and multiplicity, energy spectra) for all kinds of reactions opened, for $^{85}$Rb, $^{87}$Rb and natural rubidium. Because there are no experimental data at all for comparing, we do not give these calculated results in this paper, only give them in B-6 format output. To use conveniently for users, two kinds of B-6 format output results (one includes File 1, 2, 3, 6, 12, 14, 15, and another includes File 1~5) are given for $^{85,87,Nat}$Rb in this work.

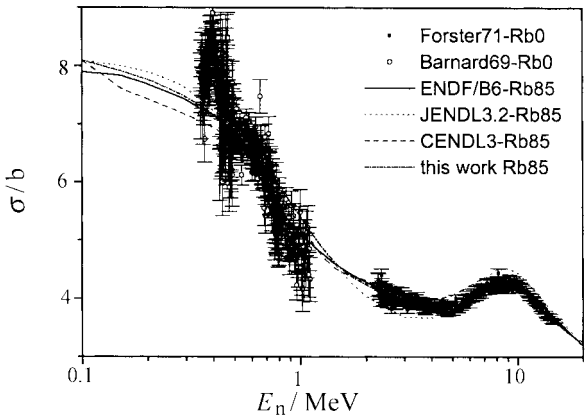


Fig. 1 (a) Totat cross sections of $^{85}$Rb

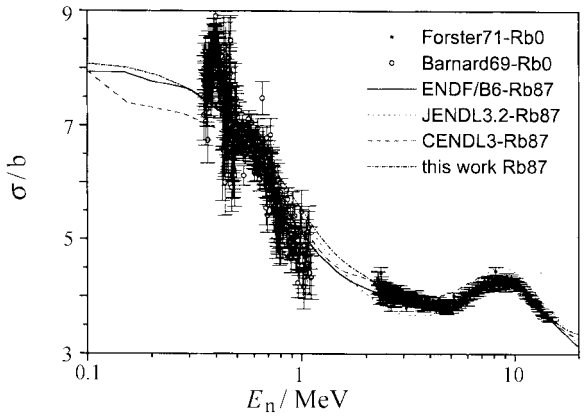


Fig. 1 (b) Totat cross sections of $^{87}$Rb

# 4 Conclusion

With new version 2001 of the code UNF and based on some newer experimental data, such as those given by YUAN Xialin et al. in 1990 and by K.Kawade in 1992, we in a consistent way recalculated and re-evaluated the complete sets of nuclear data for n + $^{85,87,Nat}$Rb below 20 MeV, and obtained better results than four existed evaluation files above mentioned.

# 5 Acknowledgement

Thanks to professor YU Baosheng for his explanation on the experiment of V.Koenig in 1965 and for other helpful discussion. Professor SHEN Qingbiao provided us some input data and some evaluation tools, Dr. ZHANG Zhengjun helped us to search the experimental data from EXFOR, Professor ZHANG Jingshang explained something about the code UNF for us; we also would like to thank them.

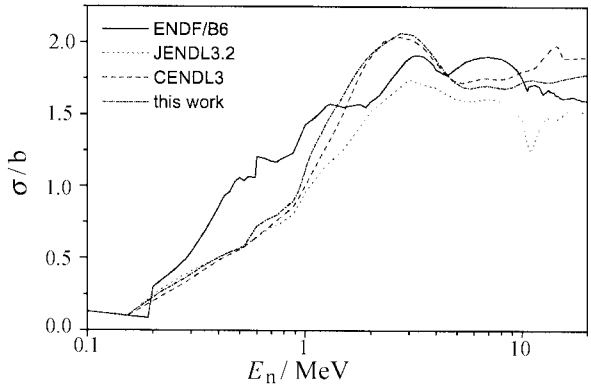


Fig. 2 (a) Nonelastic cross sections of $^{85}$Rb

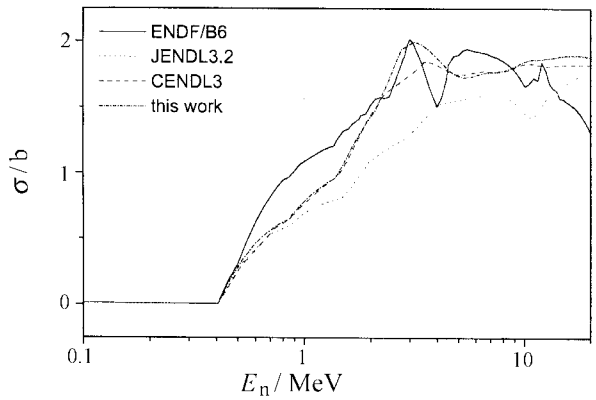


Fig. 2 (b) Nonelastic cross sections of $^{87}$Rb

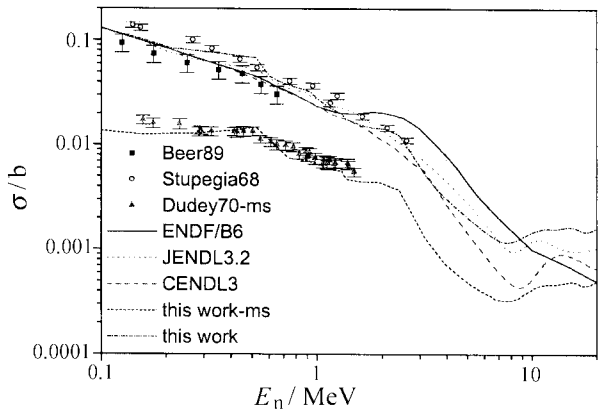


Fig. 3 (a) Capture cross sections of $^{85}$Rb

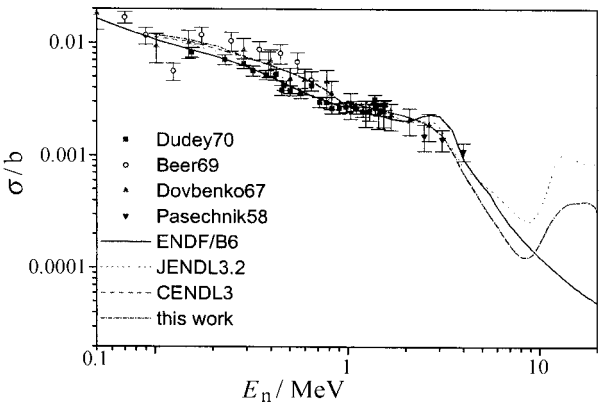


Fig. 3 (b) Capture cross sections of $^{87}$Rb

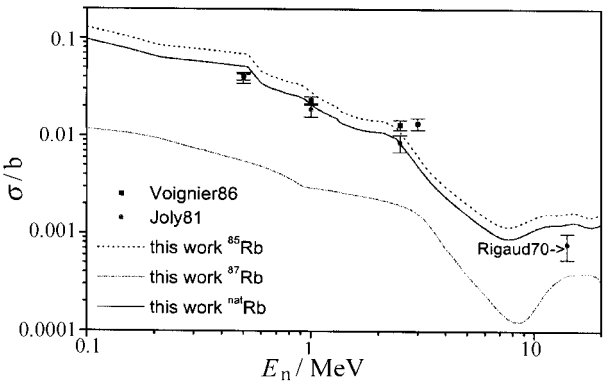


Fig. 3 (c) Capture cross sections of $^{Nat}$Rb

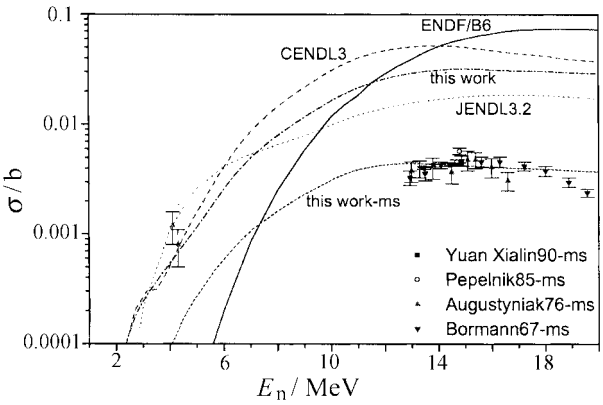


Fig. 4 (a) (n.p) reaction cross sections of $^{85}$Rb

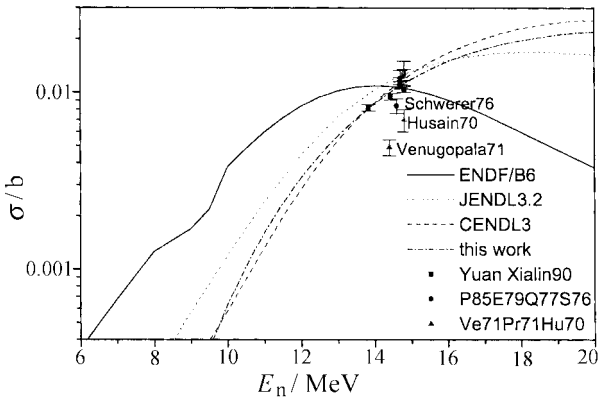


Fig. 4 (b) (n.p) reaction cross sections of $^{87}$Rb

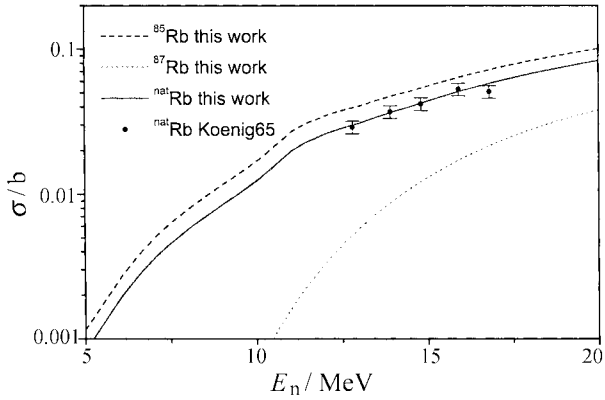


Fig. 4 (c) Inclusive (n.p) reaction cross sections of $^{Nat}$Rb

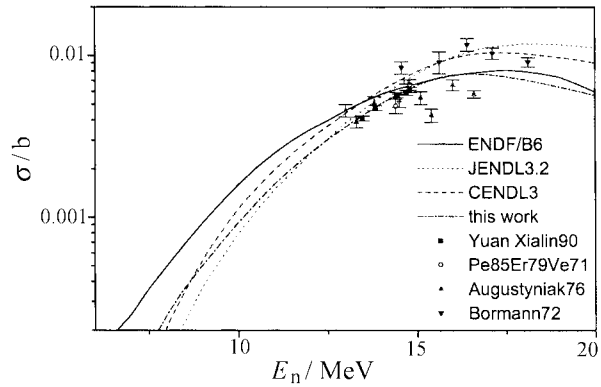


Fig. 5 (a) (n,α) reaction cross sections of $^{85}$Rb

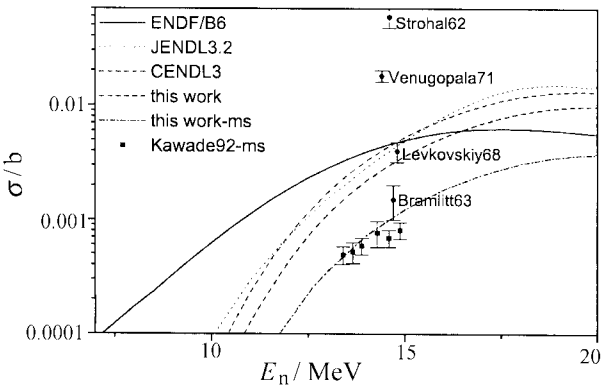


Fig. 5 (b) (n,α) reaction cross sections of $^{87}$Rb

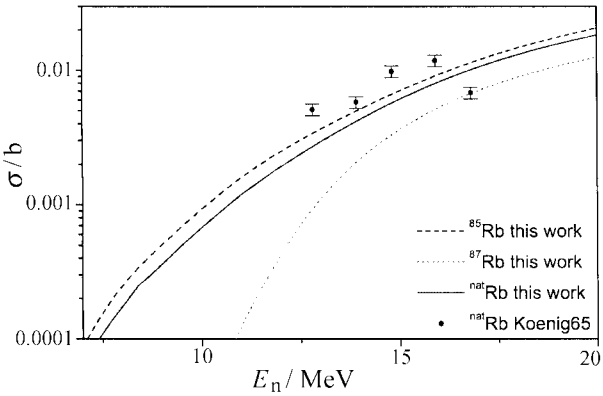


Fig. 5 (c) Inclusive (n.α) reaction cross sections of Rb

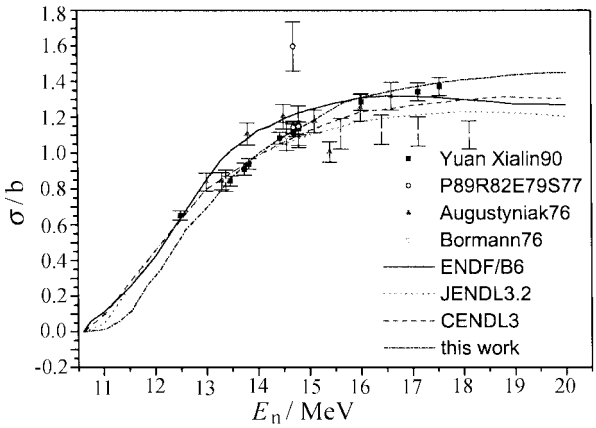


Fig. 6 (a) (n,2n) reaction cross sections of $^{85}$Rb

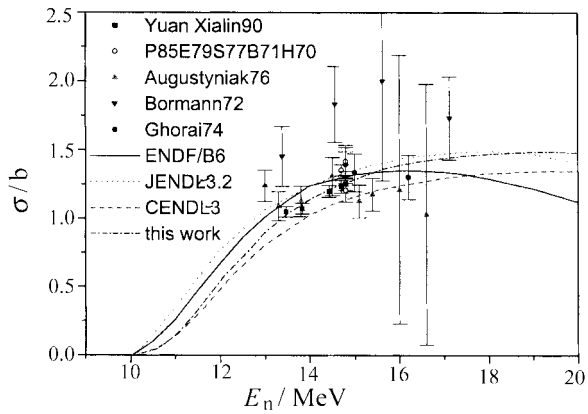


Fig. 6 (b) (n,2n) reaction cross sections of $^{87}$Rb

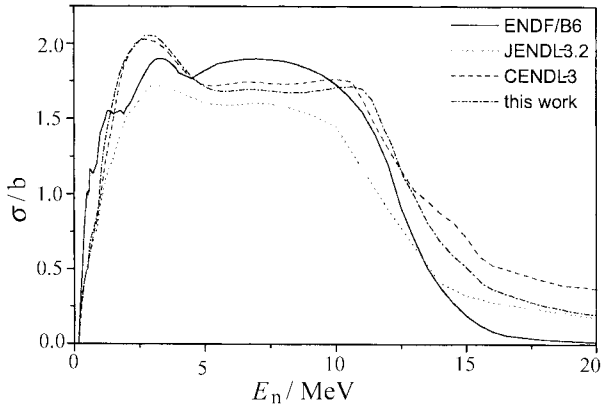


Fig. 7 (a) Inclusive cross sections of $^{85}$Rb

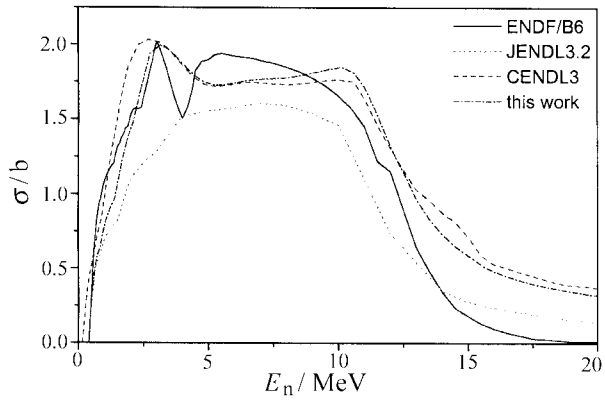


Fig. 7 (b) Inclusive cross sections of $^{87}$Rb

## References

[1] ZHANG Jingshang, User Manual of UNF Code , CNDC-0032, CNIC-01616, China Institute of Atomic Energy, P.O. Box 275(41), Dec. 2001; also New Functions in UNF Code and Illustration, Commu. Nucl. Data Progress (INDC(CRP)-053/L) No.25, p22, June 2001

[2] SHEN Qingbiao, A Code APMN for Automatically Searching Optimal Optical Potential Parameters below 300 MeV, Commu. Nucl. Data Progress (INDC(CRP)-053/L) No.25, p19, June 2001

[3] P.D.Kunz, A DWBA Code DWUCK4, University of Colorado, USA (unpublished)

# Evaluation of Complete Neutron Data for n+$^{169}$Tm Reactions below 20 MeV

CHEN Guochang YU Baosheng

*China Nuclear Data Center, CIAE, P.O.Box275(41), Beijing 102413 E-mail: cgc@iris.ciae.ac.cn*

【**abstract**】 *A complete set of neutron nuclear data, including cross sections, angular distributions, and secondary neutron spectra, of n+$^{169}$Tm reactions below 20 MeV were evaluated based on available experimental data and theoretically calculated results. The data are given in ENDF/B-6 format.*

## Introduction

Thulium-169 is a rare-earth element. Its reaction cross sections are a good indicator for nuclear science and technology applications; especially applied in astrophysics. However, there are no completely evaluated data in major evaluated nuclear data libraries in the world. The cross sections for $^{169}$Tm(n,tot), (n,el), (n,n′) (n,2n),(n,3n),(n,γ) and emission charged particle (n,x) reactions below 20 MeV were evaluated and calculated on the basis of experimental data at present work. The evaluated data can reproduce experimental data well.

## 1 Resonance Parameters

The resonance parameters referred to BNL-325 [1] and the evaluated data of ZHUANG Youxiang [2]. Here include 126 sets of resonance parameters. The cross sections at thermal energy are as follows:

$\sigma_{tot}$ =111.076 b; $\sigma_{el}$ =6.3 b; $\sigma_{\gamma}$ =104.776 b.

The cross sections of total, elastic scattering and gamma radiative capture were adjusted at boundary region in order to make the smooth cross sections connected with the calculated from resonance parameters. The relative deviations of the cross sections at boundary region are lower than $2\times10^{-4}$.

## 2 Evaluation of Smooth Cross Cections

The complete data for $^{169}$Tm up to 20 MeV were evaluated including cross sections of (n,γ), (n,2n), (n,3n) etc. The previous evaluation for $^{169}$Tm(n,*x*n) $^{166,167,168}$Tm reactions were performed up to 100 MeV. The emphasis of this evaluation is put on recommendation of these cross sections below 20 MeV.

### 2.1 $^{169}$Tm(n,2n) Reactions

There are many experimental data [3~15] from 8 MeV to 20 MeV; but there are large differences and discrepancies. The data were corrected and renormalized by using the present recommendation value[16] of the half-life and the branching ratio of the characteristic gamma ray of 198.24 keV for $^{168}$Tm, which are 93.1 day and 53.8±1.6%, respectively. At 14.6 MeV the evaluated data is 1946±24 mb; it was the normalization standard for this reaction.

J.Frehaut[11] used large Ge-loaded liquid scintillation to measure this reaction between 8.44 and 14.76 MeV, with $^{238}$U(n,f) cross section for determining the neutron flux, which was renormalized with that of ENDF/B-6; then the experimental result agreed with the data measured by LU Hanlin[14] and WANG Xiuyan[15] within error bar. B.P.Bayhurst[9] has measured this reaction in energy region of 8.65~24.47 MeV, 16.21~28.02 MeV and 26.03 MeV, respectively; in the energy region of 18~20 MeV the result is in agreement with the data measured by LU Hamlin[14] and WANG Xiuyan[15] within error bar.

The cross sections for $^{169}$Tm(n,2n)$^{168}$Tm reaction were measured by J.Frehaut [11], B.P.Bayhurst[9] and Wang Xiuyan[15] as well as Lu Hanlin [14] and adopted. Other experimental data were examined and corrected on the basis of the evaluated cross section at 14.6 MeV. The recommended data were obtained by fitting the adopted experimental data with polynomial .

### 2.2 $^{169}$Tm(n,3n) Reactions

B.P.Bayhurst[9] and R.L.Veeser[13] measured this reaction cross sections in energy region of 16.21~28.02 MeV and 16~24 MeV, respectively. In 1989, LU Hanlin[14] measured the same reaction in energy region of 15.09~18.21 MeV and the results are consistent with above mentioned within error bar from threshold to 20 MeV.

### 2.3 $^{169}$Tm(n,γ) Reactions

There are many experimental data[17~26] at thermal energy and in energy range from 0.19 keV to 3.0 MeV.

The liquid scintillation tanks were used to measure the prompt γ-ray of radiative capture events by R.C.Block[17] and J.H.Gibbons[18] in energy region of 0.19~7.0 keV and 0.0095~0.7 MeV, respectively. S.Joly[19], with NaI(Tl) spectrometer, measured in energy region of 0.52~3.0 MeV. After the 1980's, at Oak Ridge and Las Alamos laboratories average cross sections were measured by R.L.Macklin[20] in energy range from 0.003 to 2.0 MeV and there were different energy bins from 1 keV to 100 keV for different incident energy, using electron linear accelerator, and a sample of 24 cm in thick and 10 cm in diameter, a non-hydrogenous liquid scintillators. These data compared with the data measured by J.H.Gibbons[18] demonstrate that the J.H.Gibbons's[18] data are systematically higher than the results of R.L.Macklin[20].

The neutron radiative capture cross section in energy range from 0.158 to 1.47 MeV were measured it by JIANG Songsheng[21] with activation method using T(p,n) and $^{7}$LI(p,n) neutron source at 2.5 MV Van de Graaff accelerator at CIAE. The scintillation plastic anti-coincidence β-counter was used to measure the activity of $^{170}$Tm. Detection efficiency was calibrated by imitation source method[21]. The corrections of neutron multiple scattering in the target were calculated by the Monte-Carlo method. The standard cross sections for $^{197}$Au(n,γ)$^{198}$Au reaction were taken from the evaluated by himself. Then for present work, the standard cross section was corrected with the cross section of ENDF/B-6; so the corrected cross sections dropped about 2.7% and 5.4% at 0.45 and 0.55 MeV, respectively. The cross sections measured by JIANG Songsheng[21] are lower than the results of R.L.Macklin[20].

On the other hand, XU Haishan[22] of Sichuan University measured the cross sections at 1.01, 1.21 and 1.44 MeV. A large liquid scintillation detector was used for cross section measurements. In order to reduce background due to neutron capture in the hydrogen of the liquid scintillation detector, only those pluses were counted in coincidence between the two half sphere of the detector. The standard cross section of $^{197}$Au(n,γ) $^{198}$Au was corrected with the cross section of ENDF/B-6. The data are consistent with those of JIANG Songsheng[21].

The measurements in energy region of 11.2~100 keV were carried out at 2.5 MV Van de Graaff accelerator of Sichuan University by using two Moxon-Rae detectors by XIA Yijun[23]. At 23 keV the measurement was carried out by K.Siddappa [24]; however, discrepancy of the results was published in different references.

The thermal cross section was measured by LUO Dexing[25] and G.H.E.Sims[26], respectively. LUO Dexing[25] used the same method as that of JIANG Songsheng[21]. The data of G.H.E.Sims[26] was deduced indirectly. The thermal cross section is consistent between two laboratories within error bar. The value measured by LUO Dexing[25] was adopted.

The radioactive capture cross sections for $^{169}$Tm(n,γ)$^{170}$Tm reaction were measured by XIA Yijun[23], Jiang Sonsheng[21] and LUO Dexing[25] as well as S.Joly[19], those data were adopted. On the other hand, other measured data were examined and corrected on the basis of the data measured by CIAE[21] and Sichuan University[22~23]. The recommended data were obtained by fitting the adopted experimental data with polynomial .

### 2.4 $^{169}$Tm(n,x) Reactions

There is only an experimental data[27] of 1.7±0.2 mb at 14.7 MeV for $^{169}$Tm(n,α) $^{166}$Ho reaction. Therefore all the theoretical calculated data of $^{169}$Tm(n,x) reactions were adopted.

## 3 Theoretical Calculation and Recommendation

### 3.1 Theoretical calculation

This work applied EMPIRE-2 code[28] to calculate the cross sections of (n,tot), (n,n), (n,n′), (n,γ), (n,2n), (n,3n), etc. In theoretical calculation, a set of optimum neutron sphere optical parameters and Konning's optical potential parameters for proton were selected from RIPL-2 library[29] in the energy range from 1 keV to 20 MeV for $^{169}$Tm. The Gilbert-Cameron level density formula was used. In all nuclei the level density parameters were accorded with Authur systematics. Ignatyuk proposed the general calculation formula form of this dependence. The expression is as follows:

$$a(u)=\tilde{a}(1+f(u)\frac{\delta w}{u})$$

Where $\delta w$ is the shell correction, $\tilde{a}$ is the asymptotic value of the $a$-parameter and

$$f(u)=1-\exp(-\gamma u)$$

The Authur systematics available in EMPIRE-II[28] is $\tilde{a}=0.1375A-8.36\times10^{-5}A^2$ and $\gamma=0.054$. Multi-step direct and multi-step compound mechanisms were taken into account in this calculation. ORION and TRISTAN codes were applied to calculate the multi-step direct mechanism. On the other hand, NVWY formulation of the multi-step compound progress with γ-emission was implemented in the calculation. DEGAS code for exciton model with angular momentum conservation and γ-emission was included. In addition, ECIS95 code[30] was applied to calculate the direct inelastic scattering cross sections.

The code SUNF[31] was also used for theoretical calculation. The same optical potential parameters of neutron were used. Adjusting the parameters of neutron optical potential parameters, the relevant level density, pair correction value and giant dipole resonance parameters, the cross sections of (n,tot), (n,n), (n,n′), (n,γ), (n,2n), (n,3n) and (n,x) were calculated by SUNF[31] code and the direct inelastic scattering cross sections were calculated by DWUCK4[32] and ECIS95[33] code.

### 3.2 Theoretical Calculation Results and Recommendations

On the whole, the theoretical calculated results of EMPIRE-2[28] code were similar with those of SUNF[31] code; especially, for the cross sections of (n,tot), (n,n), (n,2n) etc. in the energy range from threshold to 20 MeV. Fig.1 shows the comparison of neutron total cross sections between the theoretical calculated data of EMPIRE-II[28] and the measured data[34] in the energy range from 1 keV to 20 MeV. Fig. 2~3 show the comparison of the cross sections of $^{169}$Tm(n,2n), (n,γ) reactions between the recommended data and the measured data, respectively. The cross sections of $^{169}$Tm(n,3n) reaction were recommended after adjusting other cross sections; it is similar with that of Fendl/A-2.0[35], and shown in Fig. 4. The cross sections of $^{169}$Tm(n,n′) reaction were adopted from the theoretical calculated data of EMPIRE-2[28], and shown in Fig. 5. The cross sections of $^{169}$Tm(n,x) reactions were adopted from the theoretical calculated data of EMPIRE-2[28], and shown in Fig. 6. Fig. 7~9 show the secondary neutron spectra of (n,2n), (n,3n) and (n,n') to continuous state, respectively.

## Acknowledgments

Thanks to the Chinese Nuclear Data Center for its support. The acknowledgments are also extended to Drs. WANG Shunuan, ZHUANG Youxiang, LIU Tingjin, GE Zhigang, ZHANG Zhengjun, and SUN Zhengjun etc. for their helpful discussions and instructions.

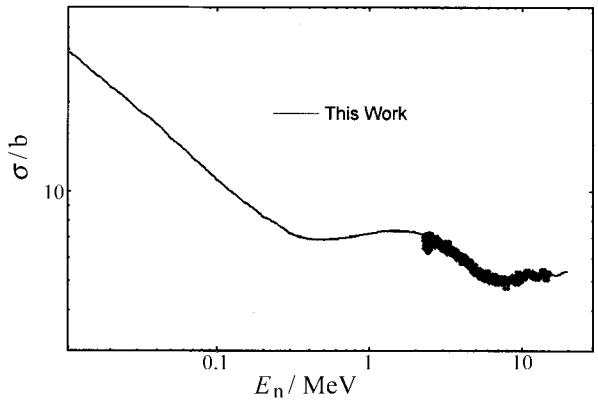


Fig. 1 Comparison between evaluated and measured data for $^{169}$Tm(n,tot)

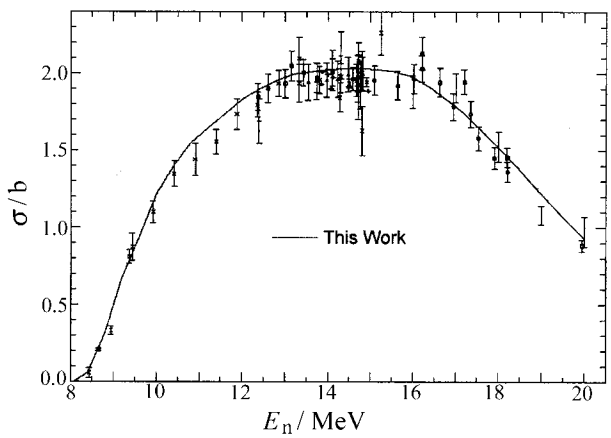


Fig. 2 Comparison between evaluated and measured data for $^{169}$Tm(n,2n)

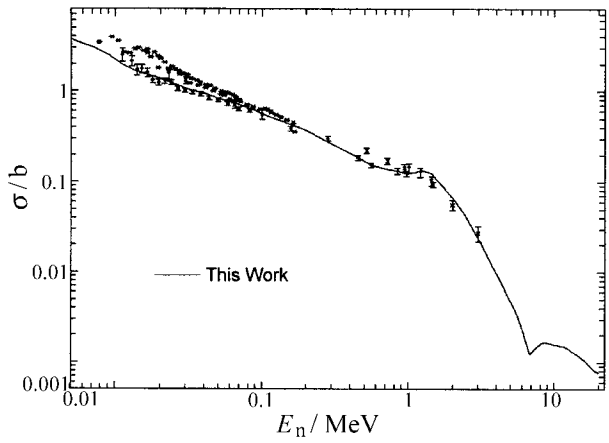


Fig. 3 Comparison between evaluated and measured data for $^{169}$Tm(n,γ)

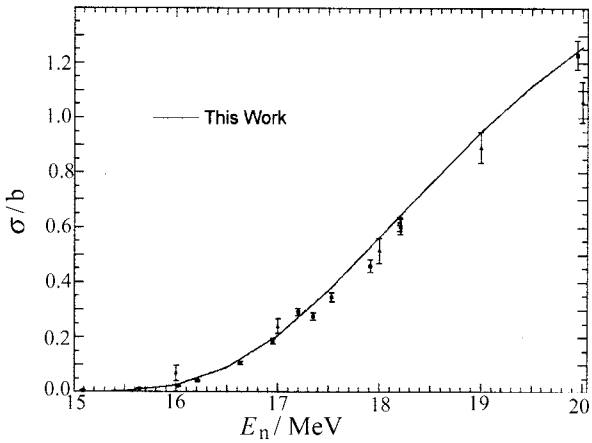


Fig. 4 Comparison between evaluated and measured data for $^{169}$Tm(n,3n)

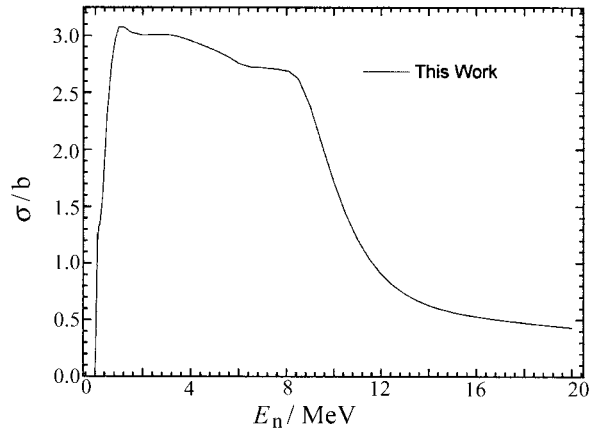


Fig. 5 The cross section of $^{169}$Tm(n,n′) reaction

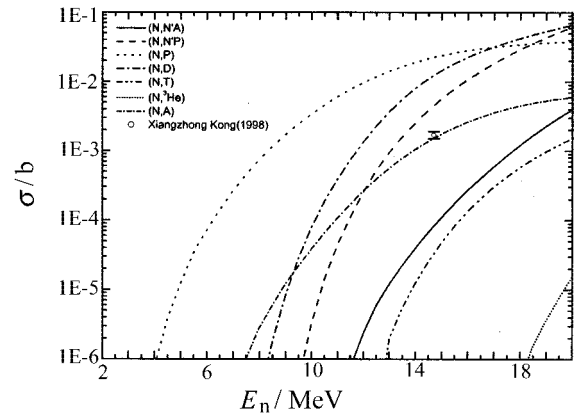


Fig. 6 Comparison between evaluated and measured data for $^{169}$Tm(n,x)

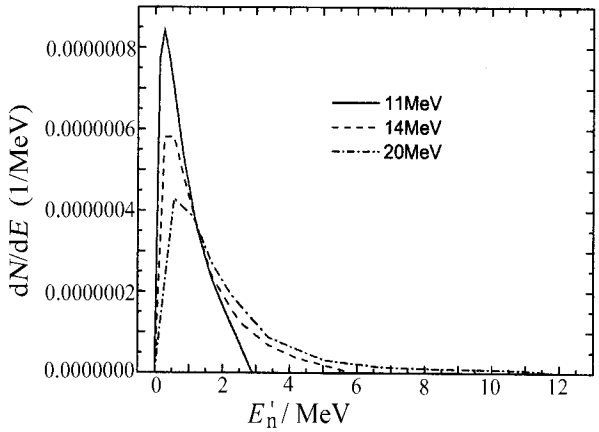


Fig. 7 Normalized secondary neutron spectra of $^{169}$Tm(n,2n) reaction

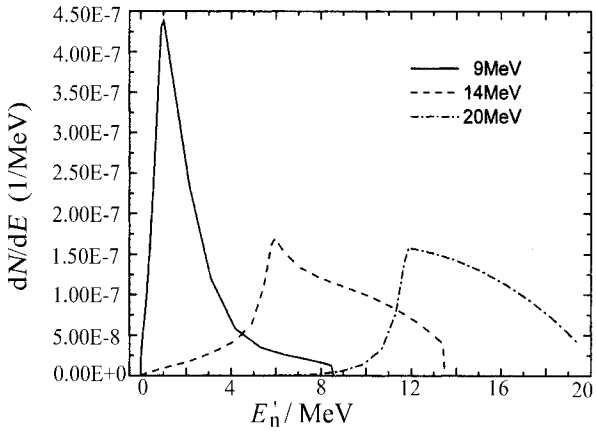


Fig. 8 Normalized secondary neutron spectra of $^{169}$Tm(n,n') to continuous state

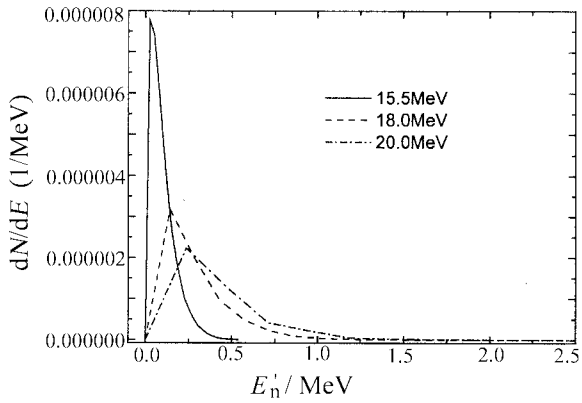


Fig. 9 Normalized secondary neutron spectra of $^{169}$Tm(n,3n) reaction

## References


[1] BNL-325, Third Edition,Volume II (1976)

[2] Youxiang Zhuang et al., Private communication (2001)

[3] W.Dilg et al., J,NP/A,118,9 (1968)

[4] A.A.Druzhinin et al., EXFOR DATA No.40171 (1971)

[5] D.R.Nethaway et al., NP/A,190,635, (1972)

[6] D.S.Mather et al., AWRE-O-72/72, (1972)

[7] R.Vos et al., EXFOR DATA No.13037, (1973)

[8] S.M.Qaim et al., EXFOR DATA No.20541, (1974)

[9] B.P.Bayhurst et al., EXFOR DATA No.10536, (1975)
[10] L.R.Greenwood et al., EXFOR DATA No.12977, (1987)
[11] J.Frehaut et al., EXFOR DATA No.20416, (1980)
[12] J.Laurec et al., EXFOR DATA No. 21709, (1981)
[13] L.R.Veeser et al., EXFOR DATA No. 10445, (1977)
[14] Lu Hanlin et al., EXFOR DATA No. 30724, (1989)
[15] Wang Xiuyuan et al., EXFOR DATA No. 30935, (1989)
[16] Xiaolong Huan et al.,Chart of nuclide (2000)
[17] R.C.Block et al., EXFOR DATA No.11935, (1961)
[18] J.H.Gibbons et al., EXFOR DATA No.11329, (1961)
[19] S.Joly et al., NSE, 70, (1), 53, (1979)
[20] R.L.Macklin et al., NSE, 78, 110, (1981)
[21] Songsheng Jiang et al., J,CNP,4,(2),136,8205, (1982)
[22] Haishan Xu et al., J,CNP,9,(2),127,8705, (1986)
[23] Yijun Xia et al., J,CNP,11,(2),75,8905,(1988)
[24] K.Siddappa et al., EXFOR DATA No.30248, (1974)
[25] Dexing Luo et al., J, CNP, 6, (1), 84, 8402, (1984)
[26] G.H.E.Sims et al., J,JIN,32,2839,7010, (1970)
[27] Xiangzhong Kong et al., EXFOR DATA No.31497, (1998)
[28] M.Herman et al., EMPIRE-II Statistical model code for nuclear reaction calculation (2002)
[29] IAEA-CRP, Reference Input Parameters Library (RIPL), IAEA-TECDOC-1034, (1998)
[30] J.Raynal etal., Notes on ECIS, (1994)
[31] Jingshang Zhang et al., CNDP, 17 (1997)
[32] P.D.Kunz et al., “Distorted wave code DWUCK4”, University of Colorado, USA
[33] Shunuan Wang, ECIS-95 for PC of CNDC
[34] D.G.Foster Jr et al., J,PR/C,3,576, 197102
[35] Fendl/A-2.0, NDS/IAEA-2000. http://www-nds.iaea.org/fendl2apic/6969/6969.htm

# The Evaluation of Cross Sections for n+$^6$Li Reaction

ZHUANG Youxiang JIN Yongli WANG Jimin

*China Nuclear Data Center, CIAE, P.O.Box 275(41), Beijing 102413 e-mail: yxzhuang@iris.ciae.ac.cn*

**【abstract】** *Neutron nuclear data of $^6$Li are important for fusion neutronics calculation. Therefore, the cross sections for n+$^6$Li reaction are evaluated in the energy range from $10^{-5}$ eV to 20 MeV. In the evaluation, $^6$Li(n, d + n)$^4$He and $^6$Li(n, d + n)$^4$He reactions are included. It is concluded that there is really only the second excited level (3.562 MeV) in the inelastic scattering, no assumed levels were taken into account. The evaluated data describe the real process of n + $^6$Li reactions and improve the existing evaluated libraries such as ENDF/B-6 and JENDL-3.*

## Introduction

Nuclear energy such as fusion reaction is a more important energy resource in future. Study of the nuclear data pertaining to the fusion reactors has grown to be one of the smart and interesting fields.

Neutron nuclear data of $^6$Li are important for fusion neutronics calculation. In particular the $^6$Li(n,t) $^4$He as well as $^7$Li(n,n't) $^4$He reaction cross sections control the tritium-production rate in fusion blankets. The $^6$Li(n,α) $^3$H reaction cross section is also used as the standard. Although the data of $^6$Li are included in some evaluated nuclear data files, including CENDL-2.1, there are following matter to be studied further:

(1) For inelastic scattering (n,n'γ), only the second excited level (3.562 MeV) really takes place; however, many assumed levels were taken into account, in order to cover (n,n'd) cross section.

(2) The $^6$Li(n,d+n)$^4$He and $^6$Li(n,n+d)$^4$He reaction channels are simply included in inelastic scattering reaction, (n,n'd) and (n,n'γ) are different reactions channels and should not be put together. Both deuteron and triton are important for fusion.

This report describes the evaluation of cross sections for n + $^6$Li reaction.

## 1 Neutron Reaction Cross Sections

### 1.1 Thermal Cross Section

The cross sections at 2200 m/s are as follows:

Total cross section $\sigma_t$ =941.6930 b
Elastic scattering $\sigma_s$ =0.6716 b
Radiative capture $\sigma_\gamma$ =0.0385 b
(n,α) cross section $\sigma_\alpha$ =940.9829 b

The (n,γ) and (n,α) cross sections were taken from BNL-325[1], and the elastic scattering (n,n) cross section was taken from ENDF-B-6[2] .

### 1.2 Total Cross Section

Below 3 MeV, the data were taken from R-matrix analysis by Hale, Dodder and Witte[3], which took into account the data of all reactions possible of $^7$Li system up to 4 MeV neutron energy. Total cross section data considered in this analysis were those of J.A.Harvey and N.W.Hill[4] and A.B.Smith et al.[5]. Between 3 and 20 MeV, the data follows the measurements of A.B.Smith et al.[6], J.D.Kellie et al.[7], H.H.Knitter et al.[8], C.A.Goulding et al.[9] and D.G.Foster et al.[10].

### 1.3 Elastic Scattering Cross Section

Below 3 MeV, the values were taken from R-matrix analysis by Hale, Dodder, and Witte[3], which includes the elastic scattering data measured by A.B.Smith et al.[6] and R.O.Lane et al.[11]. Above 3 MeV, the curve is a smooth representation of the data of H.D.Knox et al.[12], and R..Batherlor et al.[13] up to 7.5 MeV, and of that of H.H.Hogue et al.[14] between 7.5 and 13 MeV. The curve passes through the average of several measurements at 14 MeV, and is extrapolated to 20 MeV using the shape of an optical model calculation.

### 1.4 Inelastic Scattering Cross Section

$^6$Li(n,n'γ) $^6$Li inelastic scattering reaction takes place only through the second excited level (3.562 MeV). There are two sets of available experimental data measured by G.Presser et al.[15] and Besotosnyj et al[16]. A smooth curve was recommended, which was drawn through these data and from 7 to 20 MeV by eye guide, see Fig. 1.

### 1.5 $^6$Li(n,d+n) $^4$He and $^6$Li(n,n+d) $^4$He Reaction Cross Section

The $^6$Li(n,d+n) $^4$He and $^6$Li(n, n+d) $^4$He reactions include the following three channels:

(a) $n+^6Li \rightarrow n'+^6Li^*$, $Q$= –2.19 MeV, $^6Li^* \rightarrow d+\alpha$

(b) $n+^6Li \rightarrow d+^5He$, $Q$=–2.36 MeV, $^5He \rightarrow n+\alpha$

(c) $n+^6Li \rightarrow n+d+\alpha$ , $Q$=–1.47 MeV

The evaluated cross section is mainly based on the data of S.Chiba et al.[17], P.W.Lisowski et al.[18], J.C.Hopkins et al.[19] and R.Batherlor et al.[13], and the consistency of all cross sections. The evaluated result is shown in Fig. 2.

### 1.6 $^6$Li(n,2np) $^4$He Reaction Cross Section

The $^6$Li(n,2np) $^4$He reactions include the following five mechanisms:

(a) $n+^6Li \rightarrow n'+^6Li^*$, $Q$=–5.37 MeV, $^6Li^* \rightarrow p+^5He(n+\alpha)$

(b) $n+^6Li \rightarrow p+^6He$, $Q$=–2.73 MeV, $^6He \rightarrow n+n+\alpha$

(c) $n+^6Li \rightarrow n+n+p+\alpha$, $Q$=–3.70 MeV

(d) $n+^6Li \rightarrow 2n+^5Li$, $Q$=–5.66 MeV, $^5Li \rightarrow p+\alpha$

(e) $n+^6Li \rightarrow n+p+^5He$, $Q$=–4.59 MeV, $^5He \rightarrow n+\alpha$

Concerning the (n,2np) reactions, two sets of experimental data of (D.S.Mather et al.[20], V.J.Ashby et al.[21]), which were obtained by the coincident counting method, are available. The recommended curve passes through the point of Mather et al. at 14 MeV, taking into account the measurements of Ashby et al.

### 1.7 $^6$Li(n,γ)$^7$Li Radiative Capture Reaction Cross Section

The (n,γ) reaction cross section is based on the datum at thermal energy measured by E.T.Jurney[22], and the cross section was extrapolated as $1/v$ up to 200 keV, i.e.,

$$\sigma_{n,\gamma}=6.12*10^{-3}\ [E_n(\mathrm{eV})]^{-1/2}\ \text{barns.}$$

The Pendlebury's evaluation[23] at high energies was adopted.

### 1.8 $^6$Li (n,p) $^6$He Reaction Cross Section

The (n,p) cross sections were measured by G.Presser et al.[15] in the energy range from 3.1 MeV to 9.0 MeV with the activation method. Above 9 MeV, several measurements[24~27] were performed at 14 MeV. The evaluated cross sections are on the basis of the data of G.P.resser et al. from threshold to 9 MeV, extended to 20 MeV through the 14 MeV data of Ref. [22] and [23].

### 1.9 $^6$Li (n,t) $^4$He Reaction Cross Section

$^6$Li (n,t) $^4$He reaction cross section of ENDF/B-6 is used as the standard, therefore it was taken from ENDF/B-6.

## 2 Concluding Remarks

The neutron cross sections of $^6$Li were evaluated in the energy range from $10^{-5}$ eV to 20 MeV.

The major changes are as follows:

(1) $^6$Li(n,d+n) $^4$He and $^6$Li(n,n+d) $^4$He reactions are included.

(2) There is only the second excited level (3.562 MeV) in the inelastic scattering really, no assumed levels were taken into account.

The evaluated data describe the real process of $n+^6Li$ reactions and improved the mentioned-above matters of the existing evaluated libraries such as ENDF/B-6 and JENDL-3. The comparisons between them were given.

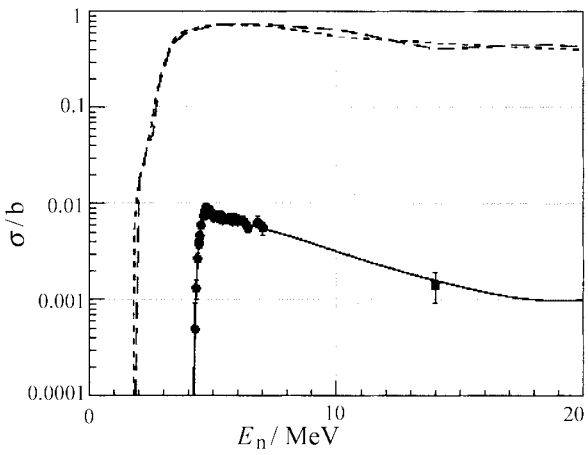


Fig. 1 $^6$Li(n, n'γ) $^6$Li total inelastic scattering reaction

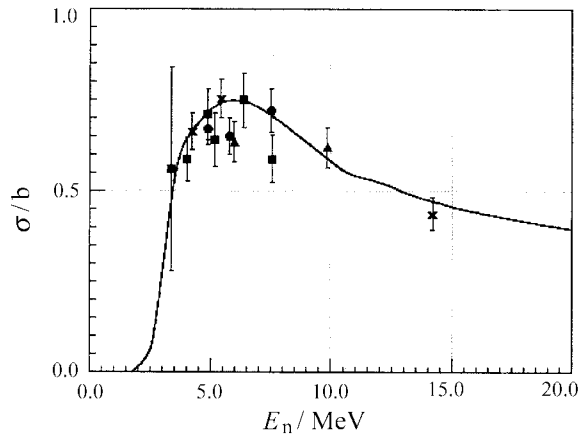


Fig. 2 $^6$Li(n,nd) $^4$He reaction cross section

### References

[1] S.F.Maghabghab, et al., BNL-325, 4th edition, 1981

[2] G.M.Hale and P.G.Young, ENDF-201, p.18, 1999

[3] G.M.Hale, IAEA TECDOC-335, 103, 1984

[4] J.A.Harvey and N.W.Hill, Washingto75, 244, 1975
[5] A.B.Smith et al., ANL/NDM-29, 1977
[6] A.B.Smith et al., Nucl. Phys. A373, 305, 1982
[7] J.D.Kellie et al., Knoxville77, 48, 1977
[8] H.H.Knitter et al., EUR5726e, 1977
[9] C.A.Goulding and P.Stoler, EANDC(US)-176U, 161, 1972
[10] D.G.Foster and D.W.Glasgow, Phys. Rev. C3, 576, 1971
[11] R.O.Lane et al., Ann. Phys. 12, 135, 1961
[12] H.D.Knox et al., N.S.E. 69, 223 1979
[13] R.Batchelor and J.H.Towle, Nucl. Phys. 47, 385, 1963
[14] H.H.Hogue et al., N.S.E. 69, 22, 1979
[15] G.Presser et al., Nucl. Phys. A131, 679, 1969
[16] Besotosnyj et al., YK-19, 77, 1975
[17] S.Chiba et al., J. Nucl. Sci. and Tech. 22, 771, 1985
[18] P.W.Lisowski et al., LA-8342, 1980
[19] J.C.Hopkins et al., Nucl. Phys. A107, 139, 1968
[20] D.S.Mather and L.F.Paine, AWRE-O-47/69, 1969
[21] V.J.Ashby et al., Phys. Rev. 129, 1771, 1963
[22] E.T.Jurney, LASL, Private Communication, 1973
[23] E.D.Pendlebury, AWRE-O-60/84, 1964
[24] M.E.Battat and F.L.Ribe, Phys. Rev. 89, 80, 1953
[25] G.M.Frye, Phys. Rev. 93, 1086, 1954
[26] R.Prasad et al., Nuovo Cimento, A3, 467, 1971
[27] F.Merchez et al., Nucl. Phys. A182, 428, 1972

# Re-Evaluation of Neutron Data for $^{89}$Y below 20 MeV

CAI Chonghai

*Department of Physics, Nankai University, Tianjin 300071, P.R.China*

【**abstract**】 *The neutron data, including all kinds of cross sections, especially the cross sections of the isomeric states in (n,γ) and (n,α) section channels, angular distributions of elastic scattering, energy spectra and/or double-differential cross sections of all emitted particles, gamma production data (production cross sections and multiplicity, energy spectra) in n+$^{89}$Y reaction below 20 MeV were calculated and evaluated. In most cases, except the channel of (n,p) reaction, the calculated cross sections are in good agreement with the measurements.*

$^{89}$Y is the only stable isotope of element yttrium, which is a fission production nucleus.

There are a few evaluated files for $^{89}$Y, such as in ENDF/B-6 and JENDL-3.2 as well as in CENDL-3; all of them do not contain double-differential cross sections and gamma production data, meanwhile something still needs to be improved. The calculations of $^{89}$Y for CENDL-3 in 1997, did not analyze the experimental data coming from different authors and different years carefully. Based on the newer and more reliable experimental data, as well as the data on isomeric states, the reevaluation of n+$^{89}$Y was performed to improve the neutron reaction data including double-differential cross sections and gamma production data in ENDF/B-6 format. In this paper the comparison with experimental data, the methods, parameters used in the model calculation and part of cross sections, secondary neutron energy spectra, angular distributions and double-differential cross sections are given. All the experimental data in figures were taken from EXFOR.

## 1 Direct Inelastic Contribution, Optical Potential and Other Parameters

Firstly, the program APMN[1] was used to search the optimal optical potential parameters of n+$^{89}$Y automatically by fitting the experimental data, such as total cross sections (C.Budtz-Jorgensen in 1984, W.P.Poenitz in 1983, D.G.Foster in 1971 and J.F.Whalen in 1968), elastic scattering cross sections (F.G.Perey in 1970, J.H.Towle in 1969, N.A.Bostrom in 1959) and their angular distributions on 60 energy points distributing from 0.889 to 21.6 MeV (G.Schreder in 1989, S.Mellema in 1987, R.D.Lawson in 1986, G.M.Honore in 1986, C.Budtz-JOrgensen in 1984, Y.Yiming in 1982, F.D.Mcdaniel in 1977, V.I.Trykova in 1975, S.A.COX in 1972, M.E.Gurtovoj in 1971 and F.G.Perey in 1970). In order to make the calculated (n,p), (n,d) and (n,α) reaction cross sections in good agreement with experimental data. We also need adjusting some optical potential parameters in proton, deuteron and alpha channels by hand. The optical potential parameters as the input parameters in the main code UNF[2] are given in Table 1.The meaning of all the optical potential parameters can be found in Ref. [1]. The same neutron optical potential parameters are also used in the calculations of the direct inelastic cross sections as well as the Legendre coefficient of their angular distributions with Dwuck4[3]. Levels and their deformation parameters $\beta_2$ used in direct inelastic calculation are given in Table 2.

Besides the optical potential parameters, the direct inelastic cross sections as well as the Legendre coefficients of angular distributions are also the input data for the main code UNF. In UNF code, Gilbert-Cammeron formula is employed for calculation of the level density. The level density parameter $a$, the pair energy correction $\Delta$ and the two peak giant resonance parameter for gamma emission were obtained from the Parameters Library in CNDC by using PREUNF code[4]. The data of levels and their spin, parity and the branch ratio of gamma emission were taken from the Parameters Library in CNDC and/or the Web of NNDC at BNL, USA. In order to make the calculated cross sections in good accordance with experimental data, some of the level density parameters $a$ and the pair energy corrections $\Delta$ need to be adjusted. The $a$ and $\Delta$'s values used in the final calculations are given in Table 3.

Besides parameters mentioned above, Kulbach parameter in exciton model CK=5500.0 the adjustable factor in (n,γ) cross section calculation CE1=5.5, and the adjustable parameter in direct (n,γ) calculation DGM=0.35 were used.

**Table 1 Optical potential parameters of $^{89}$Y used in this work**

| channel | n | p | alpha | $^3$He | d | t |
|---|---|---|---|---|---|---|
| $a_r$ | 0.6493890 | 0.47 | 0.52 | 0.72 | 0.71 | 0.72 |
| $a_s$ | 0.4711004 | 0.45 | 0.55 | 0.88 | 0.70 | 0.84 |
| $a_v$ | 0.6243670 | 0.45 | 0.55 | 0.88 | 0.70 | 0.84 |
| $a_{so}$ | 0.6493890 | 0.47 | 0.52 | 0.72 | 0.71 | 0.72 |
| $r_r$ | 1.2497820 | 1.16 | 1.40 | 1.20 | 1.30 | 1.20 |
| $r_s$ | 1.3129580 | 1.14 | 1.39 | 1.40 | 1.35 | 1.40 |
| $r_v$ | 1.2393860 | 1.14 | 1.39 | 1.40 | 1.35 | 1.40 |
| $r_{so}$ | 1.2497820 | 1.01 | 1.40 | 1.20 | 0.64 | 1.20 |
| $r_c$ | 1.3000000 | 1.25 | 1.30 | 1.30 | 1.30 | 1.30 |
| $W_{v0}$ | -0.1708760 | -2.70 | 22.4 | 0.0 | 0.0 | 0.0 |
| $W_{v1}$ | 0.1160180 | 0.22 | 0.0 | 0.0 | 0.0 | 0.0 |
| $W_{v2}$ | -0.0338120 | 0.0 | 0.0 | 0.0 | 0.0 | 0.0 |
| $V_0$ | 52.776480 | 54.0 | 164.7 | 151.9 | 90.6 | 165.0 |
| $V_1$ | -0.5965391 | -0.32 | 0.0 | -0.17 | 0.0 | -0.17 |
| $V_2$ | 0.01366303 | 0.0 | 0.0 | 0.0 | 0.0 | 0.0 |
| $V_3$ | -24.00000 | 24.0 | 0.0 | 50.0 | 0.0 | -6.4 |
| $V_4$ | -0.01222399 | 0.4 | 0.0 | 0.0 | 0.0 | 0.0 |
| $V_{so}$ | 6.200000 | 6.2 | 0.0 | 2.5 | 7.13 | 2.5 |
| $W_{s0}$ | 7.310210 | 11.8 | 0.0 | 41.7 | 12.0 | 46.0 |
| $W_{s1}$ | 0.1593175 | -0.25 | 0.0 | -0.33 | 0.0 | -0.33 |
| $W_{s2}$ | -12.00000 | 12.0 | 0.0 | 44.0 | 0.0 | -110.0 |

And $a_{s1}$=0.7, $a_{v1}$=0.7 for proton.

**Table 2 Levels and deformation parameters $\beta_2$ used in direct inelastic calculation**

| Level / MeV | $J$ | $\pi$ | $\beta_2$ |
|---|---|---|---|
| 1.50741 | 1.5 | -1 | 0.085 |
| 1.74474 | 2.5 | -1 | 0.085 |
| 2.88153 | 1.5 | -1 | 0.085 |
| 3.06776 | 1.5 | -1 | 0.085 |
| 3.10726 | 2.5 | -1 | 0.085 |
| 3.13890 | 2.5 | -1 | 0.085 |

**Table 3 The *a* and *Δ*'s values used in our final calculations**

| channel | (n,γ) | (n, n') | (n, p) | (n,α) | (n,$^3$He) | (n,d) |
|---|---|---|---|---|---|---|
| *a* | 9.53280 | 10.37206 | 8.78813 | 12.75302 | 9.81221 | 10.46237 |
| *Δ* | -0.9000 | +0.4000 | -3.0500 | -1.1400 | +1.4000 | -2.65 |
| channel | (n, t) | (n, 2n) | (n, nα) | (n, 2p) | (n, 3n) | |
| *a* | 11.18263 | 11.75555 | 10.61140 | 9.97920 | 9.61023 | |
| *Δ* | +0.3000 | -2.2000 | +0.2000 | -1.3000 | -1.0000 | |

## 2 Calculated Results, Evaluation and Discussion

By using the input parameters mentioned above, all kinds of the files were calculated with the code UNF firstly. The resonance parameters below 0.15 MeV were taken from ENDF/B-6. The values of $\sigma_{tot}$ and $\sigma_{el}$ below 0.65 MeV were also taken from ENDF/B-6, which are fluctuated rapidly. In order to make our calculated values smoothly connecting with those in resonance region, the values of $\sigma_{tot}$ and $\sigma_{el}$ within 0.65~1.1 MeV were adjusted, which are shown in Figs 1,2, respectively.

The evaluated $\sigma_{tot}$ , $\sigma_{el}$ and those of ENDF/B-6 and CENDL-3 are all in good agreement with experimental data, while those of JENDL-3.2 are not in good accordance with experimental data in $E_n$ > 8 MeV energy region. The angular distributions of elastic scattering at 8 energy points are given in Fig. 3a, 3b and 3c, respectively. The results show that our calculated values are in good accordance with experimental data for every energy points, the angular distributions at other 52 energy points not given in Fig. 3, which are also in same good agreement with experimental data as in Fig. 3.

The continuous inelastic neutron spectra are shown in Fig. 4, from which one can see that the calculated values and CENDL-3 are in good accordance with experimental data. The comparisons of the calculated double-differential cross sections of inelastic scattering with their experimental data at $E_n$=9.1, 7.94 and 7.02 MeV for 5 angles (30, 60, 90, 120 and 150 degree) are shown in Figs. 5a, 5b and 5c, respectively. At higher emitted neutron energies corresponding to discrete levels, we cannot make the calculated values in very good agreement with experimental data. There are no data of double-differential cross sections given in the ENDF/B-6, JENDL-3.2 and previous CENDL-3.

The (n,γ) reaction cross sections are shown in Fig. 6, which indicate that our evaluation values (basically the calculated values are adopted, only increase a little within 1.7~3.5 MeV based on experimental data and decrease a little within 0.15~0.18 MeV to connect with ENDF/B-6) are in very good accordance with experimental data; the calculated $\sigma_{n,\gamma}$ cross section of the isomeric state (0.6817 MeV, $J^{\pi}=7^{+}$, $T_{1/2}$=3.19 hour) is also in good agreement with experimental data except in 0.97~1.5 MeV energy region, where the calculated values are lower than experimental data.

The (n,n') reaction cross sections are shown in Fig. 7. the evaluation values (basically the calculated values are adopted, but in $E_n$ < 1.53 MeV region they are lower than the experimental data given by C.P.SWANN in 1955, so we took the values from CENDL-3 to replace the calculated values).

The (n,2n) reaction cross sections are shown in Fig. 8. In $E_n$<16 MeV region, our calculated values are not in good agreement with experimental data as ENDF/B-6, JENDL-3.2 and CENDL-3, so we took the values from CENDL-3 as the reevaluation data. In $E_n$>16 MeV energy region, considering the newer and more reliable experimental data given by HUANG Jianzhou in 1989, our calculated values are reasonable.

Fig. 9 shows the (n,p) reaction cross section. One can see that the data given by H.A.Tewes in 1960 are lower than that given by B.P.Bayhurst in 1961. The later is more reliable because near 14.5 MeV with about equal values given by N.I.Molla in 1998, so all 3 evaluated files ENDF/B-6, JENDL-3.2 and CENDL-3 gave their recommend values based on these 2 sets. Our calculated $\sigma_{n,p}$ is not in reasonable shapes, which with a small peak near 3.5~4.0 MeV, drop rapidly and form a turning line segment near 17 MeV and rise much faster in 5~11 MeV energy region than all 3 evaluated files. The reason is not yet clear at this moment, the UNF code usually gives correct and reasonable calculation results for most cases, the (n,p) channel of $^{89}$Y is a special exception case. Considering the physical reasonableness, the evaluated values for $\sigma_{n,p}$ are based on the experimental data given by N.I.Molla et al. in 1998 and by B.P.Bayhurst et al. in 1961, and give the evaluation values for inclusive $\sigma_{n,p}(=\sigma_{n,p}+\sigma_{n,,np})$ based on the experimental data given by Haight in 1981, then the evaluation values for $\sigma_{n,np}$(= inclusive $\sigma_{n,p}-\sigma_{n,p}$) were obtained.

Fig. 10 gives the (n,α) reaction cross sections, in which the data given by H.A.Tewes in 1960 is apparently lower than other experimental data, the three data near 14.5 MeV given by E.T.Bramlitt in 1963, by F.STROHAL in 1962 and by E.B.Paul in 1953, respectively, are very divergent, all of them should be given up. JENDL-3.2 and CENDL-3 have their recommended values based on the data given by B.P.Bayhurst in 1961 and other three data near 14.5 MeV given by A.Grallert in 1993 and by L.R.Greenwood in 1987, respectively. But they did not use the newest measured data given by A.A.Filatenkov in 1999. Both of our calculated (i.e. evaluated) $\sigma_{n\alpha}$ and that corresponding to residual nucleus in isomeric state (0.55605 MeV, $J=6^{-}$, $T_{1/2}$=1.017 min) are in very good agreement with experimental data given by A.A.Fllatenkov in 1999.

Fig. 11 gives the (n,d) reaction cross sections, all of ENDF/B-6, CENDL-3 and our calculated (i.e. evaluated) values pass the only one experimental data given by R.C.HAIGHT in 1981 with the different shape.

The version 2001 of the code UNF have many

improved functions, with which and based on some newer experimental data, the recalculations for neutron reaction data of n+$^{89}$Y below 20 MeV were performed and improved. For some special cases, such as the ascending segment of $\sigma_{n,2n}$ in $E_n$ < 16 MeV energy region and $\sigma_{n,n'}$ below 1.53 MeV, our calculated values is not so good as in CENDL-3, so the recommend values in CENDL-3 were adopted in our evaluation. For $\sigma_{n,p}$, $\sigma_{n,np}$ and $\sigma_{n,2n}$ in $E_n$<16 MeV energy region we did not take the calculated results but performed the new evaluation; in order to keep the consistency in $\sigma_{non}$, we also did the corresponding changes in $\sigma_{in}$. Because there are also some changes in $\sigma_{n,\gamma}$, $\sigma_{n,n'}$ and $\sigma_{el}$, we also did corresponding changes in $\sigma_{tot}$ to keep the consistency. All these consistency corrections in $\sigma_{in}$ and $\sigma_{tot}$ are small in comparison with the cross sections themselves.

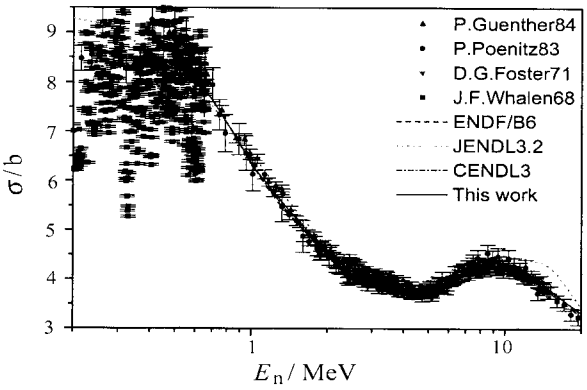


Fig. 1 Total cross section for n+$^{89}$Y

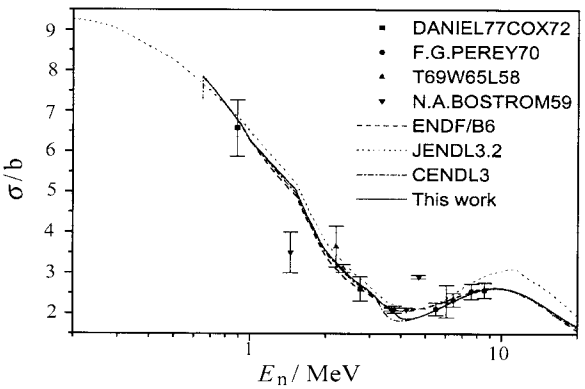


Fig. 2 Elastic scattering cross section for n+$^{89}$Y

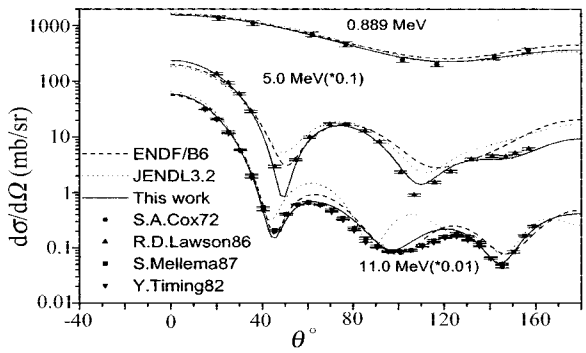


Fig. 3(a) Elastic scattering angular distributions for n+$^{89}$Y

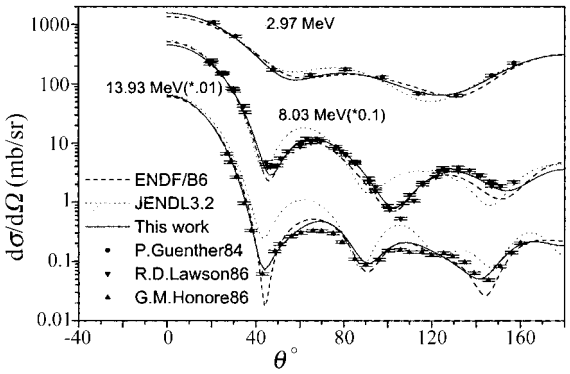


Fig. 3(b) Elastic scattering angular distributions for n+$^{89}$Y

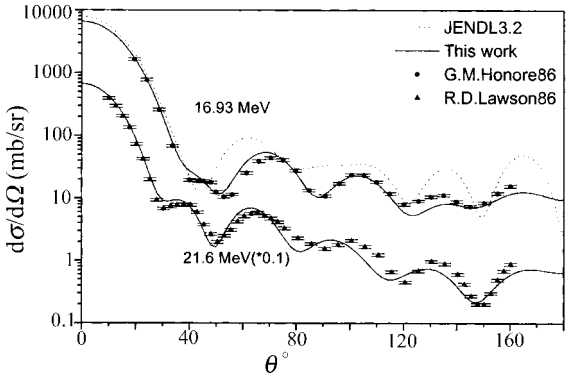


Fig. 3(c) Elastic scattering angular distributions for n+$^{89}$Y

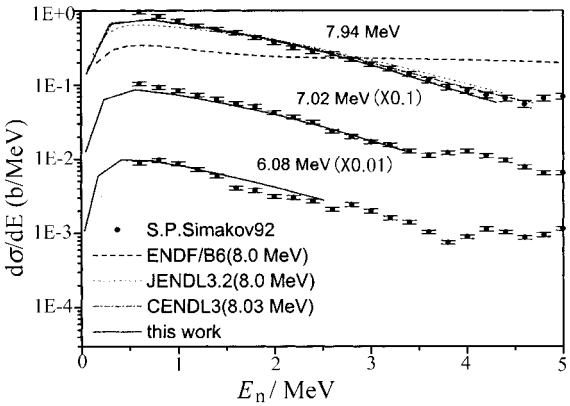


Fig. 4 Inelastic neutron spectra (MT-91) of $^{89}$Y

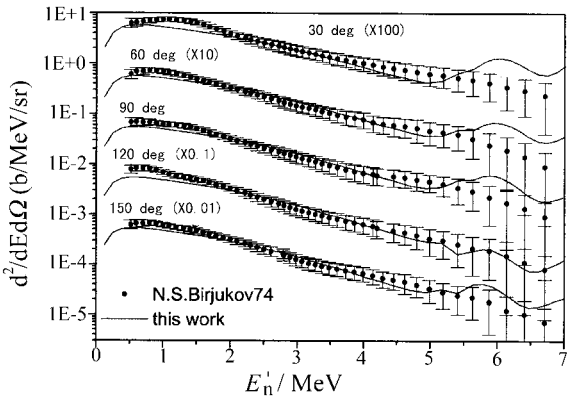


Fig. 5(a) DDCS of inelastic neutron of $^{89}$Y at $E_n$= 9.1 MeV

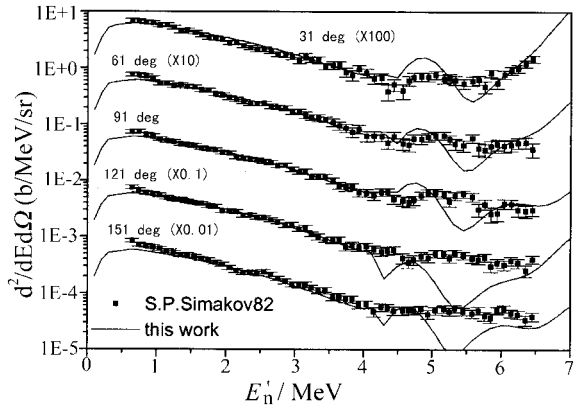


Fig. 5(b)  DDCS of inelastic neutron of $^{89}$Y at $E_n$= 7.94 MeV

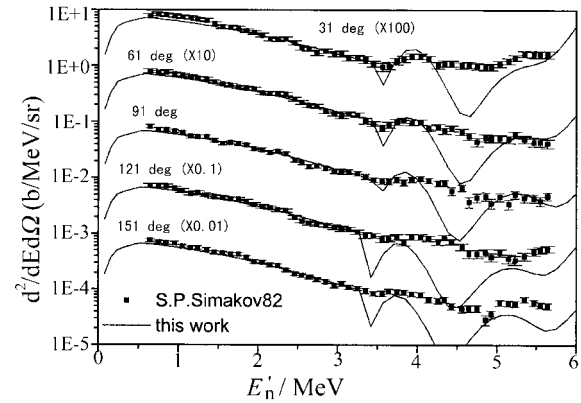


Fig. 5(c)  DDCS of inelastic neutron of $^{89}$Y at $E_n$= 7.02 MeV

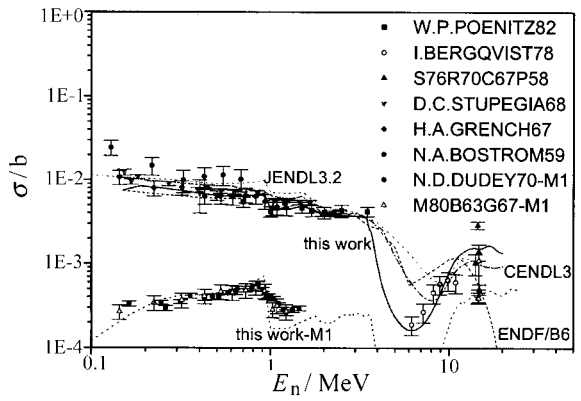


Fig. 6  (n,γ) reaction cross sections of $^{89}$Y

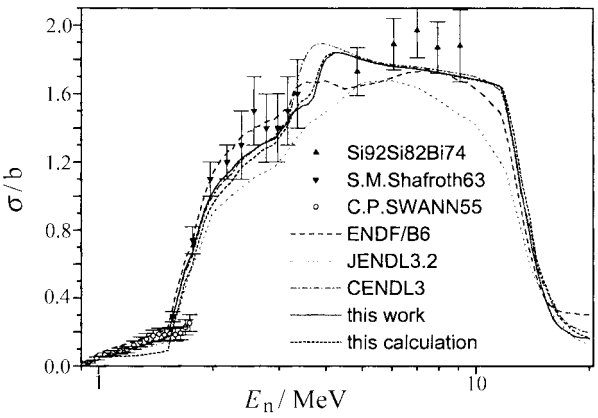


Fig. 7  (n,n′) reaction cross sections of $^{89}$Y

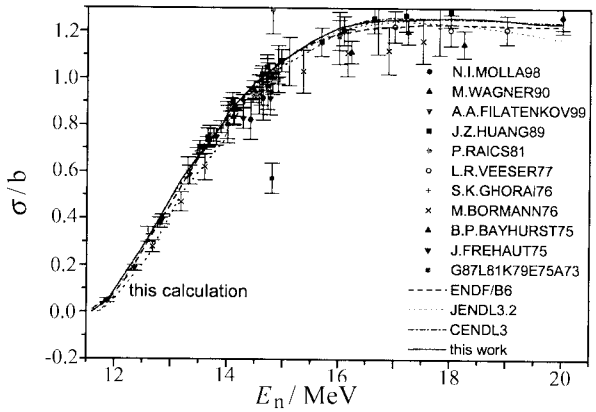


Fig. 8  (n,2n) reaction cross sections of $^{89}$Y

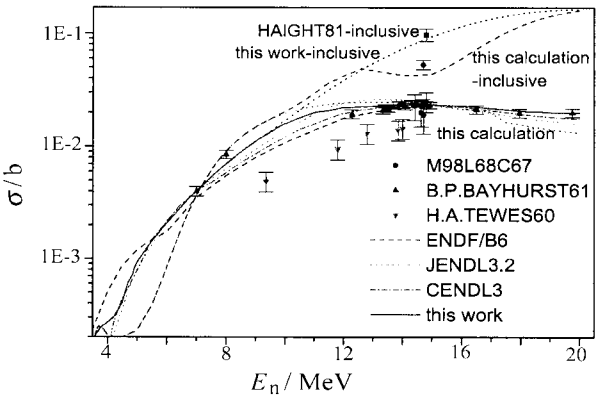


Fig. 9  (n,p) reaction cross sections of $^{89}$Y

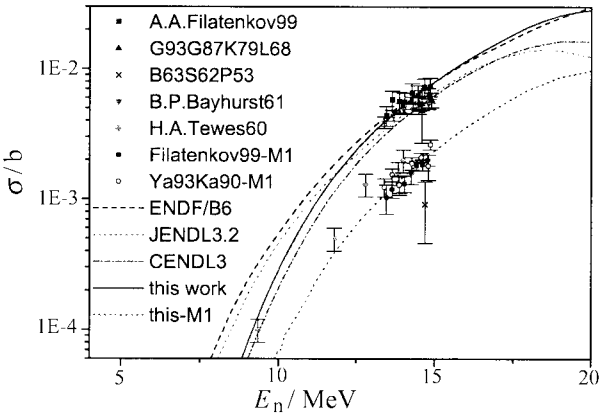


Fig. 10  (n,α) reaction cross sections of $^{89}$Y

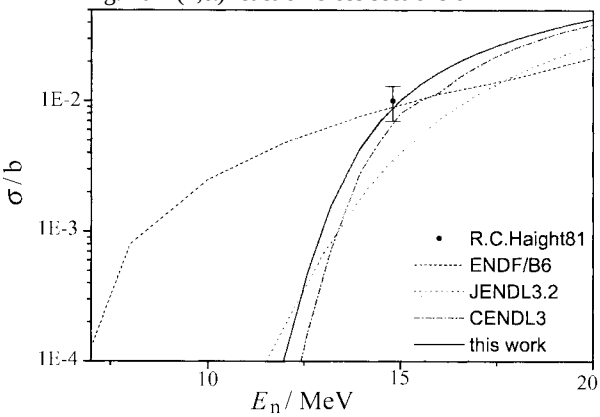


Fig. 11 (n,d) reaction cross sections of $^{89}$Y

## References

[1] SHEN Qingbiao, A Code APMN for Automatically Searching Optimal Optical Potential Parameters below 300 MeV, Commu. Nucl. Data Progress (INDC (CRP)-053/L) No.25, p19, June 2001

[2] ZHANG Jingshang, "User Manual of UNF Code", CNDC-0032, CNIC-01616, China Institute of Atomic Energy, P.O. Box 275(41), Dec. 2001; and J.S.ZHANG, "UNF Code for Fast Neutron Reaction Data Calculations", Nucl. Sci. Eng., 142, p.207, 2002

[3] P.D.Kunz, a DWBA Code DWUCK4, University of Colorado, USA (unpublished)

[4] GE Zhigang, ZHANG Jingshang and SUN Zhengjun, Commun. Nucl. Data. Prog. 27, p27 (2002)

# Data Correction to Mass Resolution

LIU Tingjin
*China Nuclear Data Center, CIAE,Beijing 102413, China tjliu@iris.ciae.ac.cn*

**【abstract】** *A method and code is presented for data correction to mass resolution (and also time, energy resolution). The problems comcerning the practical correction is discussed .*

## Introduction

Due to the mass resolution problem, the fission yield for each product nuclide measured by kinetic energy or double time of flight methods is not exact one, but a fold of the yields at this nuclide of Gaussian extension for all nuclides concerned. To get exact one, they must be corrected for the mass resolution. This paper gives a method to correct them. In fact , this method not only can be used for mass resolution correction, but also for energy resolution correction of energy spectrum, for time resolution of time spectrum measurements etc.

## 1 Correction Method and Code

According to Schmitt[1], the correction can be done with following formula:

$$Y_{\mathrm{C}}(A) = Y_{\mathrm{U}}(A) - \frac{\sigma^2}{2}\frac{\mathrm{d}^2 Y_{\mathrm{C}}(A)}{\mathrm{d}A^2} \tag{1}$$

where $Y_{\mathrm{C}}$, $Y_{\mathrm{U}}$ are the corrected and uncorrected yields respectively, and $\sigma$ is the mass resolution, half width at half maximum (it was said in Ref. [1] that $\sigma$ is full width, which is not correct).

To avoid the effect of the statistical fluctuation, the data were smoothed before correcting, fitted with 2 order function for each 5 datum points

$$Y(A) = a + bA + cA^2 \tag{2}$$

and the yield of center point was taken as new yield at the corresponding mass $A$. For the first and last two datum points, the fit values of the first and last 5 point fitting were taken.

The coefficients $a$, $b$, $c$ were got from following equation group, which was deduced by least square method for each 5 data points:

$$\begin{aligned}
&\left(\sum_{i=n}^{N} w_i\right)a + \left(\sum_{i=n}^{N} w_i A_i\right)b + \left(\sum_{Ii=n}^{N} w_i A_i^2\right)c = \sum_{i=n}^{N} w_i Y_i \\
&\left(\sum_{i=n}^{N} w_i A_i\right)a + \left(\sum_{i=n}^{N} w_i A_i^2\right)b + \left(\sum_{Ii=n}^{N} w_i A_i^3\right)c = \sum_{i=n}^{N} w_i Y_i A_i \\
&\left(\sum_{i=n}^{N} w_i A^2{}_i\right)a + \left(\sum_{i=n}^{N} w_i A_i^3\right)b + \left(\sum_{Ii=n}^{N} w_i A_i^4\right)c = \sum_{i=n}^{N} w_i Y_i A_i^2
\end{aligned} \tag{3}$$

Where $N=n+5$, $n=1,2,\ldots\ldots,(M-4)$, $M$ is the points of the data to be fitted.

The double differential of the function (2) to $A$ is $2c$, so the equation (1) becomes

$$Y_{\mathrm{C}}(A) = Y_{\mathrm{U}}(A) - c\sigma^2 \tag{4}$$

The data were corrected with formula (4). $\sigma$ is given according to the experimental condition, and usually, it is given by the author in the corresponding paper.

A code was developed. Instead of $Y_{\mathrm{c}}(A)$, $Y_{\mathrm{u}}(A)$ was used as 0 rank of approximation in the double differential, because $Y_{\mathrm{c}}(A)$ was unknown. $Y_{\mathrm{u}}(A)$ was smoothed and $a_0$, $b_0$, $c_0$ were obtained from equation group (3). By using coefficient $c_0$, $Y_{\mathrm{C1}}(A)$ was calculated from formula (4)

$$Y_{\mathrm{c}}(A)=Y_{\mathrm{u}}(A)-c_0\sigma^2 \tag{4'}$$

Smoothing $Y_{\mathrm{C1}}(A)$, coefficients $a_1$, $b_1$, $c_1$ were obtained from equation group (3), and using $c_1$, $Y_{\mathrm{C2}}(A)$ was calculated with formula (4'), and so on. Iteration was continued until it was convergent. In the code, it was defined as $\varepsilon=(Y_{\mathrm{C}n+1}(A)-Y_{\mathrm{C}n}(A))/Y_{\mathrm{C}n}(A)<0.000001$ for all mass number $A$, which makes the $Y_{\mathrm{C}n+1}(A)$ and $Y_{\mathrm{C}n}(A)$ be completely in agreement within 5 effective figures.

## 2 Code Test

The method and code were tested. In order to compare conveniently with other experimental data the Zoller's data are shown with three different lines in Figs.1, 2, including original, smoothed, and corrected one at 13 and 7 MeV respectively; and compared with the corresponding data measured with radiochemistry method by LI Ze[2,3], LIU Congqui[4], and Champan[5]. The $\sigma$ used in the correction are 3.3 and 3.675 respectively for 7 and 13 MeV, which were given by the author. It can be seen that the corrected data are in agreement within the error bar with the data measured by radiochemistry, for which there is no this kind of problem.

By using the code INTERP[6], the corrected data (smoothed for each 7 points) at 13 MeV were folded with Gaussian extension with $\sigma$=3.675, which is the same as one in the measurement. The results should be the same as measured data. As shown in Fig. 3, the folded data are in agreement with the measured ones very well, which proves the reliability of the method and code.

## 3 Practical Correction

In the practical processing, it was found that the measured data are not smoothed enough with 5 points as shown in the equations. In this case, the iteration can not be convergent, and there are some unreasonable fluctuations for the corrected data, even wrong results appear with increasing the iteration times. To solve the problem, the data can be smoothed two times, but it does not work sometimes. More efficient method is smoothing the data for each 7 points, where $N=n+7$, and $n$=1, 2, …, ($M$–6) in the equation group (3). Investigations show that in this way the iteration can be convergent and can give more reasonable corrected data (see Figs. 1, 2) for most of the data measured by Vives, Zoller and Hamilton, except for Zoller's data at 50 MeV (both post and pre neutron emission) . For the Zoller's data at 50 MeV, they were smoothed for each 9 datum points. In this case, the iteration was convergent and reasonable result was obtained. Final data were corrected in this way, namely, first smoothed for each 7 (or 9) datum points according to equation group (3), and then corrected according to equation (4).

In the correction, what extent to smooth the data is key point. If the measured data are under smoothing (take less data points in the equation group (3)) for the statistical fluctuation, the iteration would not be convergent and there would be unreasonable structures for the corrected data. If the measured data are over smoothing (take more datum points in the equation group (3)), the existed structures in physics may be wiped out. In our practical case, it is reasonable to take each 7 datum points for most of the measured data, and to take each 9 datum points for the measured data with larger fluctuation.

## 4 Data Error Correction

For the fission yield data measured by kinetic energy or double time of flight methods, not only the mass resolution effects the data themselves, but also the uncertainty of the mass (energy or time of flight) calibration could contribute to the error of the yields. It can be seen from the Figs. 1 and 2 that at the peak, volley and "ground" on two sides, the effect is smaller, but on the wings of the light and heavy peaks, where the yields vary rapidly with the mass $A$, could be larger. Comparing with the data measured with radiochemistry method (no this problem for this kind of data), the uncertainty of the mass $A$ calibration could be ±1 mass unit.

As the data were smoothed with function

$$Y=a+bA+cA^2$$

So $$dY/dA=b+2cA$$

That is $$\Delta Y=(b+2cA)\Delta A \quad (5)$$

The total error $\Delta Y$ contributed from yield measurement (mainly count statistic) $\Delta Y_1$ and mass calibration error $\Delta Y_2$ is

$$\Delta Y=(\Delta Y_1^2+\Delta Y_2^2)^{1/2} \quad (6)$$

By using the formula (5) and taking $\Delta A$=1, the error $\Delta Y_2$ from the mass calibration were calculated, and the$\Delta Y_1$ were given by the author. The total error $\Delta Y$ were calculated with formula (6). The comparison of the corrected error with original ones were given in Figs. 4, 5 as examples.

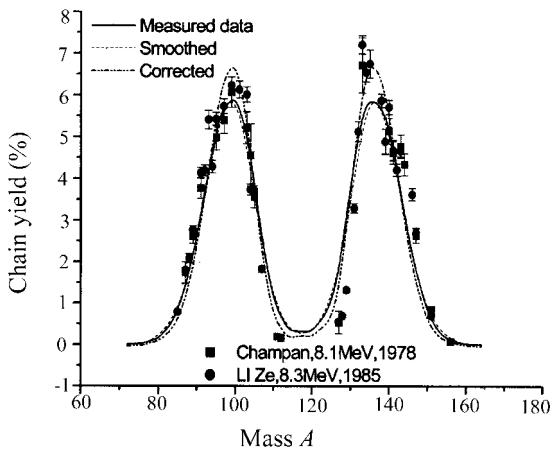


Fig.1 Comparison of corrected Zoller's data at 7 MeV with the data measured by radiochemistry method

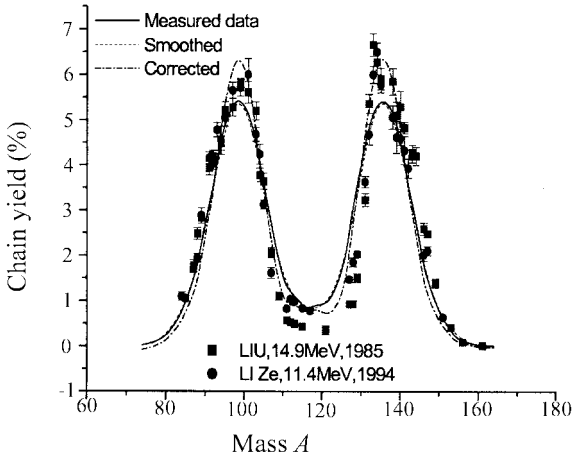


Fig.2 Comparison of corrected Zoller's data at 13 MeV with the data measured by radiochemistry method

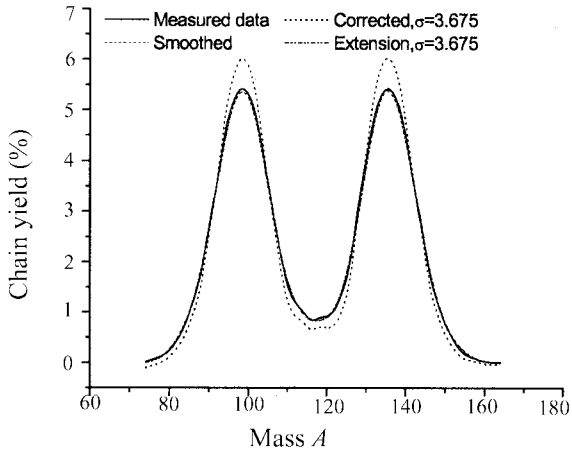


Fig.3 Comparison of corrected data extention with measured data at 13 MeV

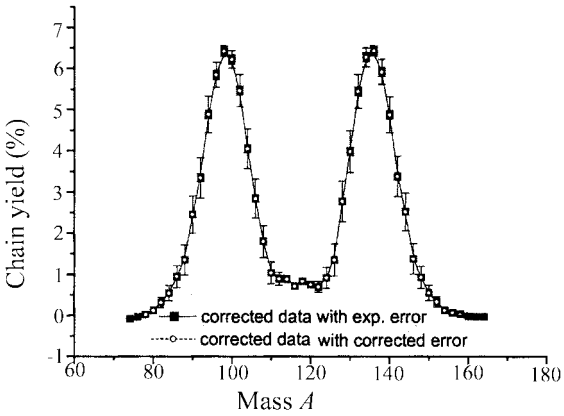


Fig.4 Intercomparison between corrected error and original exp. error at $E_n$=13 MeV

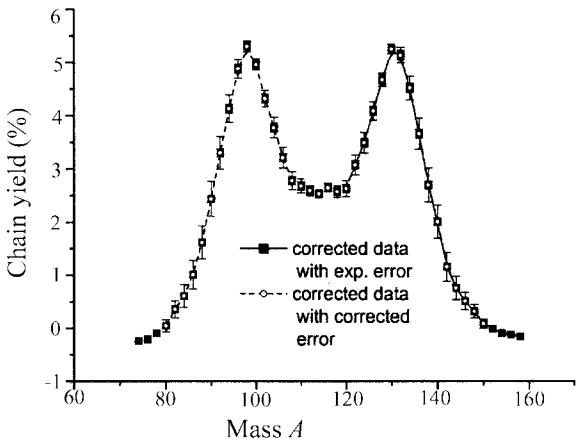


Fig.5 Intercomparison between corrected error and original exp. error at $E_n$=50 MeV

## Reference

[1] H. W. Schmitt et al, Phys. Rev., 137(4), 837 (1965) (EXFOR 13081002)

[2] LI Ze et al, Chinese Nucl . Phys., 7(2), 97(1985)

[3] LI Ze et al, Radiochimica Acta, 64, 95(1994)

[4] LIU Conggui et al, Chinese Nucl. Phys7(3),235(1985)

[5] T.C.Chapman, Phys. Rev. C17(3), 1089(1978)

[6] LIU Tingjin, Internal document(2002)

# Progress in Making Program MEND

CAI Chonghai

*Department of Physics, Nankai University, Tianjin 300071*

*ZHANG Zhengjun*

*Department of Physics, Northwest University, Xi'an 710069*

SHEN Qingbiao

*China Nuclear Data Center, CIAE, Beijing 102413*

Considering nuclear data needs for Accelerator-Driven System (ADS), high-energy radiation shielding, nuclear astrophysics, and so on, several nuclear model programs for calculating the nuclear data in medium-high energy region were developed. LAHET[1] and INC/GEM[2] are Monte-Carlo simulation programs based on the intranuclear cascade model and evaporation/ generalized evaporation model theory. The inverse reaction cross sections used in the evaporation model are given by empirical formula with parameters. The theoretically treatment to low energy region is rather roughly. GNASH[3] is a typical program to directly calculate the medium energy nuclear data based on multi-level emission process, the theoretical frames of which are optical model, exciton model and Hauser-Feshbach theory. With the complementary work of Chadwick et al.[4], GNASH can now calculate the reaction cross sections, energy spectra and the double differential cross sections of six emitting light particles and all kinds of recoil nuclei up to about 200 MeV.

Our former program CCRMN[5] is of almost the same function as GNASH, but it can not calculate energy spectra and the double differential cross sections. So based on CCRMN, we intend to develop a new program MEND for calculating the nuclear data in medium energy region. In comparison with GNASH, the following points in physics are improved:

1) In optical model calculation, the MEND can also do microscopic optical potential calculation based on Skyrme force[6] and the phenomenological optical potential calculation with CH89 or CH86 parameters[7] for n and p channel, which is very useful for those nuclide without experimental data for adjusting optical potential parameters. All inverse reaction cross sections used in statistical calculations are directly calculated with optical model instead of empirical formula.

2) GNASH code doesn't include the width fluctuation correction in Hauser-Feshbach theory, whereas MEND code includes it.

3) The pre-equilibrium emissions only in first and second emission processes are included in GNASH code. Whereas the pre-equilibrium mechanism in the first, second and third emission processes is included exactly and in the forth and fifth emission processes it is approximately considered in MEND code.

4) For emission of composite particles in pre-equilibrium statistical theory, we adopt a pick-up reaction mechanism[8]. In the calculation of state densities for the exciton model, we accommodate the Pauli principle.

5) The intranuclear cascade effect for nucleon emitting yield and energy spectra is considered in MEND code with empirical formula, but GNASH code doesn't include it.

The theoretical framework and problem solved in MEND is basically the same as in CCRMN. The improvements are:

1) In CCRMN, only pre-equilibrium and evaporation mechanisms are considered in the emissions of light particles; but in MEND, the cascade emissions of 1 to 4 nucleons with certain fractions before pre-equilibrium and evaporation are also considered in calculation (GNASH also does not consider the cascade emissions of nucleons). The cascade yield of nucleons and the energy spectra of cascade nucleons are calculated with empirical formula[9].

2) In CCRMN, the pre-equilibrium mechanism is precisely considered only in first to third emission processes of light particles; in MEND, the pre-equilibrium mechanism is also approximately considered in fourth and fifth emission processes of light particles.

3) The Hauser-Feshbach theory with width fluctuation correction is introduced in MEND, so it can also calculate the cross sections and angular distributions of the discrete levels for first emission processes of light particles in low energy region.

The improvements in program functions are:

1) In CCRMN, first to tenth emission processes are considered and they are suitable for about 1 to 100 MeV energy region. In MEND, first to eighteenth emission processes are considered and they are suitable for about 10 keV to 250 MeV;

2) In CCRMN, only the cross sections of six emitting light particles and of all kinds of recoil nuclei can be calculated. In MEND, the energy spectra and the double differential cross sections of six emitting light particles in L-frame, as well as the energy spectra of all kinds of recoil nuclei in L-frame can also be calculated. For calculation of cross sections in any emission process except the first, double-fold integration should be calculated with the excited energy of the compound nucleus as inner integration variable and that of the residual nucleus as outer integration variable in both CCRMN and MEND. For calculation of the energy spectra of the emitting particle moving against the residual nucleus, we should use the energy of relative motion (the emitting particle moving against the residual nucleus) in stead of the excited energy of the residual nucleus in outer integration. Before completing the outer integration, we keep the value of the integrand, which is just the value of the energy spectra, at every energy point. After completing the outer integration for the energy, we also obtain the same cross section value within the calculating precise degree (usually 3%). Based on the energy spectra of relative motion, we calculate the energy spectra of six emitting light particles and of all kinds of recoil nuclei in L-frame with Chadwick's approach[4]. From the energy spectra of six emitting light particles in L-frame and the corresponding pre-equilibrium fraction, we can also calculate the double differential cross sections of six emitting light particles in L-frame with Kalbach systematics[10].

In comparison with CCRM, we have also done some improvements in technical details, such as in the treatment of cross sections and angular distribution in direct reaction. Because of the calculation with higher precise degree, the normalization check in MEND for every emission process become within 2% (most of them within 0.5%), which is better than in CCRMN. The above mentioned improvements are those we have completed up to now. The most important thing is that at this moment MEND can calculate cross sections, energy spectra and the double differential cross sections of six emitting light particles and all kinds of recoil nuclei up to about 250 MeV.

In the following years, we plan to finish the following three tasks:

1) Fission mechanism and calculating methods should be researched for heavy nuclei of actinides and non-actinides in medium energy region. And then in MEND we add the function to calculate fission cross sections, the mass, charge and energy distributions of fission products as well as fission neutron spectra in all levels of fission processes.

2) All kinds of production cross sections of gamma rays and their energy spectra can be calculated in MEND.

3) The output in ENDF/B-6 format can be written in an output file.

The test calculations for p+$^{208}$Pb and p+$^{209}$Bi with MEND are performed, and the calculated results which are rather good in accordance with experimental data and reasonable in physics. Fig.1 gives the total reaction cross sections for p+$^{209}$Bi and p+$^{208}$Pb whose calculated value is a little higher than measured one. Figs. 2, 3 and 4 give the (p,n), (p,3n) and (p,4n) reaction cross sections, respectively, for p+$^{209}$Bi. The energy spectra (differential cross sections) of emitting neutrons for p+$^{208}$Pb and p+$^{209}$Bi are given in Figs. 5 and 6, respectively. All the experimental data were taken from EXFOR. The reason of the calculated neutron spectra at $E_p$=35 and 45 MeV for p+$^{208}$Pb being lower than the experimental data near high-energy ends is that the direct (p,n) reaction was not taken account. The calculated inclusive cross sections of six emitting light particles and the calculated yield cross sections of long-lived isotopes for p+$^{208}$Pb are given in Figs. 7 and 8, respectively.

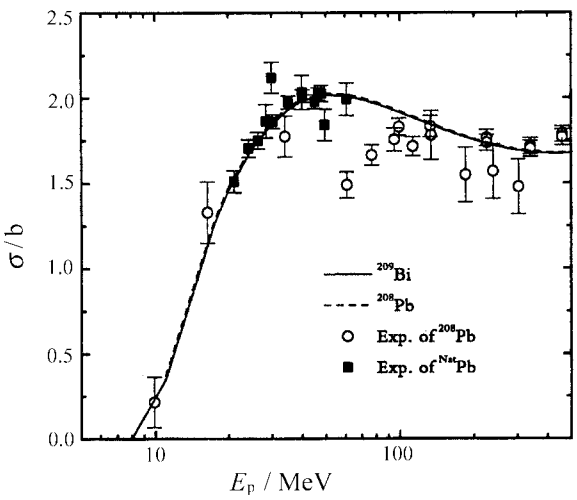


Fig. 1 The total reaction cross sections for p+$^{208}$Pb and p+$^{209}$Bi

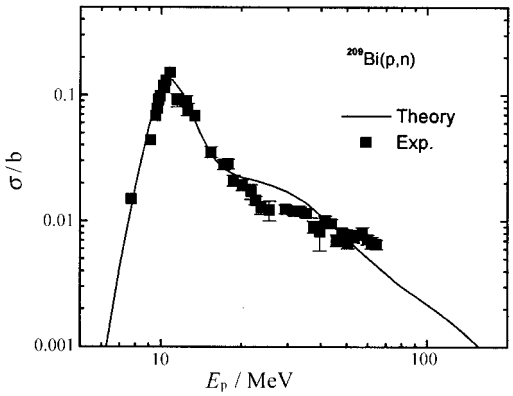


Fig. 2 (n,p) reaction cross sections for p+$^{209}$Bi

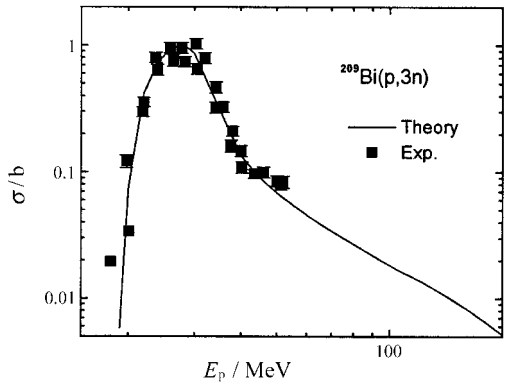


Fig. 3 (n,3p) reaction cross sections for p+$^{209}$Bi

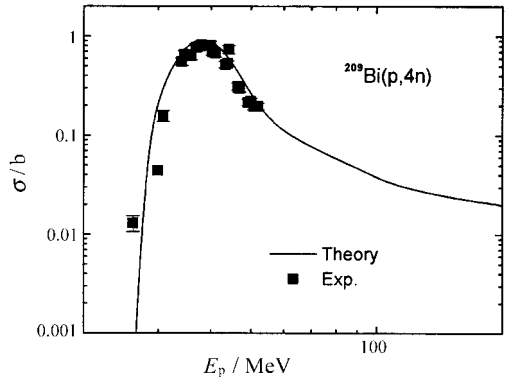


Fig. 4 (p,4n) reaction cross sections for p+$^{209}$Bi

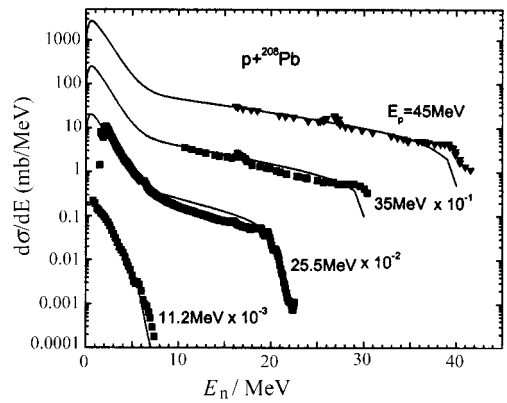


Fig. 5 Energy spectra of emitting neutrons for p+$^{208}$Pb

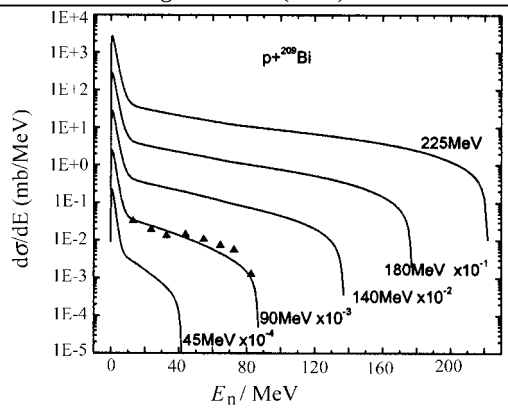


Fig. 6 Energy spectra of emitting neutrons for p+$^{209}$Bi

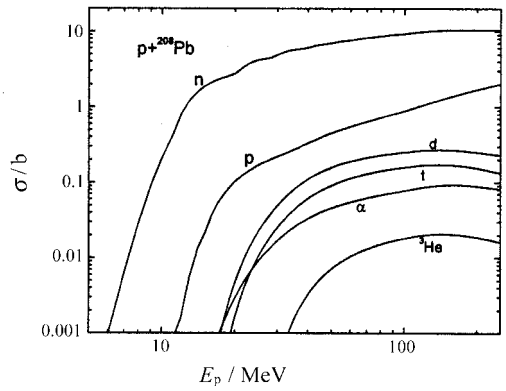


Fig. 7 Inclusive Cross sections of 6 light particles for p+$^{208}$Pb

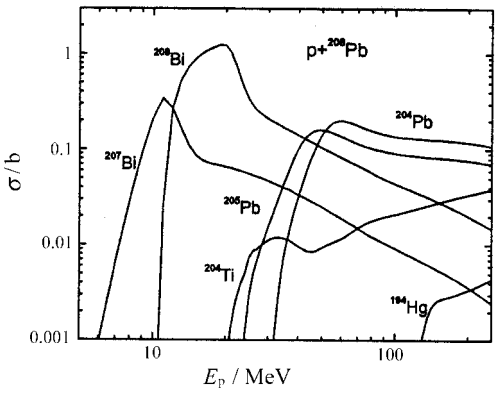


Fig. 8 Yield Cross sections of long-lived isotopes for p+$^{208}$Pb

## References


[1] R.E.Prael, LA-UR-89-3347, "LAHET benchmark calculations of differential neutron production cross sections for 113 MeV and 256 MeV protons" (1989)

[2] S.Furihata, K.Niita, S.Meigo, Y.Ikeda and F.Maekawa, JAERI-Data/Code 2001-015, "the GEM CODE"

[3] P.G.Young & E.D.Arthur, LA-6947

[4] M.B.Chadwick, P.G.Young, S.Chiba, S.C.Frankle, G.M.Hale, H.G.Hughes, A.J.Koning, R.C.Little, R.E.MacFarlane, R.E.Prael and L.S.Waters, Cross-Section Evaluations to 150 MeV for Accelerator-Driven Systems and Implementation in MCNPX, Nucl. Sci Eng. 131, 293(1999)

[5] CAI Chonghai, SHEN Qingbiao and Z.Q.Yu, CCRMN-A Program for Calculating Complex Reactions of a Medium-Heavy Nucleus with Six Light Particles, Nucl. Sci. Eng., 126, 127(1997); C.H.Cai and Q.B.Shen, Calculation Methods in Program CCRMN, Comm. Nucl. Data Prog. 15, 22(1996)
[6] SHEN Qingbiao et al., Z.Phys. A303, 69(1981)
[7] R.L.Varner et al., Phys. Rep. 201,57(1991); also Phys. Lett. B185, 6(1987)
[8] ZHANG Jingshang et al., Commun. Theor. Phys., 10, 33(1988)
[9] SHEN Qingbiao, Tian Ye, ZHAO Zhixiang, Liu Guisheng and Ding Dazhao, Calculations of Nucleon Emission and Energy Deposition of Spallation Neutron Sources Induced by Intermediate Energy Protons, Target Phy., ,231()
[10] C.Kalbach, Systematics of Continuum Angular Distributions, Phy. Rev. C, 37, 2350(1988)

# Implementation of the Resonance Analysis Code SAMMY

WANG Jimin ZHUANG Youxiang
*China Nuclear Data Center, CIAE, Beijing 102413*

【**abstract**】 *The requirement of developing the resonance analysis code SAMMY, the implementation of it in China Nuclear Data Center (CNDC), and the partial exercises results are briefly introduced.*

## Introduction

A great deal of experiments have testified that when a low energy neutron reacts with a target, there will be acute fluctuation in the low energy region of the excitation function of the nuclear reaction, that is the resonance. In the design of the nuclear reactor and other dependent calculations, the experimental data of resonance cross sections are not directly used, but the resonance parameters from fitting the experimental data are used. Therefore the cross sections in the resonance region must be parameterized. The resonance parameters can modify the effects of Doppler broadening and resolution broadening and multiple-scattering (expect for transmissions), which ensure the cross sections calculated from the resonance parameters to meet some physical requirements, and make the data simple and precious. The research on neutron resonance theory [1] has been made at CNDC.

The multi-level multi-channel R-matrix SAMMY code [2] is used for making the resonance parameters, which was developed by Oak Ridge National Laboratory (ORNL), and widely used around the USA (ORELA, KAPL, LANL, TUNL…) and around the world (Belgium, Japan, France, Bulgaria, etc.)[3]. SAMMY-M5 [4] can be used to analyze (n,alpha) or (alpha,n) reactions in addition to previously available options: transmission, elastic scattering (both angle-integrated and differential), fission, inelastic scattering, capture, and absorption cross sections, etc, self-indication, and certain types of integral data. Cross sections in the unresolved resonance region can be analyzed using SAMMY, and angle-differential reaction cross sections can also be treated in SAMMY. But it does not properly treat incident charged particles, although charged-particle final states were properly treated. In SAMMY-M6-Beta[4,5], the newest version of SAMMY, charged particles can be used for both incident and exit channels.

Chinese scientists applied SAMMY to analyze the resonance parameters at ORNL and CERN before [6]. However, it was not used in China.

The resonance parameters of CENDL[7] were taken from different evaluated neutron data files such as ENDF/B[8] or JENDL[9]. It is necessary and useful for CNDC to implement the resonance analysis code SAMMY.

## 1 The Implementation of SAMMY

The code SAMMY is an important program to CNDC. Now, we have an Alpha server 4000 and SAMMY-M5 code[2]. The code SAMMY-M5 was primarily implemented on CNDC Alpha server 4000 under VMS system by Dr. Charles Dunford from NNDC in June of 2000 during his visit at CNDC, and finally we completed it.

### 1.1. The Input and Output Files of SAMMY [2,3]

SAMMY mainly consists of three input files:

(1) INPut file. It contains details about the interaction being studied, SAMMY control information and quantum numbers.

(2) PARameter file. It contains initial values for resonance parameter and other variable parameters, a prior uncertainties, flags defining which are to be varied.

(3) DATa file. It the experimental data, including energy, measured value for cross section, and uncertainty.

In some cases, it may need more files: COVariance file (parameter covariance matrix from previous run), DCV file (Data CoVariance) (covariance information for data), AVG (AVeraGe) file (energy ranges for averaging), NDF input file (in order to produce an output file in ENDF/B-6 format), MXW file (temperatures at which to evaluate Maxwellian averages), etc. These files may be user-generated or produced by earlier SAMMY runs.

The output of SAMMY depends on the control parameters set in the INPut file. The main output file of SAMMY is SAMMY.LPT. Other output files are SAMMY.IO (initial and final values of varied parameters), SAMMY.PAR (new values of resonance parameters and other varied parameters, in the same format as the initial PARameter file), SAMMY.COV (updated COVariance matrix for the updated parameters is a binary file), SAMMY.ODF (binary file to be used for plotting), and SAM??.DAT (temporary files for communication between segments).

### 1.2 Code Testing

We have compiled and linked each segment of the SAMMY, and finally generated an executable file-sammy.exe. We did the most exercises, the results are correct. From the comparisons of the exercises results with the answers, it can be seen that the implementation is successful.

Following is one of the exercise results (ex018), in which shows how to deal with data covariance information (See Fig.1).

## 2 Future Plan

Now, the code SAMMY can run on CNDC Alpha server 4000, and scientists in China can apply SAMMY code to analyze the resonance parameters at CNDC.

We planned to evaluate one or two nucleus by using SAMMY. In the near future, we hope to get the newest version of SAMMY and to do more and better work on the resonance parameters.

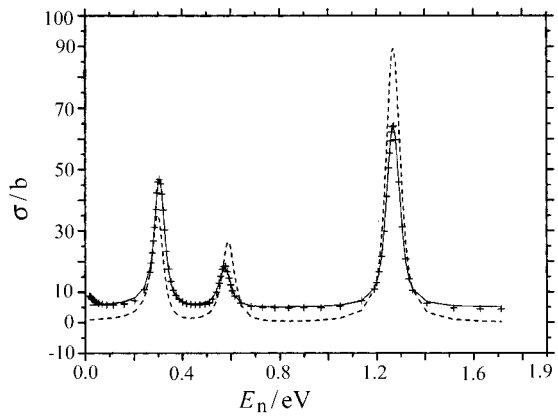


Fig.1 Fission cross section for $^{241}$Am
(fit reduced data but include data-reduction operations)
++ reduced data
--- with a prior parameter values
— SAMMY fit

### References

[1] China Nuclear Data Center，“Neutron Resonance Theory and Resonance Parameters”，in Chinese, Atomic Energy Pres.，1981

[2] Nancy.M.Larson, ORNL/TM-9179/R3, (1996); ORNL/TM-9179/R5, (2000)

[3] N.M.Larson, IAEA Workshop on “Nuclear Reaction Data and Nuclear Reactors: Physics, Design and Safety” Trieste, Italy, 25 February–28 March 2002

[4] Radiation Safety Information Computational Center, “Peripheral Shielding Routine Abstract” (December, 2000), (May, 2002)

[5] N.M.Larson, Jour of Nucl. Sci. and Tech., p.92-95, (2002)

[6] ZHAO Zhixiang et al., NNDC, BNL-NCS-17541, 4th Edition of ENDF/B-VI, p.120, 1991

[7] ZHUANG Youxiang et al., Jour. of Nucl. Sci. and Tech., p.37-39, (2002)

[8] NNDC, BNL-NCS-17541, 4th Edition of ENDF/B-6, 1991

[9] NDC/JAERI, JAERI-M-92-007, INDC(JPN)-161/L, 1992

# The Benchmark Testing of $^{9}$Be of CENDL-3

LIU Ping

*China Nuclear Data Center P. O. Box 275(41), Beijing 102413, China. Email: ping@iris.ciae.ac.cn*

**【abstract】** *CENDL-3, the latest version of China Evaluated Nuclear Data Library was finished. The data of $^{9}$Be were updated, and distributed for benchmark analysis recently. The calculated results were presented, and compared with the experimental data and the results based on other evaluated nuclear data libraries. The results show that CENDL-3 is better than others for most benchmarks.*

## Introduction

The $^{9}$Be data of CENDL-3 were updated again recently by Prof. ZHANG Jingshang et. al. by using a new approach[1]. In order to test the reliability of $^{9}$Be data of CENDL-3, some benchmarks were used. In addition to the values of $k_{eff}$ , the leakage spectrum of Be sphere was calculated. The data processing was carried out by using the NJOY[2] nuclear data processing code system. The calculations and analysis of benchmarks were done with Monte Carlo code MCNP[3]. The comparisons of calculated results with the results obtained with other evaluated nuclear data libraries were also performed. The aim of the comparison between different evaluated nuclear data libraries is to identify the source of the discrepancies with the experimental results.

## 1 Data Processing

The cross sections from CENDL-3, ENDF/B-6.4, JENDL-3.2 and CENDL-2.1 were processed with the NJOY97 code system in the MCNP-format of continuous-energy. The cross sections from the ENDF/B-5 in the MCNP-format of MCNP library [4] were also used for the benchmarks calculations.

## 2 Data Testing Calculations

The continuous energy Monte Carlo code MCNP was used to do the benchmark testing calculations. The characteristics of the benchmark assemblies are shown in Table 1 and Table 2 briefly. The benchmarks for the calculations of $k_{eff}$ are given in the International Handbook of Evaluation Criticality Safety Benchmark Experiments[5]. The benchmark for the calculation of the leakage of Be sphere surface is a 50 cm radius beryllium sphere.[6] The calculated results of $k_{eff}$ are given in Table 3 and Table 4. The leakage spectrum of Be sphere surface is given in Fig. 1.

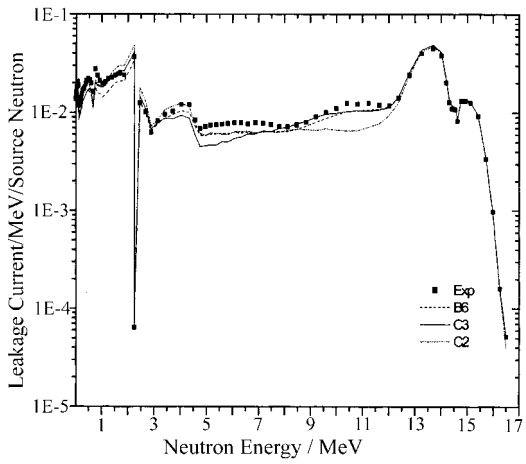


Fig.1 The leakage spectrum of Be sphere surface

## 3 Discussions

It can be seen that CENDL-3 shows good agreements with experiment for most assemblies. The calculated $k_{eff}$ for the assembly of spheres of plutonium surrounded by highly enriched uranium and reflected by beryllium or beryllium oxide is slightly lower compared with other evaluated libraries; this may be due to the uranium data are from ENDF/B-5. While uranium data were used from CENDL-3, the calculated results would be better for the assembly. The calculated results based on CENDL-3 are significantly improved compared with the results based on CENDL-2.1, which is the old version of CENDL. ENDF/B-6 also gives better results for most assemblies.

It can be seen in the Fig.1 that CENDL-3 shows good agreement with the experiment, and the ENDF/B-6 is underestimated below 3 MeV. From 3~7.5 MeV, CENDL-3 is underestimated, maybe the original spectrum of Be is soften in the energy region. CENDL-3 also shows good agreement with the experiment above 7.5 MeV, but ENDF/B-6 and CENDL-2.1 are lower in this energy region.

**Table 1　Composition of Isotopes (Atom/barn-cm)**

| Assembles | Core | | | Reflector | | |
|---|---|---|---|---|---|---|
| | Isotope | Composition | | Isotope | Composition | |
| 1. A Delta-phase plutonium sphere reflected by beryllium | $^{239}$Pu | $3.7291*10^{-2}$ | | Beryllium | $1.1984*10^{-1}$ | |
| | $^{240}$Pu | $1.9277*10^{-3}$ | | Oxygen | $1.3776*10^{-3}$ | |
| | $^{241}$Pu | $1.2196*10^{-4}$ | | | | |
| | Gallium | $1.3628*10^{-3}$ | | | | |
| 2. Sphere of plutonium reflected by beryllium | $^{239}$Pu | $3.3930*10^{-2}$ | | Be | $1.2081*10^{-1}$ | |
| | $^{240}$Pu | $3.5043*10^{-3}$ | | O | $8.2064*10^{-3}$ | |
| | $^{241}$Pu | $3.9189*10^{-4}$ | | C | $1.0020*10^{-4}$ | |
| | Ga | $2.2105*10^{-3}$ | | Fe | $5.0939*10^{-5}$ | |
| | C | $3.0246*10^{-4}$ | | | | |
| | Fe | $3.2525*10^{-4}$ | | | | |
| | W | $7.4100*10^{-5}$ | | | | |
| | Ni | $1.4187*10^{-3}$ | | | | |
| 3a. Beryllium reflected cylinders of plutonium | $^{239}$Pu | $4.4422*10^{-2}$ | | Beryllium | $1.2099*10^{-1}$ | |
| | $^{240}$Pu | $2.1326*10^{-3}$ | | Oxygen | $1.0449*10^{-3}$ | |
| | $^{241}$Pu | $9.2538*10^{-5}$ | | | | |
| | C | $1.9515*10^{-4}$ | | | | |
| | Fe | $8.1943*10^{-5}$ | | | | |
| 3b. Beryllium oxide reflected cylinders of plutonium | $^{239}$Pu | $4.4422*10^{-2}$ | | Beryllium | $6.9041*10^{-2}$ | |
| | $^{240}$Pu | $2.1326*10^{-3}$ | | Oxygen | $6.9041*10^{-2}$ | |
| | $^{241}$Pu | $9.2538*10^{-5}$ | | | | |
| | C | $1.9515*10^{-4}$ | | | | |
| | Fe | $8.1943*10^{-5}$ | | | | |
| 4a. Highly enriched uranium-233 spheres reflected by beryllium | $^{233}$U | $4.7253*10^{-2}$ | | Beryllium | $1.1984*10^{-1}$ | |
| | $^{234}$U | $5.2705*10^{-4}$ | | Oxygen | $1.3776*10^{-3}$ | |
| | $^{238}$U | $3.2975*10^{-5}$ | | | | |
| 4b. Highly enriched uranium-233 spheres reflected by beryllium | $^{233}$U | $4.7312*10^{-2}$ | | Beryllium | $1.1984*10^{-1}$ | |
| | $^{234}$U | $5.2770*10^{-4}$ | | Oxygen | $1.3776*10^{-3}$ | |
| | $^{238}$U | $3.3015*10^{-5}$ | | | | |
| 5a,5b. Beryllium reflected and beryllium oxide-reflected cylinders of highly enriched uranium | | Bottom | Top | | Bottom | Top |
| | | | | | Be reflector | |
| | $^{235}$U | $4.5798*10^{-2}$ | $4.5754*10^{-2}$ | Beryllium | $1.2149*10^{-1}$ | $1.2049*10^{-1}$ |
| | $^{238}$U | $1.3387*10^{-3}$ | $1.3374*10^{-3}$ | Oxygen | $1.0492*10^{-3}$ | $1.0406*10^{-3}$ |
| | $^{234}$U | $5.6819*10^{-4}$ | $5.6764*10^{-4}$ | | BeO reflector | |
| | $^{12}$C | $1.0276*10^{-4}$ | $1.0266*10^{-4}$ | Beryllium | $6.8675*10^{-2}$ | $6.9459*10^{-2}$ |
| | Fe | $5.0229*10^{-5}$ | $5.0180*10^{-5}$ | Oxygen | $6.8675*10^{-2}$ | $6.9459*10^{-2}$ |
| | W | $1.2206*10^{-6}$ | $1.2194*10^{-6}$ | | | |
| 6. $^{235}$U（94%）spheres surrounded By beryllium | $^{234}$U | $4.8554*10^{-4}$ | | Beryllium | $1.2295*10^{-1}$ | |
| | $^{235}$U | $4.4508*10^{-2}$ | | | | |
| | $^{238}$U | $2.3775*10^{-3}$ | | | | |

Cont. Table 1

| Assembles | Core | | | Reflector | |
|---|---|---|---|---|---|
| | Isotope | | Composition | | Isotope |
| 7a,7b. Spheres of plutonium surrounded by highly enriched uranium and reflected by beryllium or beryllium oxide | Plutonium Atom Densities | | | Be reflector | BeO reflector |
| | $^{239}$Pu | $3.4304*10^{-2}$ | Be | $1.1994*10^{-1}$ | $6.7508*10^{-2}$ |
| | $^{240}$Pu | $3.4950*10^{-3}$ | O | $8.1470*10^{-5}$ | $6.7508*10^{-2}$ |
| | $^{241}$Pu | $3.9076*10^{-4}$ | C | $9.9480*10^{-5}$ | |
| | Ga | $2.1289*10^{-3}$ | Fe | | |
| | C | $3.0536*10^{-4}$ | | | |
| | Fe | $3.2837*10^{-4}$ | | | |
| | W | $7.4811*10^{-5}$ | | | |
| | Ni | $8.6774*10^{-4}$ | | | |
| | HEU Atom Densities | | | | |
| | $^{235}$U | $4.1030*10^{-2}$ | | | |
| | $^{238}$U | $4.1009*10^{-3}$ | | | |
| | $^{234}$U | $5.2286*10^{-4}$ | | | |
| | $^{236}$U | $8.7989*10^{-5}$ | | | |
| | C | $3.9571*10^{-4}$ | | | |
| | Fe | $1.3507*10^{-4}$ | | | |
| | W | $1.2436*10^{-5}$ | | | |
| | Cu | $7.2150*10^{-4}$ | | | |
| | Ni | $3.3480*10^{-4}$ | | | |
| | Duralumin Atom Densities | | | | |
| | Al | 5.8077E-2 | | | |
| | Mg | 1.0332E-3 | | | |
| | Mn | 1.8284E-4 | | | |
| | Cu | 1.1329E-3 | | | |
| 8. Critical experiments performed using spherical composite cores reflected by beryllium | $^{239}$Pu | $4.5536*10^{-2}$ | Be | $1.2295*10^{-1}$ | |
| | $^{240}$Pu | $2.7719*10^{-3}$ | | | |
| | $^{241}$Pu | $1.7313*10^{-4}$ | | | |
| | $^{235}$U | $4.4401*10^{-2}$ | | | |
| | $^{238}$U | $3.2137*10^{-3}$ | | | |

**Table 2 The benchmark assemblies reflected by beryllium or beryllium oxide**

| Assemblies | *w* % (Beryllium) | Reflector Density / g/cm$^3$ | Reflector Thickness / cm |
|---|---|---|---|
| 1 | 98.0 | 1.83 | 3.6881 |
| 2 | 98.51 | 1.8169 | 5.65 |
| 3a | 98.49 | 1.83846 | 9.995 |
| 3b | 98.49 | 2.8675 | 9.995 |
| 4a | 98.0 | 1.83 | 4.1961 |
| 4b | 98.0 | 1.83 | 2.0447 |
| 5a | 98.49 | 1.83 | 9.995 |
| 5b | 98.49 | 2.86 | 9.995 |
| 6 | 99.058 | 1.84 | 4.699 |
| 7a | 98.49 | 1.83 | 9.15 |
| 7b | 98.49 | 1.93 | 9.15 |
| 8 | 100 | 1.84 | 16.2 |

**Table 3 The $k_{eff}$ values for assemblies**

| Assembles | Exp | CENDL3 | ENDFB6 | ENDFB5 | JENDLl3.2 | CENDL2.1 |
|---|---|---|---|---|---|---|
| 1 | 1.0000 | 0.99953 | 0.99946 | 0.99932 | 1.0054 | 1.00082 |
| 2 | 0.9992 | 0.99995 | 1.00185 | 1.00055 | 1.00713 | 1.0022 |
| 3a | 1.0000 | 1.00413 | 1.00457 | 1.00466 | 1.01000 | 1.00540 |
| 3b | 1.0000 | 0.99691 | 0.99759 | 0.99647 | 1.00166 | 0.99897 |
| 4a | 1.0000 | 0.99527 | 0.99589 | 0.99474 | 0.99930 | 0.99732 |
| 4b | 1.0000 | 0.99722 | 0.99822 | 0.99549 | 1.00322 | 0.99732 |
| 5a | 0.9996 | 0.99752 | 0.99690 | 0.99626 | 1.00179 | 0.99666 |
| 5b | 0.9996 | 1.00221 | 1.00267 | 1.00193 | 1.00568 | 1.00131 |
| 6 | 1.0000 | 1.00028 | 1.00040 | 0.99987 | 1.00482 | 1.00050 |
| 7a | 0.9993 | 0.99697 | 0.99842 | 0.99734 | 1.00009 | 0.99753 |
| 7b | 0.9993 | 0.99740 | 0.99860 | 0.99942 | 0.99962 | 0.99785 |
| 8 | 1.0000 | 1.00797 | 1.00783 | 1.00622 | 1.01647 | 1.01150 |

**Table 4 The $k_{eff}$ differences relative to the experimental results ( Δ k)***

| Assembles | Exp | CENDL3 | ENDFB6 | ENDFB5 | JENDL3.2 | CENDL2.1 |
|---|---|---|---|---|---|---|
| 1 | 1.0000 | -47 | -54 | -68 | 540 | 82 |
| 2 | 0.9992 | 75 | 265 | 135 | 793 | 300 |
| 3a | 1.0000 | 413 | 457 | 466 | 1000 | 540 |
| 3b | 1.0000 | -309 | -241 | -353 | 166 | -103 |
| 4a | 1.0000 | -473 | -411 | -526 | -70 | -268 |
| 4b | 1.0000 | -278 | -178 | -451 | 322 | -268 |
| 5a | 0.9996 | -208 | -270 | -334 | 219 | -294 |
| 5b | 0.9996 | 261 | 307 | 233 | 608 | 171 |
| 6 | 1.0000 | 28 | 40 | -13 | 482 | 50 |
| 7a | 0.9993 | -233 | -88 | -196 | 49 | -177 |
| 7b | 0.9993 | -177 | -70 | 12 | 32 | -145 |
| 8 | 1.0000 | 797 | 783 | 622 | 1647 | 1150 |

*: Δ k in units of 1.E-5. Note: All materials are from ENDF/B-5 except Beryllium, which is from different evaluated data file.

## References


[1] ZHANG J S et.al., Nucl. Sci. & Eng. 133, 218-234 (1999)

[2] R.E. MacFarlane and D. W. Muir, "The NJOY Data Processing System Version 94,"LA-12740-M (1994)

[3] MCNP-A General Monte Carlo N-Particle Transport Code(Version 4C),LA-13709-M, Judith F. Briesmeister, Editor. April 10 2000

[4] J. S. Hendricks, S. C. Frankle, J. D. Court, "ENDF/B-6 Data for MCNP", Los Alamos National Laboratory report LA-12891 (1994)

[5] International Handbook of Evaluated Criticality Safety Benchmark Experiments. NEA/NSC/DOC(95), September 2000 Edition

[6] Y. Murakami, K. Yoshioka, "Leakage Neutron Spectra from Beryllium Sphere" , Version 1.0 compiled on March 8, 1994

# CINDA INDEX

| Nuclide | Quantity | Energy/ eV | | Lab | Type | Documentation | | | | | Author, Comments |
|---|---|---|---|---|---|---|---|---|---|---|---|
| | | Min | Max | | | Ref | Vol | Page | Date | | |
| $^{6}$Li | Evaluation | 1.0–5 | 2.0+7 | AEP | Eval | Jour CNDP | 28 | 43 | Dec | 2002 | ZHUANG Yuoxiang +, SIG |
| $^{28}$Si | (n,γ) | 1.0–5 | 2.0+7 | BJG | Eval | Jour CNDP | 28 | 13 | Dec | 2002 | TANG Guoyou +, SIG, DA, DA/DE |
| $^{29}$Si | Evaluation | 1.0–5 | 2.0+7 | BJG | Eval | Jour CNDP | 28 | 13 | Dec | 2002 | TANG Guoyou +, SIG, DA, DA/DE |
| $^{30}$Si | Evaluation | 1.0–5 | 2.0+7 | BJG | Eval | Jour CNDP | 28 | 13 | Dec | 2002 | TANG Guoyou +, SIG, DA, DA/DE |
| $^{Nat}$Si | Evaluation | 1.0–5 | 2.0+7 | BJG | Eval | Jour CNDP | 28 | 13 | Dec | 2002 | TANG Guoyou +, SIG, DA, DA/DE |
| $^{50}$Cr | Evaluation | 5.0+4 | 1.0+6 | SIU | Expt | Jour CNDP | 28 | 1 | Dec | 2002 | XIA Yijun +, CS, TBL, ACTIN |
| $^{85}$Rb | Evaluation | 1.0–5 | 2.0+7 | NKU | Eval | Jour CNDP | 28 | 31 | Dec | 2002 | CAI Chonghai, SJG, DA, DE |
| $^{87}$Rb | Evaluation | 1.0–5 | 2.0+7 | NKU | Eval | Jour CNDP | 28 | 31 | Dec | 2002 | CAI Chonghai, SJG, DA, DE |
| $^{Nat}$Rb | Evaluation | 1.0–5 | 2.0+7 | NKU | Eval | Jour CNDP | 28 | 31 | Dec | 2002 | CAI Chonghai, SJG, DA, DE |
| $^{89}$Y | Evaluation | 1.0–5 | 2.0+7 | NKU | Eval | Jour CNDP | 28 | 46 | Dec | 2002 | CAI Chonghai, SJG, DA, DE |
| $^{Nat}$Ag | (n,γ) | 1.0+4 | 5.0+6 | ZHN | Theo | Jour CNDP | 28 | 8 | Dec | 2002 | LIU Jianfeng +, SJG, DE |
| $^{169}$Tm | Evaluation | 1.0–5 | 2.0+7 | AEP | Eval | Jour CNDP | 28 | 38 | Dec | 2002 | CHEN Guochang +, SJG, DA, DE |
| $^{181}$Ta | (n,γ) | 1.0+4 | 5.0+6 | ZHN | Theo | Jour CNDP | 28 | 8 | Dec | 2002 | LIU Jianfeng +, SJG, DE |
| $^{197}$Au | (n,γ) | 1.0+4 | 1.0+7 | ZHN | Theo | Jour CNDP | 28 | 8 | Dec | 2002 | LIU Jianfeng +, SJG, DE |
| $^{197}$Au | Evaluation | 1.0–5 | 2.0+7 | AEP | Eval | Jour CNDP | 28 | 26 | Dec | 2002 | FAN Sheng +, SIG, DA, DA/DE |
| $^{238}$U | Fission Yield | 1.0–5 | 2.0+8 | AEP | Eval | Jour CNDP | 28 | 18 | Dec | 2002 | LIU Tingjin, FISS YLD |
| $^{239}$Pu | Fission Yield | 1.0–5 | 2.0+8 | AEP | Eval | Jour CNDP | 28 | 18 | Dec | 2002 | LIU Tingjin, FISS YLD |
| $^{242}$Pu | Fission Yield | 1.0–5 | 2.0+8 | AEP | Eval | Jour CNDP | 28 | 18 | Dec | 2002 | LIU Tingjin, FISS YLD |